IN-MEDIUM NUCLEON-NUCLEON SCATTERING UP TO 1 GEV

Eivind Brodal

Contents

Chapter 1

Scattering Theory

In this chapter much of the theoretical theory for the Nucleon-Nucleon (NN) scattering is derived, focusing on deriving practical expressions for numerical calculations of phase shifts and inelasticities. Phase shifts and inelasticities are derived from S-matrix, which is again determined from the T-matrix.

We will use two different T-matrix equations derived from approximations of the Bethe-Salpeter equation, which covariantly describes the NN scattering in quantum field theory, These approximations are known as the Thompson (Th) method and the Blankenbecler-Sugar (BbS) method. Both (Th) and (BbS) have much in common with the Lippmann-Schwinger equation, which can be derived from classical two-particle scattering. In this chapter much of the space will therefore be dedicated to formulas from classical scattering theory. One also has to introduce a special T-matrix for coupled channels. The deuteron, for example, is such a coupled state. To deal with coupled channels, one has to define a mixing parameter, along with two phase shifts and two inelasticities.

More simple potentials arising from the NN interactions such as the box potential and the Yukawa potential, will be derived. Even though the box potential and the Yukawa potential are not as accurate as the more sophisticated NN-potentials, they can still provide a very good physical understanding of the NN system. The phase shifts from a box potential can also be calculated both numerically and analytically, and it can therefore be used to test the computational methods in the numerical calculations of phase shifts. If we use a complex box potential we are able to test the inelasticities in the same way as for the phase shifts.

1.1 Perturbation theory used in classical two-particle scattering

A two nucleon system or a general multiple nucleon system is described by a Hamiltonian $\hat{H}$ which can be divided into two parts; $\hat{H} = \hat{H}_0 + \hat{V}$. For a two-nucleon system the dominant part is the unperturbed Hamiltonian $\hat{H}_0$, which contains information of each nucleon in the absence of the other, and $\hat{V}$ is this interaction term between

the nucleons. The time-independent Schrödinger equation can be written as

$$\big(\hat{H}_0 + \hat{V}\big)|\psi_{\mathbf{k}}\rangle = E_{\mathbf{k}}|\psi_{\mathbf{k}}\rangle, \tag{1.1}$$

where $|\psi_{\mathbf{k}}\rangle$ can be divided into two orthogonal parts as $|\psi_{\mathbf{k}}\rangle = |\phi_{\mathbf{k}}\rangle + |\chi_{\mathbf{k}}\rangle$. Given $|\phi_{\mathbf{k}}\rangle = |\mathbf{k}\rangle$ as the free part, and $|\chi_{\mathbf{k}}\rangle$ as the perturbed part. We have the familiar unperturbed equation

$$\hat{H}_0|\phi_{\mathbf{k}}\rangle = \frac{\hat{\mathbf{k}}^2}{2m}|\phi_{\mathbf{k}}\rangle = \varepsilon_{\mathbf{k}}|\phi_{\mathbf{k}}\rangle. \tag{1.2}$$

Using the free Green function defined as

$$\hat{G}_0^{(\pm)}(E) = \lim_{\epsilon\to 0}\frac{1}{E - \hat{H}_0 \pm i\epsilon}, \tag{1.3}$$

where ϵ is a regulator that decides if the green operator is carrying the state forward or backward in time, we can rewrite $|\psi_{\mathbf{k}}\rangle$ as an iterative equation

$$|\psi_{\mathbf{k}}^{\pm}\rangle = |\phi_{\mathbf{k}}\rangle + \hat{G}_0^{(\pm)}(E_{\mathbf{k}})\ \hat{V}\ |\psi_{\mathbf{k}}^{\pm}\rangle. \tag{1.4}$$

It is easy to verify that this state satisfies the time-independent Schrödinger equation

$$(E_{\mathbf{k}} - \hat{H}_0)\ |\psi_{\mathbf{k}}^{\pm}\rangle = \hat{V}|\psi_{\mathbf{k}}^{\pm}\rangle, \tag{1.5}$$

since we have

$$(E_{\mathbf{k}} - \hat{H}_0)\ |\phi_{\mathbf{k}}\rangle = 0 \tag{1.6}$$

and

$$(E_{\mathbf{k}} - \hat{H}_0)\ \hat{G}_0^{(\pm)}(E_{\mathbf{k}})\ \hat{V}\ |\psi_{\mathbf{k}}^{\pm}\rangle = \hat{V}\ |\psi_{\mathbf{k}}^{\pm}\rangle. \tag{1.7}$$

Eq(1.4) is therefore exact. We use the expression "Born approximation of order n" to describe how many times we iterate this equation and where we end the last iterating with the approximation $|\psi_{\mathbf{k}}\rangle = |\phi_{\mathbf{k}}\rangle$. If we use $|\phi_{\mathbf{k}}\rangle = |\mathbf{k}\rangle$ and iterate infinitely many times, we obtain

$$|\psi_{\mathbf{k}}^{\pm}\rangle = \big(1 + \hat{G}^{(\pm)}(E_{\mathbf{k}})\ \hat{V}\big)\ |\mathbf{k}\rangle, \tag{1.8}$$

where

$$\begin{aligned}\hat{G}^{(\pm)} &= \hat{G}_0^{(\pm)} + \hat{G}_0^{(\pm)}\hat{V}\hat{G}^{(\pm)} \\ &= \hat{G}_0^{(\pm)} + \hat{G}_0^{(\pm)}\hat{V}\hat{G}_0^{(\pm)} + \hat{G}_0^{(\pm)}\hat{V}\hat{G}_0^{(\pm)}\hat{V}\hat{G}_0^{(\pm)} + \ldots.\end{aligned} \tag{1.9}$$

If we now make use of the general operator relation

$$\frac{1}{\hat{A}+\hat{B}} = \frac{1}{\hat{A}} + \frac{1}{\hat{A}}\hat{B}\frac{1}{\hat{A}} + \frac{1}{\hat{A}}\hat{B}\frac{1}{\hat{A}}\hat{B}\frac{1}{\hat{A}} + \ldots, \tag{1.10}$$

we see that

$$\hat{G}^{(\pm)}(E) = \frac{1}{E - \hat{H}_0 - \hat{V} \pm i\epsilon}, \tag{1.11}$$

where $\hat{G}^{(\pm)}(E)$ is the Green function for the full Hamilton operator $\hat{H} = \hat{H}_0 + \hat{V}$. We can therefore rewrite the time independent Schrödinger equation from eq(1.1) as

$$\big(E_{\mathbf{k}} - \hat{H}\big)|\psi_{\mathbf{k}}^{\pm}\rangle = 0, \tag{1.12}$$

with $|\psi_{\mathbf{k}}^{\pm}\rangle$ given by eq(1.8).

1.2 The S- and the T-matrix derived from two-particle scattering

1.2.1 For a general potential

The scattering matrix S is defined as

$$S(\mathbf{p},\mathbf{k}) = \langle \mathbf{p}|\hat{\mathbf{S}}|\mathbf{k}\rangle = \langle \psi^-_{\mathbf{p}}|\psi^+_{\mathbf{k}}\rangle. \tag{1.13}$$

This definition tells us that $S(\mathbf{p},\mathbf{k})$ represents the probability of finding a free incoming particle in state $|\mathbf{k}\rangle$, which is an eigenstate of the free Hamiltonian, and a free outgoing particle in state $|\mathbf{p}\rangle$, which is another eigenstate of the same free Hamiltonian. Both $\hat{V}$ and $\hat{H}_0$ are Hermitian, since they are operators of observables. i.e., $\hat{V} = \hat{V}^\dagger$ and $\hat{H}_0 = \hat{H}_0^\dagger$. From this follows

$$(\hat{G}^{(\pm)})^\dagger = \hat{G}^{(\mp)}. \tag{1.14}$$

By taking the Hermitian adjunct on both sides of eq(1.8), we obtain

$$\langle \psi^\pm_{\mathbf{k}}| = \langle \hat{k}|\big(1 + \hat{V}\,\hat{G}^{(\mp)}(E_{\mathbf{k}})\big). \tag{1.15}$$

From the definition above, the two probability amplitudes $\langle \psi^+_{\mathbf{p}}|\psi^+_{\mathbf{k}}\rangle$ and $\langle \mathbf{p}|\mathbf{k}\rangle$ must be the same, i.e.

$$\langle \psi^+_{\mathbf{p}}|\psi^+_{\mathbf{k}}\rangle = \langle \mathbf{p}|\mathbf{k}\rangle. \tag{1.16}$$

We can rewrite this as follows

$$\begin{aligned}\langle \psi^-_{\mathbf{p}}|\psi^+_{\mathbf{k}}\rangle &= \langle \psi^+_{\mathbf{p}}|\psi^+_{\mathbf{k}}\rangle + \big(\langle \psi^-_{\mathbf{p}}| - \langle \psi^+_{\mathbf{p}}|\big)|\psi^+_{\mathbf{k}}\rangle \\ &= \langle \mathbf{p}|\mathbf{k}\rangle + \left(\frac{1}{E_{\mathbf{p}} - E_{\mathbf{k}} + i\epsilon} - \frac{1}{E_{\mathbf{p}} - E_{\mathbf{k}} - i\epsilon}\right)\langle \mathbf{p}|\hat{\mathbf{V}}|\psi^+_{\mathbf{k}}\rangle. \end{aligned} \tag{1.17}$$

Using the relations

$$\frac{1}{x + i\epsilon} = \mathcal{P}\frac{1}{x} - i\pi\delta(x), \tag{1.18}$$

$$\frac{1}{x - i\epsilon} = \mathcal{P}\frac{1}{x} + i\pi\delta(x), \tag{1.19}$$

where $\mathcal{P}$ is Cauchy's principal value. We then derive the well-known expression for the S-matrix given as

$$S(\mathbf{p},\mathbf{k}) = \langle \psi^{(-)}_{\mathbf{p}}|\psi^{(+)}_{\mathbf{k}}\rangle = \langle \mathbf{p}|\mathbf{k}\rangle - 2\pi i\delta(E_{\mathbf{p}} - E_{\mathbf{k}})\langle \mathbf{p}|\hat{T}|\mathbf{k}\rangle, \tag{1.20}$$

which can be written in operator form as

$$\hat{S} = \hat{1} - 2\pi i\delta(\hat{H}_0 - E)\hat{T}, \tag{1.21}$$

where E is the kinetic energy of the two nucleons. We have also introduced the transition operator $\hat{T}$, which is defined as

$$\hat{V}|\psi^{(+)}_{\mathbf{k}}\rangle = \hat{T}|\mathbf{k}\rangle. \tag{1.22}$$

From eq(1.4) and eq(1.9), we see that $\hat{T}$ can also be written as

$$\hat{T} = \hat{V} + \hat{V}\hat{G}^{(+)}\hat{V} = \hat{V} + \hat{V}\hat{G}_0^{(+)}\hat{T}, \tag{1.23}$$

which is the Lippmann-Schwinger equation on a general operator form.

A useful feature of the S-matrix in elastic scattering, is the unitarity, i.e., $S S^\dagger = \hat{1}$, since this can be a good test to use in the numerical calculations. We can prove this unitarity by showing that $\langle \mathbf{p}|\hat{S}\hat{S}^\dagger|\mathbf{k}\rangle = \langle \mathbf{p}|\mathbf{k}\rangle$, but first we note that

$$\hat{S}|\mathbf{k}\rangle = |\mathbf{k}\rangle - 2\pi i\delta(H_0 - E_\mathbf{k})\hat{T}|\mathbf{k}\rangle \tag{1.24}$$

$$\langle \mathbf{p}|\hat{S}^\dagger = \langle \mathbf{p}| + \langle \mathbf{p}|\hat{T}^\dagger 2\pi i\delta(H_0 - E_\mathbf{p}). \tag{1.25}$$

Putting these two equations together, we get

$$\begin{aligned}\langle \mathbf{p}|\hat{S}^\dagger\hat{S}|\mathbf{k}\rangle &= \langle \mathbf{p}|\mathbf{k}\rangle - 2\pi i\delta(E_\mathbf{k} - E_\mathbf{p})\langle \mathbf{p}|(\hat{T} - \hat{T}^\dagger)|\mathbf{k}\rangle \\ &\quad -(2\pi i)^2\langle \mathbf{p}|\hat{T}^\dagger\delta(E_\mathbf{k} - H_0)\delta(E_\mathbf{p} - H_0)\hat{T}|\mathbf{k}\rangle.\end{aligned} \tag{1.26}$$

We have to show that the second and the third term on the right-hand side of eq(1.26) cancel each other. From eq(1.23) we have $\hat{T} = \hat{V} + \hat{V}\hat{G}_0^{(+)}\hat{T}$. From this we get the relation

$$\hat{T}^\dagger = \hat{V} + \hat{T}^\dagger\hat{G}_0^{(-)}\hat{V}. \tag{1.27}$$

If we use eq(1.23) to remove the last $\hat{V}$ in eq(1.27), we get

$$\hat{T}^\dagger = \hat{V} + \hat{T}^\dagger\hat{G}_0^{(-)}\hat{T} - \hat{T}^\dagger\hat{G}_0^{(-)}\hat{V}\hat{G}_0^{(+)}\hat{T}. \tag{1.28}$$

A similar expression for $\hat{T}$ can be found by substituting the last $\hat{V}$ in eq(1.23) with eq(1.27):

$$\hat{T} = \hat{V} + \hat{T}^\dagger\hat{G}_0^{(+)}\hat{T} - \hat{T}^\dagger\hat{G}_0^{(-)}\hat{V}\hat{G}_0^{(+)}\hat{T}, \tag{1.29}$$

and we obtain the relation

$$\begin{aligned}\hat{T}^\dagger - \hat{T} &= \hat{V} + \hat{T}^\dagger\hat{G}_0^{(-)}\hat{T} - \hat{T}^\dagger\hat{G}_0^{(-)}\hat{V}\hat{G}_0^{(+)}\hat{T} \\ &\quad -\left[\hat{V} + \hat{T}^\dagger\hat{G}_0^{(+)}\hat{T} - \hat{T}^\dagger\hat{G}_0^{(-)}\hat{V}\hat{G}_0^{(+)}\hat{T}\right] \\ &= \hat{T}^\dagger\hat{G}_0^{(-)}\hat{T} - \hat{T}^\dagger\hat{G}_0^{(+)}\hat{T} \\ &= \hat{T}^\dagger\left[\hat{G}_0^{(-)} - \hat{G}_0^{(+)}\right]\hat{T} \\ &= \hat{T}^\dagger\left[\frac{1}{E - \hat{H}_0 - i\epsilon} - \frac{1}{E - \hat{H}_0 + i\epsilon}\right]\hat{T} \\ &= 2\pi i\hat{T}^\dagger\delta(E - \hat{H}_0)\hat{T},\end{aligned} \tag{1.30}$$

where E is the kinetic energy of the two nucleons. In the last step we have also used eq(1.18) and eq(1.19). By inserting

$$\delta(E_\mathbf{k} - H_0)\delta(E_\mathbf{p} - H_0) = \delta(E_\mathbf{k} - E_\mathbf{p})\delta(E - H_0), \tag{1.31}$$

and eq(1.30) in eq(1.26), we have proven the unitary properties of the S-matrix.

A complete set of eigenstates in the NN scattering process will only include the states with positive energies E. i.e., we remove the bound states from the complete set of eigen states. If we choose to work with eq(1.23) in a momentum space basis, we are left with the continuous spectrum of momentum vectors.

It is convenient to work in momentum space, since we then have an integral equation instead of an integro-differential equation, when we solve the Schrödinger equation in coordinate space. If we now use the ket relation found in eq(1.4) with the definition of T from eq(1.22), we have

$$\begin{aligned} |\psi_{\mathbf{k}}^{+}\rangle &= |\mathbf{k}\rangle + \hat{G}_0^{(+)}(E_{\mathbf{k}})\ \hat{V}\ |\psi_{\mathbf{k}}^{+}\rangle \\ &= |\mathbf{k}\rangle + \frac{1}{E_{\mathbf{k}} - \hat{H}_0 + i\epsilon}\ \hat{T}\ |\mathbf{k}\rangle \\ &= |\mathbf{k}\rangle + \frac{1}{(2\pi)^3}\int_{-\infty}^{\infty} d^3q \quad |\mathbf{q}\rangle\langle\mathbf{q}|\frac{1}{E_{\mathbf{k}} - E_{\mathbf{q}} + i\epsilon}\ \hat{T}\ |\mathbf{k}\rangle, \end{aligned} \tag{1.32}$$

where we in the last step inserted a complete set of positive energy states. By multiplying this equation with $\langle\mathbf{p}|\hat{V}$ from the left, we get

$$\langle\mathbf{p}|\hat{T}(E)|\mathbf{k}\rangle = \langle\mathbf{p}|\hat{V}|\mathbf{k}\rangle + \frac{1}{(2\pi)^3}\int_{-\infty}^{\infty} d^3q \quad \langle\mathbf{p}|\hat{V}|\mathbf{q}\rangle\langle\mathbf{q}|\frac{1}{E - E_{\mathbf{q}} + i\epsilon}\ \hat{T}(E)\ |\mathbf{k}\rangle, \tag{1.33}$$

where E is also known as the on-shell energy when derived from NN-interactions in covariant field theory.

1.2.2 In partial waves for central potentials

The Lippmann-Schwinger equation in eq(1.33) has almost the same form as the non-relativistic Blankenbecler-Sugar equation, which is a commonly used 3D-reductions of the Bethe-Salpeter equation in NN phase shift analysis. Many of the NN potentials developed from NN interactions will require a partial wave form of the Lippmann-Schwinger equation. A partial wave decomposition of eq(1.33) can be practical if the potential is central. A central potential is only a function of the relative coordinates $r = |\mathbf{r}|$, i.e., on the form $V(\mathbf{r}_2 - \mathbf{r}_1) = V(\mathbf{r}) = V(r)$. An OBEP will be spherical symmetric with respect to the $\mathbf{r}$ in the center of mass system. If we calculate the phase shifts in the center of mass system from the OBEP, we will therefore have reduced the two particle problem to a one particle problem.

We can make a local potential by using meson theory for NN scattering in free space. For NN scattering in a nuclei, the potential from the strong interactions will not be local. However, for some nucleon systems we can regard the potential as an effective local potential. Phase shifts from in-medium NN scattering are derived from the G-matrix, which is similar to the T-matrix and is defined through a different perturbation. The in-medium scattering will be discussed in another chapter.

We expect to see axial symmetry around the direction of the incoming particle $\hat{\mathbf{k}}$ for a central $V(r)$ potential. This symmetry allows us to separate the part depending

on the parameters $k = |\mathbf{k}|$ and $p = |\mathbf{p}|$ in the equations above. This method is known as partial wave decomposition, where each partial wave is related to a phase shift and an inelasticity.

We note that the angle part $\hat{\mathbf{k}}\hat{\mathbf{r}}$ and the momentum part $\mathbf{kr}$ can be separated in $\exp(i\mathbf{kr})$, since this function can be written in terms of Legendre polynomials $P_l(\hat{\mathbf{k}}\hat{\mathbf{r}})$ and spherical Bessel functions $j_l(kr)$, where $\hat{\mathbf{k}}\hat{\mathbf{r}}$ denotes the angle between the two vectors. This is known as the Bauer series, which is given as

$$\exp(i\mathbf{kr}) = \sum_{l=0}^{\infty}(2l+1)i^l j_l(kr)P_l(\hat{\mathbf{k}}\hat{\mathbf{r}}), \tag{1.34}$$

where the orbital momentum l has been introduced. A local potential in momentum space can then be expressed as

$$\begin{aligned}
&\langle\mathbf{p}|\hat{V}|\mathbf{k}\rangle = \int_{-\infty}^{\infty} d^3r \exp(-i\mathbf{pr})V(r)\exp(i\mathbf{kr}) \\
= &\int_{-\infty}^{\infty} d^3r \sum_{l'=0}^{\infty}(2l'+1)i^{-l'}j_{l'}(pr)P_{l'}(\hat{\mathbf{p}}\hat{\mathbf{r}})V(r)\sum_{l=0}^{\infty}(2l+1)i^l j_l(kr)P_l(\hat{\mathbf{k}}\hat{\mathbf{r}}) \qquad (1.35)\\
= &\ 2\pi\sum_{l,l'=0}^{\infty}(2l'+1)(2l+1)i^{(l-l')}\int_{-1}^{1}d(\cos\theta)P_{l'}(\hat{\mathbf{p}}\hat{\mathbf{r}})P_l(\hat{\mathbf{k}}\hat{\mathbf{r}})\int_0^{\infty}dr\ r^2V(r)j_{l'}(pr)j_l(kr)
\end{aligned}$$

(1.36)

We then define the partial wave decomposition of V as

$$V_{l'l}(p,k) = \langle p|\hat{V}_{l'l}|k\rangle = \int_0^{\infty} dr\ r^2V(r)j_{l'}(pr)j_l(kr), \tag{1.37}$$

where $V_l'l$ is independent of the angle $\hat{\mathbf{p}}\hat{\mathbf{k}}$. From the definition of $\hat{T}$ we have $\hat{V}|\psi_{\mathbf{k}}^{(+)}\rangle = \hat{T}|\mathbf{k}\rangle$. The partial wave decomposition of T is defined in a similar way as $\hat{V}_{l'l}|\psi_k^{(+)}\rangle = \hat{T}_{l'l}|k\rangle$. With this definition of $\hat{V}_{l'l}$, we can rewrite eq(1.35) as

$$V(\mathbf{p},\mathbf{k}) = 2\pi\sum_{l,l'=0}^{\infty}A_{l'l}(\hat{\mathbf{p}}\hat{\mathbf{r}},\hat{\mathbf{k}}\hat{\mathbf{r}})V_{ll}(p,k), \tag{1.38}$$

where we have used the short-hand notation

$$A_{l'l}(\hat{\mathbf{p}}\hat{\mathbf{r}},\hat{\mathbf{k}}\hat{\mathbf{r}}) = (2l'+1)(2l+1)i^{(l-l')}\int_{-1}^{1}d(\cos\theta)P_{l'}(\hat{\mathbf{p}}\hat{\mathbf{r}})P_l(\hat{\mathbf{k}}\hat{\mathbf{r}}) \tag{1.39}$$

The relation between $\hat{T}$ and $\hat{T}_{l'l}$ will therefore yield

$$\langle\mathbf{p}|T|\mathbf{k}\rangle = 2\pi\sum_{l,l'=0}^{\infty}A_{l'l}(\hat{\mathbf{p}}\hat{\mathbf{r}},\hat{\mathbf{k}}\hat{\mathbf{r}})\langle p|T_{l'l}|k\rangle. \tag{1.40}$$

By using these relations, we obtain

$$\begin{aligned}
&\frac{1}{(2\pi)^3}\int_{-\infty}^{\infty} d^3q \quad \langle \mathbf{p}|\hat{V}|\mathbf{q}\rangle\langle \mathbf{q}|\frac{1}{E-E_{\mathbf{q}}+i\epsilon}\,\hat{T}(E)\,|\mathbf{k}\rangle \\
= &\sum_{l,l',l'',l'''=0}^{\infty}\int_{-\infty}^{\infty}\frac{d^3q}{2\pi}A_{l'l''}(\hat{\mathbf{p}}\hat{\mathbf{r}},\hat{\mathbf{q}}\hat{\mathbf{r}})V_{l'l'''}(p,q)\frac{1}{E-E_{\mathbf{q}}+i\epsilon}A_{l'''l}(\hat{\mathbf{q}}\hat{\mathbf{r}},\hat{\mathbf{k}}\hat{\mathbf{r}})\langle q|\hat{T}_{l'''l}(E)|k\rangle \\
= &\ 4\sum_{l,l'l''=0}^{\infty}A_{l'l''}(\hat{\mathbf{p}}\hat{\mathbf{r}},\hat{\mathbf{k}}\hat{\mathbf{r}})\int_0^{\infty}dq \quad q^2V_{ll''}(p,q)\frac{1}{E-E_{\mathbf{q}}+i\epsilon}\langle q|\hat{T}_{l''l}(E)\,|k\rangle, \qquad (1.41)
\end{aligned}$$

where we in the last step have rewritten the integrals and used the Legendre polynomial relation

$$\int_{-1}^{1}d(\cos\theta)P_l(\hat{\mathbf{p}}\hat{\mathbf{r}})P_{l'}(\hat{\mathbf{k}}\hat{\mathbf{r}}) = \frac{2}{2l+1}\,P_l(\hat{\mathbf{p}}\hat{\mathbf{k}})\,\delta_{l,l'} \qquad (1.42)$$

We now have partial wave expressions for all the terms in the Lippmann-Schwinger equation given in eq(1.33). By inserting these terms in the Lippmann-Schwinger equation, we obtain

$$\langle p|\hat{T}_{l'l}(E)|k\rangle = \langle p|\hat{V}_{l'l}|k\rangle + \frac{2}{\pi}\sum_{l''}\int_0^{\infty}dq\;q^2 \quad \langle p|\hat{V}_{l'l''}|q\rangle\frac{1}{2E-2E_{\mathbf{q}}+i\epsilon}\langle q|\,\hat{T}_{l''l}(E)\,|k\rangle, \qquad (1.43)$$

which only depends on the partial wave decomposition of the potential $V_{l'l}$ and the on-shell energy E in the center of mass system. Note that, eq(1.43) contains coupled orbital momentum states. From eq(1.18) and eq(1.19) we have

$$\begin{aligned}
\frac{1}{2E_{\mathbf{k}}-2E_{\mathbf{q}}\pm i\epsilon} &= \mathcal{P}\frac{1}{2E_{\mathbf{k}}-2E_{\mathbf{q}}}\mp i\pi\delta_{l'l}\delta(2E_{\mathbf{k}}-2E_{\mathbf{q}}) \\
&= \mathcal{P}\frac{1}{2E_{\mathbf{k}}-2E_{\mathbf{q}}}\mp\frac{i\pi\delta_{l'l}\delta(k-q)}{2\left|\frac{\partial E_{\mathbf{q}}}{\partial q}\right|_k}, \qquad (1.44)
\end{aligned}$$

where we in the last step used the general formula for the delta function

$$\delta(f(x)) = \frac{1}{\left|\frac{\partial f(x)}{\partial x}\right|_{x_0}}\delta(x_0). \qquad (1.45)$$

For non-relativistic energies $E_{\mathbf{q}} = \frac{q^2}{2m}$, we have

$$\left|\frac{\partial E_{\mathbf{q}}}{\partial q}\right|_k = \frac{k}{m}. \qquad (1.46)$$

The Lippmann-Schwinger equation can therefore be rewritten in partial waves as

$$\begin{aligned}
\langle p|\hat{T}_{l'l}(E_k)|k\rangle &= \langle p|\hat{V}_{l'l}|k\rangle + \frac{2m}{\pi}\sum_{l''}\Bigg[\mathcal{P}\int_0^{\infty}dq\;q^2\langle p|\hat{V}_{l'l''}|q\rangle\frac{1}{k^2-q^2}\langle q|\hat{T}_{l''l}(E_k)|k\rangle \\
&\quad -ikm\;\langle p|\hat{V_{l'l''}}|k\rangle\;\langle k|\hat{T}_{l''l}(E_k)\,|k\rangle\Bigg]. \qquad (1.47)
\end{aligned}$$

With this expression of $\hat{T}_{l'l}$, one can calculate the phase shifts and the inelasticities, which can be compared with experimental results obtained from NN scattering. To be able to find the phase shifts and the inelasticities we need to define a partial wave expression for the scattering operator $\hat{S}_{l'l}$.

As shown earlier in this chapter the $\hat{S}$ operator is unitary when we are dealing with elastic scattering , i.e.

$$\langle \mathbf{p}|\hat{S}^\dagger \hat{S}|\mathbf{k}\rangle = \int_{-\infty}^{\infty} d^3r \ \langle \mathbf{p}|\hat{S}^\dagger|\mathbf{r}\rangle\langle \mathbf{r}|\hat{S}|\mathbf{k}\rangle = \langle \mathbf{p}|\ \hat{1}\ |\mathbf{k}\rangle = (2\pi)^3\ \delta(\mathbf{p}-\mathbf{k}). \tag{1.48}$$

To find the partial wave decomposition of the S-matrix relative to $\hat{T}_{l'l}$, we rewrite $\langle \mathbf{r}|\hat{S}|\mathbf{k}\rangle$ as a partial wave expansion

$$\begin{aligned}
\langle \mathbf{r}|\hat{S}|\mathbf{k}\rangle &= \int_{-\infty}^{\infty} \frac{d^3q}{(2\pi)^3}\ \langle \mathbf{r}|\mathbf{q}\rangle\langle \mathbf{q}|\hat{S}|\mathbf{k}\rangle \\
&= \int_{-\infty}^{\infty} \frac{d^3q}{(2\pi)^3}\ \exp(i\mathbf{rq})\big(\ \langle \mathbf{q}|\mathbf{k}\rangle - 2\pi i\ \delta(2E_{\mathbf{q}} - 2E_{\mathbf{k}})\ \langle \mathbf{q}|\hat{T}|\mathbf{k}\rangle\ \big) \\
&= \exp(i\mathbf{rk}) - \Big[\frac{i^{l+l'-l''+1}}{2} m \int_0^{\infty} dq\ q\ \delta(q-k) \\
&\quad \times \sum_{l,l',l''=0}^{\infty} j_l(kr)(2l+1)(2l'+1)(2l''+1)\ \langle q|\hat{T}_{l'l}\ |k\rangle \\
&\quad \times \int_{-1}^{1} d(\cos\theta')\ P_l(\hat{\mathbf{q}}\hat{\mathbf{r}}) \int_{-1}^{1} d(\cos\theta)\ P_{l'}(\hat{\mathbf{q}}\hat{\mathbf{r}}) P_{l''}(\hat{\mathbf{k}}\hat{\mathbf{r}})\Big] \\
&= \sum_{l',l=0}^{\infty} (2l+1) i^l j_l(kr) P_l(\hat{\mathbf{k}}\hat{\mathbf{r}})\big[\delta_{l'l} - 2imk\ \langle k|\hat{T}_{l'l}\ |k\rangle\big],
\end{aligned} \tag{1.49}$$

where we have used eq(1.42), eq(1.45), eq(1.46) and non-relativistic energies $E_{\mathbf{k}} = \frac{\mathbf{k}^2}{2m}$ in $\delta(2E_{\mathbf{q}} - 2E_{\mathbf{k}})$. We define $\hat{S}_l$ to be

$$\hat{S}_{l'l}\ = \delta_{l'l} - 2imk\ \langle k|\hat{T}_{l'l}\ |k\rangle, \tag{1.50}$$

resulting in

$$\langle \mathbf{r}|\hat{S}|\mathbf{k}\rangle = \sum_{l',l=0}^{\infty} (2l+1) i^l j_l(kr) P_l(\hat{\mathbf{k}}\hat{\mathbf{r}})\ \hat{S}_{l'l}. \tag{1.51}$$

One can also show that $\hat{S}_{l'l}$ is unitary if we have elastic scattering. By using eq(1.48), eq(1.51) and setting $|\hat{S}_{ll}| = 1$ for all l, we obtain

$$\int_{-\infty}^{\infty} d^3r\ \langle \mathbf{p}|\hat{S}^\dagger|\mathbf{r}\rangle\langle \mathbf{r}|\hat{S}|\mathbf{k}\rangle = \int_{-\infty}^{\infty} d^3r\ \exp(i\mathbf{r}(\mathbf{k}-\mathbf{p})) = (2\pi)^3\delta(\mathbf{p}-\mathbf{k}). \tag{1.52}$$

From which we see that $|\hat{S}_{ll}| = 1$ for all l has given us the correct result.

For inelastic scattering we always have $|\hat{S}_l| \leq 1$, since the probability for elastic scattering can not be greater than 100%. Including intermediate inelastic processes in the potential, will yield a complex potential. The creations of other particles have to follow certain rules such as the nucleon number, total spin, isospin, momentum, energy and charge are all conserved in the process. These matters will be discussed later since we need the quantum field theory to explain creations of new particles.

1.3 Scattering amplitudes, phase shifts and inelasticities

The scattering process we look at, is a situation in which a particle is scattered from a local, stationary potential $V(\mathbf{r})$, which is the same situation we have in the center of mass system if two nucleons are interacting through a central potential. We can use the time independent Schrödinger equation eq(1.1) to solve the scattering caused by this potential. By using non-relativistic energies $E = \frac{k^2}{m}$, we can rewrite the Schrödinger equation as

$$(\nabla^2 + k^2)\psi(\mathbf{r}) = 2m\, V(\mathbf{r})\, \psi(\mathbf{r}), \tag{1.53}$$

where $\psi(\mathbf{r}) = \langle \mathbf{r}|\psi\rangle$ is the wave function. The behavior of the wave function is very complex near the scattering center. For larger r the potential grows weaker, and for an even larger r it can be neglected since the strong force has a short range. The Schrödinger equation for the NN system will therefore produce free particle solutions outside of the range of the strong force. The incoming particle is a plane wave and the outgoing/scattered particle is a radial wave. The total wave function is then

$$\psi(\mathbf{r}) = \psi_{in}(\mathbf{r}) + \psi_{out}(\mathbf{r}) \qquad for \quad r \to \infty, \tag{1.54}$$

where the the incoming plane wave is

$$\psi_{in}(\mathbf{r}) = \exp(i\mathbf{kr}). \tag{1.55}$$

For an elastic scattering the kinetic energy is conserved, and the scattered wave must have the same wave number $k = |\mathbf{k}|$ as the incoming wave.

$$\psi_{out}(\mathbf{r}) = f(\theta, \varphi)\frac{\exp(ikr)}{r}, \tag{1.56}$$

where $f(\theta, \varphi)$ describes the distribution in the different directions, and is known as the scattering amplitude. For large r we have

$$\psi(\mathbf{r}) = \exp(i\mathbf{kr}) + f(\theta, \varphi)\frac{\exp(ikr)}{r}. \tag{1.57}$$

From eq(1.4) we also have an expression of $\psi(\mathbf{r})$, given as

$$\langle \mathbf{r}|\psi^+_{\mathbf{k}}\rangle = \langle \mathbf{r}|\mathbf{k}\rangle + \int_{-\infty}^{\infty} d^3r'\, \langle \mathbf{r}|\hat{G}_0^{(+)}(E_{\mathbf{k}})|\mathbf{r}'\rangle\, V(\mathbf{r}')\, \langle \mathbf{r}'|\psi^+_{\mathbf{k}}\rangle, \tag{1.58}$$

where we need to know the Green function with respect to coordinate space. We have

$$\begin{aligned}
\langle \mathbf{r}|\hat{G}_0^{(+)}|\mathbf{r}'\rangle &= \int_{-\infty}^{\infty} \frac{d^3q}{(2\pi)^3}\,\langle \mathbf{r}|\frac{1}{E_{\mathbf{k}}-\hat{H}_0+i\epsilon}|\mathbf{q}\rangle\,\langle \mathbf{q}|\mathbf{r}'\rangle \\
&= \frac{4\pi m}{(2\pi)^3}\int_0^{\infty} dq\; q^2 \int_0^{\pi} d\theta\,\frac{\sin\theta}{k^2-q^2+i\epsilon}\,\exp(iq|\mathbf{r}-\mathbf{r}'|\cos\theta) \\
&= \frac{-4\pi mi}{(2\pi)^3|\mathbf{r}-\mathbf{r}'|}\int_0^{\infty} dq\frac{q}{k^2-q^2+i\epsilon}\left[\exp(iq|\mathbf{r}-\mathbf{r}'|)-\exp(-iq|\mathbf{r}-\mathbf{r}'|)\right] \\
&= \frac{-4\pi mi}{(2\pi)^3|\mathbf{r}-\mathbf{r}'|}\int_{-\infty}^{\infty} dq\frac{q}{k^2-q^2+i\epsilon}\,\exp(iq|\mathbf{r}-\mathbf{r}'|) \\
&= -\frac{m}{2\pi|\mathbf{r}-\mathbf{r}'|}\exp(ik|\mathbf{r}-\mathbf{r}'|), \qquad (1.59)
\end{aligned}$$

where we in the last step calculated the simple pole at $q=+\sqrt{2mE}=k$ in the integrand. If we use the approximation

$$k|\mathbf{r}-\mathbf{r}'| = k\sqrt{r^2-2\mathbf{r}\mathbf{r}'+r'^2} = kr - k\frac{\mathbf{r}\cdot\mathbf{r}'}{r}+\mathcal{O}(\frac{1}{r}) \qquad \text{for} \quad r\gg r' \qquad (1.60)$$

in eq(1.59), we can rewrite eq(1.58) as

$$\langle \mathbf{r}|\psi_{\mathbf{k}}^+\rangle \simeq \exp(i\mathbf{k}\mathbf{r}) - \frac{\exp(ikr)}{r}\,\frac{m}{2\pi}\int_{-\infty}^{\infty} d^3r'\,\exp\left(-ik\frac{\mathbf{r}\cdot\mathbf{r}'}{r}\right)V(\mathbf{r}')\,\langle \mathbf{r}'|\psi_{\mathbf{k}}^+\rangle. \qquad (1.61)$$

If we compare this with eq(1.57), we see that the scattering amplitude can be written as

$$\begin{aligned}
f(\theta,\varphi) &= -\frac{m}{2\pi}\int_{-\infty}^{\infty} d^3r'\,\exp\left(-ik\frac{\mathbf{r}\cdot\mathbf{r}'}{r}\right)V(\mathbf{r}')\,\langle \mathbf{r}'|\psi_{\mathbf{k}}^+\rangle \\
&= -\frac{m}{2\pi}\int_{-\infty}^{\infty} d^3r'\,\langle k\hat{\mathbf{r}}|\mathbf{r}'\rangle\langle \mathbf{r}'|\hat{V}|\psi_{\mathbf{k}}^+\rangle, \qquad (1.62)
\end{aligned}$$

or its relation to the T-matrix as

$$f(\theta,\varphi) = -\frac{m}{2\pi}\langle k\hat{\mathbf{r}}|\hat{T}|\mathbf{k}\rangle \qquad (1.63)$$

For a local potential one can write the wave function as

$$\psi(\mathbf{r},\theta,\varphi) = \sum_{l=0}^{\infty}\sum_{m'=-l}^{l} c_{lm'}R_l(r)Y_{lm'}(\theta,\varphi), \qquad (1.64)$$

where $Y_{lm'}$ are the spherical harmonics, $c_{lm'}$ are constants and $R_l(r)$ are radial functions satisfying the radial part of the Schrödinger equation

$$\frac{d^2}{r^2}(rR_l)+\left[k^2-2mV(\mathbf{r})-\frac{l(l+1)}{r^2}\right](rR_l)=0. \qquad (1.65)$$

If the z-axis is in the direction of the incoming particle, we will get axial symmetry when $m' = 0$. The spherical harmonics $Y_{lm'}(\theta, \varphi) \propto P_l^{|m'|} \cos\theta e^{im'\phi}$ can be written as Legendre polynomials $Y_{lm'}(\theta) \propto P_l(\cos\theta)$ and the wave function will be

$$\psi(\mathbf{r}, \theta) = \sum_{l=0}^{\infty} C_l R_l(r) P_l(\cos\theta), \tag{1.66}$$

where C_l are constants. The next step is to find an estimate for this partial wave expression of $\psi(\mathbf{r})$. Using the Schrödinger equation equation given in eq(1.53), and the large r limit where the potential can be neglected. Such a potential must be $V(r) \propto 1/r^n$, where $n \gg 1$. In this large r limit we have

$$(\nabla^2 + k^2)\psi(\mathbf{r}) = 0 \qquad for \quad r \to \infty. \tag{1.67}$$

This equation for elastic scattering has the general solution

$$\psi(\mathbf{r}) = c_l e^{\pm i(\mathbf{kr} + \delta_l)}, \tag{1.68}$$

where δ_l is known as the phase shift of the partial wave with orbital momentum l, and c_l is an arbitrary constant satisfying the relation $|c_l| = \eta_l \leq 1$. For elastic scattering the inelasticity $\eta_l = 1$. We note that only the outgoing spherical wave has a physical meaning. The incoming spherical wave can be interpreted as the part of the wave function lost through inelastic processes.

The incoming wave function is not influenced by the potential because of causality, and will therefore remain unchanged. The incoming wave function can be removed from the total wave function given in eq(1.68):

$$\psi(\mathbf{r}) - e^{i\mathbf{kr}} = c_l e^{i(\mathbf{kr} + \delta_l)} - e^{i\mathbf{kr}}. \tag{1.69}$$

This can be written in terms of partial waves as

$$\psi(\mathbf{r}) - e^{i\mathbf{kr}}\Big|_{r\to\infty} = \sum_{l=0}^{\infty} (2l+1)\; i^l \Big[c_l j_l(kr + \delta_l) - j_l(kr)\Big]\; P_l(\cos\theta)\Big|_{r\to\infty}. \tag{1.70}$$

In the asymptotic region where $r \to \infty$ the spherical Bessel function $j_l(kr)$ is found to be

$$j_l(kr)\Big|_{r\to\infty} = \frac{1}{kr} \sin\left(kr - \frac{\pi}{2} l\right). \tag{1.71}$$

We need to find the difference between the Bessel functions in eq(1.70):

$$\begin{aligned} c_l j_l(kr + \delta_l) - j_l(kr)\Big|_{r\to\infty} &= \frac{1}{kr}\left[c_l \sin\left(kr - \frac{\pi}{2} l + \delta_l\right) - \sin\left(kr - \frac{\pi}{2} l\right)\right] \\ &= \frac{1}{2ikr}\left[(c_l e^{\delta_l} - 1) e^{i(kr - \frac{\pi}{2} l)} - (c_l e^{-\delta_l} - 1) e^{-i(kr - \frac{\pi}{2} l)}\right] \\ &= \frac{1}{2i^{l+1} kr}\left[(c_l e^{\delta_l} - 1) e^{ikr} - (1 - c_l e^{-\delta_l}) e^{-ikr}\right]. \end{aligned} \tag{1.72}$$

The second term on the right-hand-side represents the incoming spherical wave, and is unphysical for elastic scattering. For inelastic scattering it can be related to the inelastic part of the wave function. Since we assumed that the outgoing wave function only was shifted compared to the incoming wave function, we also assumed that the particles were identical before and after the scattering. The incoming spherical wave can therefore be interpreted as the unknown inelastic part of the wave function, and we focus our interest in the elastic part. Note that the inelastic part of the wave function will be removed, in elastic scattering with $\eta_l = 1$, if we choose $c_l = \eta_l e^{i\delta_l}$. When inserting eq(1.72) in eq(1.70), we obtain

$$\psi(\mathbf{r}) - e^{i\mathbf{kr}}\Big|_{r\to\infty} = \frac{e^{ikr}}{2ikr}\sum_{l=0}^{\infty}(2l+1)(\eta_l e^{2\delta_l} - 1)P_l(\cos\theta) + \psi_{\text{inel}}(\mathbf{r}). \quad (1.73)$$

The inelastic wave function can then be removed from both sides. From the definition of the scattering amplitude eq(1.57) we obtain the elastic part $f_{\text{el}}(\theta) = f(\theta) - f_{\text{inel}}(\theta)$. The scattering amplitude is no longer dependent on φ because of the axial symmetry around the direction of the incoming particle

$$f_{\text{el}}(\theta) = \frac{1}{2ik}\sum_{l=0}^{\infty}(2l+1)(\eta_l e^{2i\delta_l} - 1)P_l(\cos\theta), \quad (1.74)$$

or alternatively by using $e^{2i\delta_l} - 1 = 2ie^{i\delta_l}\sin\delta_l$ for an elastic scattering, we get

$$f(\theta) = \frac{1}{k}\sum_{l=0}^{\infty}(2l+1)e^{i\delta_l}\ \sin\delta_l\ P_l(\cos\theta). \quad (1.75)$$

This is the partial wave expansion of the scattering amplitude. Note that the S-wave phase shifts can easily be extracted from the differential scattering measurements of $d\sigma/d\omega$ v.s. θ because they do not depend on θ. If we insert the relation for the elastic scattering amplitude from eq(1.74) in the expression of $\langle p|T_{l'l}|k\rangle$ found in eq(1.40), we obtain $T_{l'l}$ as a function of partial wave phase shifts and inelasticities:

$$\langle k|T_{l'l}|k\rangle = \frac{1}{2mik}\left[\delta_{l'l} - \eta_{l'l}e^{2i\delta_{l'l}}\right], \quad (1.76)$$

where we have not indicated that this expression of the T-matrix is only valid for elastic scattering

$$N + N \to N + N, \quad (1.77)$$

since it is a well known fact that phase shifts are meaningless for inelastic scattering, due to different wave numbers before and after scattering. The S-matrix is obtained by eliminating $T_{l'l}$ from eq(1.76) and eq(1.50), we have:

Uncoupled states

$$S_l = \eta_l\ e^{2i\delta_l}. \quad (1.78)$$

Coupled states

$$S_{l'l} = \begin{pmatrix} \eta_{ll}\ e^{2i\delta_{ll}} & \eta_{ll'}\ e^{2i\delta_{ll'}} \\ \eta_{l'l}\ e^{2i\delta_{l'l}} & \eta_{l'l'}\ e^{2i\delta_{l'l'}} \end{pmatrix}. \quad (1.79)$$

From the definition, both η_l and δ_l are always real.

1.4 Cross sections

The total cross section is defined as

$$\sigma_{\text{tot}} = \sigma_{\text{el}} + \sigma_{\text{inel}} = \int_0^{\pi} |f(\theta)|^2 2\pi \sin(\theta) d\theta. \tag{1.80}$$

In the center-of-mass system the elastic cross section is given as

$$\sigma_{\text{el}} = \frac{1}{k^2} \sum_{l=0}^{\infty} (2l+1)(\eta_l e^{2i\delta_l} - 1)^2 \tag{1.81}$$

and the inelastic cross section is given as

$$\sigma_{\text{inel}} = \frac{1}{k^2} \sum_{l=0}^{\infty} (2l+1)(1 - \eta_l^2). \tag{1.82}$$

Note that there has been done an angle average over the differential cross sections. Only the S-wave phase shifts will have an uniform cross section in all θ directions.

1.5 Interpretation of phase shifts and inelasticities

Phase shifts are very important for the understanding of the strong force. The phase shift δ is a result from the de Broglies postulate, which states that particles also behaves as waves. Particles have a wave length λ, called the de Broglie wavelength. The wave length is related to the particle's momentum k as

$$\lambda = \frac{2\pi\hbar}{k}, \tag{1.83}$$

where λ depends on the energy of the particle. A wave packet/(particle) in an external potential will therefore be in a different phase relative to the phase the particle would have been in without the potential. This is illustrated in fig 1.5, where we have an incoming partial wave packet expressed as $\sin(kr)$ and the outgoing wave packet as $\sin(kr + \delta)$ where δ is the phase shift.

The physical interpretation of δ can be divided into three regions

- $\delta > 0$ Attraction
- $\delta > 0$ Neither attraction nor repulsion
- $\delta > 0$ Repulsion

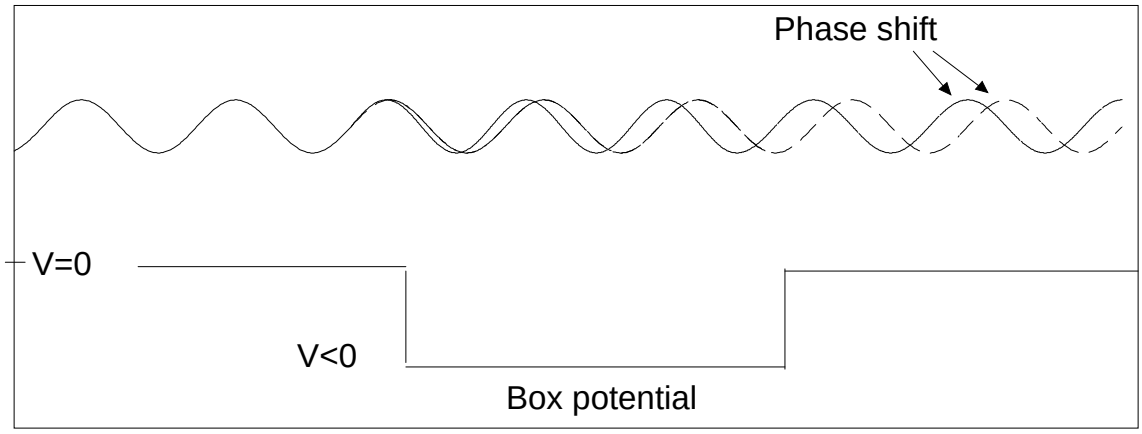

Figure 1.1: *An illustration phase shift. We see here how the wave function will be affected by an attractive box potential (solid line), when compared to the wave function without the potential (dashed line).*

However, the phase shift δ only refers to the average effects from the interactions. There can be both repulsion and attractions in this process, but the δ will tell us which one is the most important.

Since the potential created by strong force has a short range ($R \to 0$), we would expect that only partial waves with $l \leq kR$ are affected when the energy of the incoming particle goes to zero, i.e. the S-states where $l = 0$. The S-wave scattering amplitude can be found from eq(1.75) for forward scattering to yield

$$f_0 = \frac{1}{k} e^{i\delta_0} \sin\delta_0. \tag{1.84}$$

The cross section contribution from the S-state will be

$$\sigma_0 = \frac{4\pi}{k^2} \sin^2\delta_0. \tag{1.85}$$

Note that, for all the other partial waves will also $f \propto \sin\delta$. If the attractive potential is strong enough, the waves can be pulled in enough for a state to be bound. This is the case when $f = 0$, which we obtain when $\delta = \pi$. For a given potential this can only happen for an exact energy. We therefore observe discrete binding energies. Other potentials than the free NN interactions can have more bound states, according to Levinson's theorem, when the phase shift is $\delta = n\pi$, where "n" is a positive integer. The number of bound states will depend on the strength and range of the potential. For example the long range potential like the Coulomb force, turns out to have infinite bound states as the incoming particle energy goes to zero.

Phase shifts can not be obtained directly from experiments, but can be calculated from observables in NN scattering. The most important observables are differential cross sections and spin polarizations. From these experimental data one can calculate the NN scattering amplitudes and cross-sections.

The physical meaning of the inelasticity $|\eta|^2$ can be interpreted as the probability of having elastic scattering, i.e. eq(1.77). All the other processes where particles are created, are inelastic. The most important inelastic process in NN scattering is

$$N + N \to N + N + \pi. \tag{1.86}$$

The definition of inelasticity η does not contain any information about the relation between all the inelastic processes. e.g., the probability of creating two free pions in the scattering. These inelastic processes are easy to detect experimentally, and give us information about the different interactions between particles involved in the scattering. From this information one can make models for these inelastic interactions. e.g. one can calculate coupling constants, if one has a valid interaction Lagrangian for the interaction between the particles.

The T-matrix can include intermediate inelastic states as long as the total scattering is elastic. The S-matrix for such a system can be found by solving a coupled T-matrix system, where also the inelastic T-matrices are important for the elastic T-matrix. One can alternatively include a complex box-diagram potentials, which include inelastic intermediate states. Inelasticity is entering the scattering at about 300 MeV in the lab system, where the lightest π-mesons can be created.

1.6 Coupled channels

In a NN scattering process, we have conservation of energy, total spin, charge, barion number and the three components of momentum. However, also the Pauli principle and CPT invariance will be important for the system.

CPT invariance states that the total wave function squared is unchanged if all the particles are changed with their antiparticles; C (charge conjugation), the space coordinates are reflected; P (parity) and the time is reversed; T. The wave functions yields

$$|\psi(q_1, q_2, t, \mathbf{r}_1, \mathbf{r}_2)| = |\psi(-q_1, -q_2, -t, -\mathbf{r}_1, -\mathbf{r}_2)|. \tag{1.87}$$

This symmetry/antisymmetry can be rewritten as

$$|\psi(S, L)| = |\psi(-S, -L)|, \tag{1.88}$$

where S is the total spin (intrinsic) and L is the total orbital momentum. These wave functions can be separated into two orthogonal wave functions since S and L are independent.

The weak force and the Coulomb force can be neglected in the regime where the strong force is present. Since parity conservation only can be violated in week interactions, this approximation leads to conservation of parity P.

Another approximation often used in NN interaction models, is charge independence. Here "charge" refers to the character of the nucleon (proton or neutron) and

not to electrical charge. In the absence of the coulomb force the EM-self energy connected to the quarks electrical charge will disappear. The strong force independence will similarly remove the self energy of the quarks created by the strong force. The small mass differences in the u and d quarks, created from Coulomb and strong forces, will disappear in this approximation, i.e. $m_q = m_d$. Noether's theorem tells us that this new symmetry is equivalent with a new conserved quantity. Namely, the total isospin (T) conservation in the NN system. From this symmetry one can group the different Hadrons into isospin multiplets of T. The proton and neutron are treated as two different states of a single particle (the nucleon) from the $T = 1/2$ group. The projection T_3 is related to the particles charge. The proton has $T_3 = 1/2$ and the neutron has $T_3 = -1/2$. A NN system of pp or nn will be isovector states ($T = 1$) since the projection will be respectively $T_3 = 1$ and $T_3 = -1$, while the $T_3 = 0$ for the np states can have both $T = 0$ and $T = 1$.

The isospin symmetry must also be included in the wave function, and the nucleons are regarded as identical particles with regard to Pauli exclusion principle.

$$\psi(L, S, T) = \varphi(L)\chi(S)\phi(T). \tag{1.89}$$

These parts of the wave function include the symmetries

$$\psi(L) = (-1)^L\psi(-L), \quad \chi(S) = (-1)^{S+1}\psi(-S) \quad \text{and} \quad \phi(T) = (-1)^{T+1}\phi(-T). \tag{1.90}$$

The Pauli principle states that: Because the nucleons are fermions, the total wave function has to be antisymmetric for two nucleons. For two-nucleon scattering we have

$$-1 = (-1)^L(-1)^S(-1)^T \tag{1.91}$$

From parity conservation, the $(-1)^L$ term can not change. The total spin J is also conserved in the process, and is defined as $\vec{J} = \vec{L} + \vec{S}$. For NN scattering we have $S = 0, 1$. If we use normal spin addition rules, we find L from S and J as follows:

$$L = S, \qquad J = 0 \quad \text{for} \quad S = 0, 1 \tag{1.92}$$

$$L = J \pm S, \quad J \geq 1 \quad \text{for} \quad S = 1 \tag{1.93}$$

$$L = J, \qquad J \geq 1 \quad \text{for} \quad S = 0, 1 \tag{1.94}$$

If we use these relations in eq(1.91), we find the allowed isospin in the different partial waves. The results for the first partial states are shown in table 1.1, where the states are written in $^{2S+1}\mathrm{L_J}$ formalism. Table 1.1 contains one coupled channel, which is the $^3\mathrm{S}_1$ - $^3\mathrm{D}_1$ state. The coupled channels are results from parity conservation and eq(1.93), where transition between states with different orbital momentum are allowed. Note that the Pauli principle does not prevent the possibility of the isoscalar np states, only the isovector nn, np and pp states.

States	$^1S_0$	$^1P_1$	$^1D_2$	$^3S_1$ - $^3D_1$	$^3P_0$	$^3P_1$
Parity $(-1)^L$	+	−	+	+	−	−
Spin interchange $(-1)^S$	+	+	+	−	−	−
Isospin $(-1)^T$	1	0	1	0	1	1
Allowed NN states	nn np pp	− np −	nn np pp	− np −	nn np pp	nn np pp

Table 1.1: Some of the allowed partial wave states for NN-scattering. The first coupled channel state ($^3S_1$ - $^3D_1$) is also included.

From observations of the coupled system deuteron, we know that L can change under the exchange of virtual mesons. The deuteron and other unbound states, where two states with different orbital momentum can interfere with each other, are known as coupled channels. The first mixed state is the $^3S_1 - {}^3D_1$ state. This is a bound isoscalar np state, and it is the only bound NN system. From the magnetic dipole moment of the deuteron one can calculate that the mixed state contains only about 4% of $^3D_1$. This is done in [7].

For a given total spin S state, the general T-matrix in partial waves is defined as

$$\begin{aligned}\langle mn|T^{JS}|ij\rangle &= \langle \mathbf{p}SM'_S|T(\omega)|\mathbf{k}SM_S\rangle \\ &= \frac{(4\pi)^2}{\Omega}\sum_{ll'mJ} Y^*_{lm}(\hat{\mathbf{k}})Y_{l'm'}(\hat{\mathbf{p}})\langle l'm'SM'_S|JM\rangle\langle lmSM_S|JM\rangle \\ &\qquad \times T^{\alpha}_{l'l}(p,k;\omega), \end{aligned} \tag{1.95}$$

where ω is the on-shell energy and we have used the short-hand notation

$$T^{\alpha}_{l'l}(p,k;\omega) \equiv \langle k'l'STJM|T(\omega)|klSTJM\rangle. \tag{1.96}$$

Here, α represent the quantum numbers S, T and J with projection M. For given S and J, T-matrix can now be determined by the coupled channel equation

$$T^{JS}_{l'l}(p,k;\omega) = V^{JS}_{l'l}(p,k) + \frac{2}{\pi}\sum_{l''}\int q^2 dq V^{JS}_{l'l''}(p,q)\frac{1}{\omega - E(q) + i\varepsilon}T^{JS}_{l''l}(q,k;\omega), \tag{1.97}$$

where $E(q)$ is the kinetic energy in the intermediate state. If we use non relativistic energies $\omega = \frac{k^2}{m}$, the partial wave expansion of the Lippmann-Schwinger equation can be rewritten as:

Spin singlet

$$\hat{T}^{J0}_{J,J}(p,k) = \hat{V}^{J0}_{J,J}(p,k) + \frac{2m}{\pi}\int_0^\infty dq\, q^2\, \frac{1}{k^2 - q^2 + i\epsilon}\hat{V}^{J0}_{J,J}(p,q)\hat{T}^{J0}_{J,J}(q,k). \tag{1.98}$$

Uncoupled spin triplet

$$\hat{T}^{J1}_{J,J}(p,k) = \hat{V}^{J1}_{J,J}(p,k) + \frac{2m}{\pi}\int_0^\infty dq\, q^2\, \frac{1}{k^2 - q^2 + i\epsilon}\hat{V}^{J1}_{J,J}(p,q)\hat{T}^{J1}_{J,J}(q,k). \tag{1.99}$$

Coupled triplet states

$$\hat{T}^{J1}_{++}(p,k) = \hat{V}^{J1}_{++}(p,k) + \frac{2m}{\pi}\int_0^\infty dq\, q^2 \frac{1}{k^2-q^2+i\epsilon}\big[\hat{V}^{J1}_{++}(p,q)\hat{T}^{J1}_{++}(q,k) + \hat{V}^{J1}_{+-}(p,q)\hat{T}^{J1}_{-+}(q,k)\big], \tag{1.100}$$

$$\hat{T}^{J1}_{--}(p,k) = \hat{V}^{J1}_{--}(p,k) + \frac{2m}{\pi}\int_0^\infty dq\, q^2 \frac{1}{k^2-q^2+i\epsilon}\big[\hat{V}^{J1}_{--}(p,q)\hat{T}^{J1}_{--}(q,k) + \hat{V}^{J1}_{-+}(p,q)\hat{T}^{J1}_{+-}(q,k)\big], \tag{1.101}$$

$$\hat{T}^{J1}_{+-}(p,k) = \hat{V}^{J1}_{+-}(p,k) + \frac{2m}{\pi}\int_0^\infty dq\, q^2 \frac{1}{k^2-q^2+i\epsilon}\big[\hat{V}^{J1}_{++}(p,q)\hat{T}^{J1}_{+-}(q,k) + \hat{V}^{J1}_{+-}(p,q)\hat{T}^{J1}_{--}(q,k)\big], \tag{1.102}$$

$$\hat{T}^{J1}_{-+}(p,k) = \hat{V}^{J1}_{-+}(p,k) + \frac{2m}{\pi}\int_0^\infty dq\, q^2 \frac{1}{k^2-q^2+i\epsilon}\big[\hat{V}^{J1}_{-+}(p,q)\hat{T}^{J1}_{++}(q,k) + \hat{V}^{J1}_{--}(p,q)\hat{T}^{J1}_{-+}(q,k)\big], \tag{1.103}$$

where we have introduced the abbreviations $\hat{T}^{J1}_{++} = \hat{T}^{J1}_{J+1,J+1}$, $\hat{T}^{J1}_{+-} = \hat{T}^{J1}_{J+1,J-1}$, $\hat{T}^{J1}_{-+} = \hat{T}^{J1}_{J-1,J+1}$, and $\hat{T}^{J1}_{--} = \hat{T}^{J1}_{J-1,J-1}$. In a non-relativistic consideration, it is the tensor force that couples triplet states with $L = J \pm 1$.

To describe the S-matrix in a system where states with different orbital momentum are coupled, we need the 2×2 matrix from eq(1.79). However, these four S-matrix elements are not independent. Since it is convenient to work with as few parameters as possible, we choose to diagonalize the S-matrix with an unitary rotation. We are then left with the diagonal elements $S'_{ll} = \eta_l\, e^{2i\delta_l}$ and $S'_{l'l'} = \eta_{l'}\, e^{2i\delta_{l'}}$. In order not to loose information about the original S-matrix, we need a new parameter that contains the information about the rotation. There are many possible unitary rotations which will diagonalize the S-matrix, but only two are used in nuclear physics. We will get back to those later, but first we need to define the 2×2 potential.

$$\langle l|\hat{V}^{J1}(p,k)|l'\rangle = \begin{pmatrix} \langle J+1|\hat{V}^{J1}(p,k)|J+1\rangle & \langle J+1|\hat{V}^{J1}(p,k)|J-1\rangle \\ \langle J-1|\hat{V}^{J1}(p,k)|J+1\rangle & \langle J-1|\hat{V}^{J1}(p,k)|J-1\rangle \end{pmatrix}, \tag{1.104}$$

where we have simplified the notation by using the $\hat{V}^{JS}$ formalism. Similarly the coupled S-matrix be

$$\langle l|\hat{S}^{J1}(\omega)\ |l'\rangle = \begin{pmatrix} \langle J+1|\hat{S}^{J1}(\omega)\ |J+1\rangle & \langle J+1|\hat{S}^{J1}(\omega)\ |J-1\rangle \\ \langle J-1|\hat{S}^{J1}(\omega)\ |J+1\rangle & \langle J-1|\hat{S}^{J1}(\omega)\ |J-1\rangle \end{pmatrix}. \tag{1.105}$$

This S-matrix can be parameterized into the "bar" (also called "Stapp" formalism [9]). Introducing the special "bar" mixing parameter $\bar{\varepsilon}$ and using the transformation

$$\langle l|\hat{S}^{J1}(\omega)\ |l'\rangle = \begin{pmatrix} e^{i\beta_+} & 0 \\ 0 & -e^{i\beta_-} \end{pmatrix} \begin{pmatrix} \cos 2\bar{\varepsilon}^{J1} & i\sin 2\bar{\varepsilon}^{J1} \\ i\sin 2\bar{\varepsilon}^{J1} & \cos 2\bar{\varepsilon}^{J1} \end{pmatrix} \begin{pmatrix} e^{i\beta_+} & 0 \\ 0 & -e^{i\beta_-} \end{pmatrix}, \tag{1.106}$$

where $e^{i\beta_\pm} = \sqrt{\bar{\eta}_\pm^{J1}} e^{i\bar{\delta}_\pm^{J1}}$ and $\pm$ denotes $J \pm 1$. From this equation we can evaluate the "bar" phase shifts and inelasticities. This leads to

$$\bar{\varepsilon}^J = \frac{1}{2}\arctan \frac{-i(\langle J+1|\hat{S}^{J1}|J-1\rangle + \langle J-1|\hat{S}^{J1}|J+1\rangle)}{\sqrt{\langle J+1|\hat{S}^{J1}|J+1\rangle\langle J-1|\hat{S}^{J1}|J-1\rangle}}, \tag{1.107}$$

$$\bar{\delta}_\pm^J = \frac{1}{2}\arctan \frac{\mathcal{I}m\{\langle J\pm 1|\hat{S}^{J1}|J\pm 1\rangle/\cos 2\bar{\varepsilon}^J\}}{\mathcal{R}e\{\langle J\pm 1|\hat{S}^{J1}|J\pm 1\rangle/\cos 2\bar{\varepsilon}^J\}} \tag{1.108}$$

and

$$\bar{\eta}_\pm^J = \left|\langle J\pm 1|\hat{S}^{J1}|J\pm 1\rangle/\cos 2\bar{\varepsilon}^J\right|. \tag{1.109}$$

These parameters are related to new parameters from the "Blatt-Biedenharn"-formalism, which is also a commonly used convention. Both formalisms are used in my program.

The Blatt-Biedenharn scattering parameters are defined (see [8]) as

$$\langle l|\hat{S}^{J1}\ |l'\rangle == U^{-1} \begin{pmatrix} \eta_+ e^{2i\delta_+} & 0 \\ 0 & \eta_- e^{2i\delta_-} \end{pmatrix} U, \tag{1.110}$$

with

$$U = \begin{pmatrix} \cos\varepsilon & \sin\varepsilon \\ -\sin\varepsilon & \cos\varepsilon \end{pmatrix}. \tag{1.111}$$

The Blatt-Biedenharn parameters can be calculated from this equation by diagonalizing S^{J1} in eq(1.110)

$$U\langle l|\hat{S}^{J1}\ |l'\rangle U^{-1} = \begin{pmatrix} S_+ & 0 \\ 0 & S_- \end{pmatrix}. \tag{1.112}$$

The following calculations are lengthy, but straight forward. From the off-diagonal elements of the S-matrix, one obtains the mixing parameter

$$\varepsilon^J = \frac{1}{2}\arctan\left(\frac{S_{+-}^{J1} + S_{-+}^{J1}}{S_{++}^{J1} - S_{--}^{J1}}\right). \tag{1.113}$$

From the diagonal elements one also obtains the phase shifts

$$\delta_\pm^J = \frac{1}{2}\arctan\left(\frac{2\mathcal{R}e\{S_\pm\}}{1 - 2\mathcal{I}m\{S_\pm\}}\right) \tag{1.114}$$

and inelasticities

$$\eta_\pm^J = \sqrt{1 + 4\Big[\big(\mathcal{R}e\{S_\pm\}\big)^2 + \big(\mathcal{I}m\{S_\pm\}\big)^2 - \mathcal{I}m\{S_\pm\}\Big]}, \tag{1.115}$$

where

$$S_{\pm} = \frac{1}{4i}\left(S^{J1}_{++} - S^{J1}_{--} - 2 \mp i\sqrt{(S^{J1}_{++} - S^{J1}_{--})^2 + 4S^{J1}_{+-}S^{J1}_{-+}}\right). \tag{1.116}$$

If the potential is real, i.e. elastic scattering, then the Blatt-Biedenharn parameters are related to the *Stapp/bar* parameters as

$$\bar{\delta^J}_+ + \bar{\delta^J}_- = \delta^J_+ + \delta^J_-, \tag{1.117}$$

$$\sin(\bar{\delta}^J_- - \bar{\delta}^J_+) = \tan 2\bar{\varepsilon}^J / \tan 2\varepsilon^J, \tag{1.118}$$

$$\sin(\delta^J_- - \delta^J_+) = \tan 2\bar{\varepsilon}^J / \tan 2\varepsilon^J. \tag{1.119}$$

1.7 The optical theorem

In eq(1.30) we found that

$$2\,\mathcal{I}m\{\hat{T}\} = \hat{T} - \hat{T}^\dagger = -2\pi\hat{T}^\dagger\delta(E - \hat{H}_0)\hat{T}, \tag{1.120}$$

where we have used energies in the laboratory system for the delta function. If we take the matrix element of this equation, we get

$$\langle p|\hat{T}|k\rangle - \langle k|\hat{T}|p\rangle^\dagger = -\frac{2\pi m}{(2\pi)^3}\int_{-\infty}^{\infty} d^3q\langle k|\hat{T}|q\rangle^\dagger\langle q|\hat{T}|k\rangle\delta(k-q). \tag{1.121}$$

We can therefore rewrite eq(1.120) as

$$\mathcal{I}m\{\langle \mathbf{k}|\hat{T}|\mathbf{k}\rangle\} = -\pi mk|\langle \mathbf{k}|\hat{T}|\mathbf{k}\rangle|^2, \tag{1.122}$$

or in partial waves, we have

$$\mathcal{I}m\{\langle k|\hat{T}_{l'l}|k\rangle\} = -2mk|\langle k|\hat{T}_{l'l}|k\rangle|^2. \tag{1.123}$$

If we use the relation between scattering amplitude f and the T-matrix given in eq(1.63), the total cross section σ for the special case of forward scattering is found to be:

$$\sigma = \int d\Omega|f(\theta)|^2 = \frac{4\pi}{k}\mathcal{I}m\{f(0)\}. \tag{1.124}$$

This is known as the optical theorem, and it relates the scattering cross section to the imaginary part of the scattering amplitude in the forward direction of the laboratory system.

Since we will mostly work in the center of mass system we note that eq(1.120) together with the center of mass delta function $\delta(2E_k - 2E_q)$ can be rewritten as

$$\mathcal{I}m\{\langle k|\hat{T}_{l'l}|k\rangle\} = -mk|\langle k|\hat{T}_{l'l}|k\rangle|^2. \tag{1.125}$$

Note that, in elastic scattering $\mathcal{I}m\{\langle k|\hat{T}_{l'l}|k\rangle\}$ is given by $\mathcal{R}e\{\langle k|\hat{T}_{l'l}|k\rangle\}$. This shows that all the information contained in the complex T-matrix, can be expressed in terms of a real matrix.

1.8 Relativistic approaches for the S- and T-matrix

So far we have only considered non-relativistic scattering. For relativistic scattering [17] the on shell scattering amplitude can be written as

$$f_{rel}(\theta) = \frac{E}{m} f_{class}(\theta) = \frac{E}{km} \sum_{l=0}^{\infty} (2l+1) e^{i\delta_l} \sin\delta_l \, P_l(\cos\theta), \tag{1.126}$$

where E is the on-shell energy in the center of mass system. From eq(1.63) the non-relativistic T-matrix is given as

$$\langle p|T_{l'l}|k\rangle = -\frac{m}{2\pi} f_{class}(\theta). \tag{1.127}$$

A new relativistic transition operator will have the same relation to the relativistic scattering amplitude. This invariant on-shell T-matrix is defined as

$$\langle p|\mathcal{T}_{l'l}|k\rangle \equiv -\frac{m}{2\pi} f_{rel}(\theta). \tag{1.128}$$

The relation between the non-relativistic and the relativistic T-matrix is then for the on-shell case

$$\langle \mathbf{p}|T|\mathbf{k}\rangle = \frac{m}{E_p} \langle \mathbf{p}|\mathcal{T}|\mathbf{k}\rangle. \tag{1.129}$$

This modified T-matrix can then be used in the Lippmann-Schwinger equation.

There are, however, many different possible Lippmann-Schwinger equations, corresponding to different Green operators. The two most commonly used Lippmann-Schwinger equations in the center of mass system for NN scattering are the non-relativistic

$$\hat{G}_0^{\pm}(E_k) = \frac{m}{k^2 + 2\hat{H} \pm i\epsilon}, \tag{1.130}$$

where $\hat{H}|\mathbf{k}\rangle = \frac{k^2}{2m}|\mathbf{k}\rangle$, and the relativistic

$$\hat{G}_0^{\pm}(E_k) = \frac{m}{2\sqrt{k^2+m^2} + 2\hat{H}' \pm i\epsilon}, \tag{1.131}$$

where $\hat{H}'|\mathbf{k}\rangle = \sqrt{k^2+m^2}|\mathbf{k}\rangle$.

Both of these approaches have their advantages and disadvantages. Relativistic energies in the propagator can not be transformed exactly from momentum space to coordinate space, because of the square root in the propagator. This method has been recommended by Thompson. Models where one can work in both momentum space and coordinate space are often preferred when potentials from the NN interactions are made. The non-relativistic Green operator will give such a system, since the Green operator can be Fourier transformed exactly. This is known as the Blankenbecler-Suger method, and will have the disadvantage of non-relativistic energies in the propagator.

1.8.1 The Blankenbecler-Suger equation

The relativistic T-matrix can also be substituted in the S-matrix eq(1.21). With non-relativistic energies in the propagator we have

$$\langle \mathbf{p}|\hat{S}|\mathbf{k}\rangle = \langle \mathbf{p}|\mathbf{k}\rangle - 2\pi i\delta(2\frac{k^2}{2m} - 2\frac{p^2}{2m})\frac{m}{E_k}\langle \mathbf{p}|\mathcal{T}|\mathbf{k}\rangle, \tag{1.132}$$

where $E = \frac{k^2}{2m}|\mathbf{k}\rangle$.

The Lippmann-Schwinger equation from eq(1.33) can be found with respect to the invariant $\mathcal{T}$ by inserting the relation found in eq(1.129). We have

$$\langle \mathbf{p}|\hat{\mathcal{T}}(E)|\mathbf{k}\rangle = \langle \mathbf{p}|\bar{V}|\mathbf{k}\rangle + \frac{1}{(2\pi)^3}\int_{-\infty}^{\infty} d^3q\ \frac{m^2}{E_q}\langle \mathbf{p}|\bar{V}|\mathbf{q}\rangle\frac{1}{\mathbf{k}^2 - \mathbf{q}^2 + i\epsilon}\ \langle \mathbf{q}|\hat{\mathcal{T}}(E)\ |\mathbf{k}\rangle, \tag{1.133}$$

which is known as the Blankenbecler-Sugar equation. The potential $\langle \mathbf{p}|\bar{V}|\mathbf{k}\rangle$ can be derived from field theory by using a special three-dimensional reduction of the Bethe-Salpeter equation.

Most potentials are redefined so the Blankenbecler-Sugar equation will be identical to the non-relativistic Lippmann-Schwinger equation. This method is known as minimal relativity. The new potential will be defined as

$$\langle \mathbf{p}|\hat{V}|\mathbf{k}\rangle = \frac{m}{\sqrt{E_pE_k}}\langle \mathbf{p}|\bar{V}|\mathbf{k}\rangle, \tag{1.134}$$

and the new T-matrix related to this potential will be

$$\langle \mathbf{p}|\hat{T}|\mathbf{k}\rangle = \frac{m}{\sqrt{E_pE_k}}\langle \mathbf{p}|\hat{\mathcal{T}}|\mathbf{k}\rangle. \tag{1.135}$$

Using these definitions, the partial wave version of the "minimal relativity" equation, will be the same as for the non-relativistic Lippmann-Schwinger equation found in eq(1.47):

$$\begin{aligned}\langle p|\hat{T}_{l'l}(E_k)|k\rangle &= \langle p|\hat{V}_{l'l}|k\rangle + \frac{2m}{\pi}\sum_{l''}\Bigg[\mathcal{P}\int_0^{\infty} dq\ q^2\langle p|\hat{V}_{l'l''}|q\rangle\frac{1}{k^2-q^2}\langle q|\hat{T}_{l''l}(E_k)\ |k\rangle \\ &\quad -ikm\langle p|\hat{V_{l'l''}}|k\rangle\ \langle k|\hat{T}_{l''l}(E_k)\ |k\rangle\Bigg].\end{aligned} \tag{1.136}$$

The S-operator in partial wave decomposition from eq(1.50), obtained from a non-relativistic energies, is

$$\hat{S}_{l'l} = \delta_{l'l} - 2imk\ \langle k|\hat{T}_{l'l}\ |k\rangle, \tag{1.137}$$

where we used the relation

$$\delta(2\frac{k^2}{2m} - 2\frac{p^2}{2m}) = \frac{m}{2k}\delta(k-p). \tag{1.138}$$

1.8.2 The Thompson equation

We derive the Thompson equation [13] in almost the same way as we did for the Blankenbecler-Sugar equation. We use a three-dimensional reduction of the Bethe-Salpeter equation [11] to find the invariant T-matrix, which can be redefined to yield the Lippmann-Schwinger equation with a relativistic propagator. The Thompson equation is

$$\langle \mathbf{p}|\hat{\mathcal{T}}'(E)|\mathbf{k}\rangle = \langle \mathbf{p}|\bar{V}|\mathbf{k}\rangle + \frac{1}{(2\pi)^3}\int_{-\infty}^{\infty} d^3q\ \frac{m^2}{2E_q^2}\langle \mathbf{p}|\bar{V}|\mathbf{q}\rangle \frac{1}{E_k - E_q + i\epsilon}\ \langle \mathbf{q}|\hat{\mathcal{T}}'(E)\ |\mathbf{k}\rangle. \tag{1.139}$$

The invariant T-matrix, $\mathcal{T}'$, is related to the S-matrix by

$$\langle \mathbf{p}|\hat{S}|\mathbf{k}\rangle = \langle \mathbf{p}|\mathbf{k}\rangle - 2\pi i\delta(2E_p - 2E_k)\frac{m}{E_k}\langle \mathbf{p}|\mathcal{T}'|\mathbf{k}\rangle, \tag{1.140}$$

where $E_q = \sqrt{q^2+m^2}$. Just like we got the "minimal relativity" equation, by redefining the potential in the Blankenbecler-Sugar equation, we get its Thompson version, which is just the Lippmann-Schwinger equation with relativistic energies in the propagator. This is achieved if we define

$$\langle \mathbf{p}|T|\mathbf{k}\rangle = \frac{m^2}{E_pE_k}\langle \mathbf{p}|\mathcal{T}'|\mathbf{k}\rangle \tag{1.141}$$

and

$$\langle \mathbf{p}|\bar{V}|\mathbf{k}\rangle = \frac{E_pE_k}{m^2}\langle \mathbf{p}|\hat{V}|\mathbf{k}\rangle. \tag{1.142}$$

Eq(1.139) will with these new definitions be

$$\langle \mathbf{p}|\hat{T}(E)|\mathbf{k}\rangle = \langle \mathbf{p}|\hat{V}|\mathbf{k}\rangle + \frac{1}{(2\pi)^3}\int_{-\infty}^{\infty} d^3q\ \langle \mathbf{p}|\hat{V}|\mathbf{q}\rangle \frac{1}{2E_k - 2E_q + i\epsilon}\ \langle \mathbf{q}|\hat{T}(E)\ |\mathbf{k}\rangle. \tag{1.143}$$

The Green function can be rewritten using the relation

$$\frac{1}{2(E_k - E_q)} = \frac{E_k + E_q}{2(k^2 - q^2)}. \tag{1.144}$$

The partial wave decomposition of this T-matrix is

$$\begin{aligned}\langle p|\hat{T}_{l'l}(E_k)|k\rangle \;=\; & \langle p|\hat{V}_{l'l}|k\rangle + \frac{2}{\pi}\sum_{l''}\left[\mathcal{P}\int_0^{\infty} dq\ \langle p|\hat{V}_{l'l''}|q\rangle\ \frac{q^2(E_k+E_q)}{2(k^2-q^2)}\ \langle q|\hat{T}_{l''l}(E_k)\ |k\rangle\right. \\ & \left. -ikE_k\langle p|\hat{V_{l'l''}}|k\rangle\ \langle k|\hat{T}_{l''l}(E_k)\ |k\rangle\right].\end{aligned} \tag{1.145}$$

The corresponding S-matrix, $S_{l'l}$, can be found from eq(1.49)

$$\hat{S}_{l'l} \;= \delta_{l'l} - 2ikE_k\delta_{l'l}\langle k|\hat{T}_{l'l}\ |k\rangle, \tag{1.146}$$

where relativistic energies in the delta function

$$\delta(2\sqrt{k^2+m^2}-2\sqrt{p^2+m^2}) = \frac{E_k}{2k}\delta(k-p) \tag{1.147}$$

have been used.

The Thompson equation looks like the Lippmann-Schwinger equation, where all the classical energies have been replaced with relativistic energies in the propagator. Since relativistic theory is used everywhere in the Thompson equation, one might be tempted to think that this relativistic equation would be exact. This is not the case, because there have already been approximations done in deriving the equation for $\mathcal{T}$ from Bethe-Salpeter equation. It can also be noted that it is impossible to go from the Thompson equation to the Blankenbecler-Sugar equation by redefining new potentials and T-matrices. One should therefore not be surprised to see, in these two cases, that the parameters in the two methods are fitted differently to the experimental data [1].

1.9 The Bethe-Salpeter equation

From field theory we find that the NN scattering is described covariantly by

$$\mathcal{M} = \mathcal{V} + \mathcal{V}\mathcal{G}\mathcal{M}, \tag{1.148}$$

which is known as the Bethe-Salpeter equation [11] in operator notation. $\mathcal{M}$ is the invariant amplitude, $\mathcal{V}$ is the sum of all connected two-particle irreducible diagrams and $\mathcal{G}$ is the relativistic two-particle propagator. The $\mathcal{V}, \mathcal{G}$ and $\mathcal{M}$ are operators in spinor space, and they will therefore be 16×16 matrices. As this four dimensional integral equation is very difficult to solve [30], three dimensional reductions have been proposed for numerically calculations.

To make the $\mathcal{V}$ easier to work with, one often do a ladder approximation, which is the fundamental philosophy in OBE-models, since the NN interactions will then only depend on the one-meson exchanges between the nucleons. Furthermore, it has been shown by Gross [31] that the full Bethe-Salpeter equation in ladder approximation does not generate the desired one-body equation in the one-body limit, (i.e., when one of the particles becomes very massive) in contrast to a large family of three-dimensional quasi-potential equations. The Bethe-Salpeter integral equation has four dimensions, i.e. four variables which arrives from the four-momentum $k = (k_0, \mathbf{k})$. The integral version of the Bethe-Salpeter equation is

$$\mathcal{M}(p,k|P) = \mathcal{V}(p,k|P) + \int d^4q \quad \mathcal{V}(p,q|P)\mathcal{G}(q|P)\mathcal{M}(q,k|P) \tag{1.149}$$

with

$$\begin{aligned}\mathcal{G}(q|P) &= \frac{i}{(2\pi)^4}\frac{1}{(\frac{1}{2}\not{P}+\not{q}-m+i\epsilon)^{(1)}}\frac{1}{(\frac{1}{2}\not{P}+\not{q}-m+i\epsilon)^{(2)}} \\ &= \frac{i}{(2\pi)^4}\left(\frac{\frac{1}{2}\not{P}+\not{q}+m}{(\frac{1}{2}P+q)^2-m^2+i\epsilon}\right)^{(1)}\left(\frac{\frac{1}{2}\not{P}+\not{q}+m}{(\frac{1}{2}P-q)^2-m^2+i\epsilon}\right)^{(2)},\end{aligned} \tag{1.150}$$

where k, q and p are the initial, intermediate and final relative four momenta. The superscripts refers to nucleon (1) and (2), and m is the nucleon mass. We also used the notation $\not{k} = \gamma^\mu k_\mu$. The total four momenta $P = (P_0, \mathbf{P})$ and the total energy $\sqrt{s}$, will be $P = (\sqrt{s}, 0)$ and $\sqrt{s} = 2E_q = 2\sqrt{\mathbf{q}^2 + m^2}$ in the center of mass system.

The first step in the three-dimensional reduction is to rewrite eq(1.148) as

$$\mathcal{M} = \mathcal{V} + \mathcal{V} g \mathcal{M} + \mathcal{V}(\mathcal{G} - g)\mathcal{M}, \tag{1.151}$$

where g is a three-dimensional propagator with the same elastic unitarity cut as $\mathcal{G}$. It is common, for the derivation of all three-dimensional reductions, that the time component of the relative momentum is fixed in some covariant way, so that the time no longer appears as an independent variable in the propagator. Eq(1.151) can be divided into two coupled equations, if g is chosen to cancel the last term on the right-hand-side. We will choose a g that has an unitary S-matrix for elastic NN scattering. This can be done if g has the same imaginary part as $\mathcal{G}$. By this definition of g we will still have the same relation between the invariant amplitude $\mathcal{M}$ and the scattering operator $\hat{S}$. There is an infinite number of choices for g satisfying these restrictions. One commonly used family of g with these properties is

$$\begin{aligned} g(q,s) = & -\frac{1}{(2\pi)^3}\int_{4m^2}^{\infty}\frac{ds' f(s',s)}{s'-s-i\epsilon}\delta^{(+)}\big[\frac{1}{2}(P'+q)^2 - m^2\big]\delta^{(+)}\big[\frac{1}{2}P'-q)^2 - m^2\big] \\ & \big(\frac{1}{2}\not{P}' + \not{q} + m\big)^{(1)}\big(\frac{1}{2}\not{P}' + \not{q} + m\big)^{(2)}, \end{aligned} \tag{1.152}$$

where $P' \equiv \frac{\sqrt{s'}}{\sqrt{s}}P$ and the on-shell function $f(s,s) = 1$ must be satisfied. The Blankenbecler-Sugar (BbS) uses $f(s',s) = 1$ and the Thompson (Th) variant uses $f(s',s) = \frac{\sqrt{s}+\sqrt{s'}}{2\sqrt{s}}$. The virtual anti nucleons have been neglected to be able to simplify the problem with $\delta^{(+)}$ functions. The $\delta^{(+)}$ indicates that only the positive energy root of the argument is included in the delta function. The BbS propagator in the center of mass system after integration yields

$$g_{BbS} = \delta(q_0)\frac{1}{(2\pi)^3}\frac{m^2}{E_q}\frac{\Gamma_+^{(1)}(\mathbf{q})\Gamma_+^{(2)}(-\mathbf{q})}{\frac{1}{4}s - E_q^2 + i\epsilon}, \tag{1.153}$$

where

$$\Gamma_+^{(i)}(\mathbf{q}) = \left(\frac{\gamma^0 E_k - \gamma\cdot\mathbf{k} + m}{2m}\right)^{(i)} \tag{1.154}$$

$$= \frac{1}{2m}\sum_{\lambda_i=1,2} u(\mathbf{q},\lambda_i)\bar{u}(\mathbf{q},\lambda_i) \tag{1.155}$$

represents the positive energy projection operator nuclei i with a positive-energy Dirac spinor $u(\mathbf{q})$ with momentum $\mathbf{q}$; γ_i denotes either the helicity or the spin projection of the respective nucleon. The projection operators implies that virtual antinucleon contributions are suppressed. It has been shown in [32] that these contributions are

small when the pseudovector coupling is used for the pion. We replace $\mathcal{G}$ in eq(1.149) by g_{BbS} , which yields

$$\begin{aligned}\mathcal{M}(0,\mathbf{p};0,\mathbf{k}|\sqrt{s}) &= \mathcal{V}(0,\mathbf{p};0,\mathbf{k}) \\ &\quad + \int d^3q \mathcal{V}(0,\mathbf{p};0,\mathbf{q}) g_{BbS}(\mathbf{q},s) \mathcal{M}(0,\mathbf{q};0,\mathbf{k}|\sqrt{s}), \quad (1.156)\end{aligned}$$

where both nucleons in intermediate states are equally far off their mass shell. The total energy in the center of mass is

$$\sqrt{s} = 2E_q = 2\sqrt{\mathbf{q}^2 + m^2}. \quad (1.157)$$

We can now rewrite eq(1.156), simplifying our notation,

$$\begin{aligned}\mathcal{M}(\mathbf{p},\mathbf{k}) &= \mathcal{V}(\mathbf{p},\mathbf{k}) \\ &\quad + \int \frac{d^3q}{(2\pi)^3} \mathcal{V}(\mathbf{p},\mathbf{q}) \frac{m^2}{E_q} \frac{\Gamma_+^{(1)}(\mathbf{q})\Gamma_+^{(2)}(-\mathbf{q})}{\mathbf{k}^2 - \mathbf{q}^2 + i\epsilon} \mathcal{M}(\mathbf{q},\mathbf{k}), \quad (1.158)\end{aligned}$$

where both nucleons in intermediate states are equally far off their mass shell, and the exchanged mesons transfer three-momentum only, i.e., the meson propagator is (for scalar mesons)

$$\frac{i}{-(\mathbf{p}-\mathbf{k})^2 - m_\alpha^2}. \quad (1.159)$$

Taking the matrix elements between positive-energy spinors yields an equation for the scattering amplitude, which can be recognized as the invariant transition matrix satisfying the Blankenbecler-Sugar equation:

$$\langle \mathbf{p}|\hat{\mathcal{T}}(E)|\mathbf{k}\rangle = \langle \mathbf{p}|\hat{V}|\mathbf{k}\rangle + \frac{1}{(2\pi)^3} \int_{-\infty}^{\infty} d^3q \, \frac{m^2}{E_q} \langle \mathbf{p}|\hat{V}|\mathbf{q}\rangle \frac{1}{\mathbf{k}^2 - \mathbf{q}^2 + i\epsilon} \, \langle \mathbf{q}|\hat{\mathcal{T}}(E) \, |\mathbf{k}\rangle, \quad (1.160)$$

where, as before, spin (helicity) and isospin indices are suppressed. Within the OBE model, the quasi potential $\langle \mathbf{p}|\hat{V}|\mathbf{k}\rangle$ is a sum of OBE amplitudes.

The BbS propagator is the most widely used approximation. Another choice that has been frequently applied is the version suggested by Thompson [13], which reads, in reduced form

$$g_{BbS} = \delta(q_0) \frac{1}{(2\pi)^3} \frac{m^2}{2E_q^2} \frac{\Gamma_+^{(1)}(\mathbf{q})\Gamma_+^{(2)}(-\mathbf{q})}{\frac{1}{2}\sqrt{s} - E_q + i\epsilon}. \quad (1.161)$$

1.10 Yukawa potentials

In 1935 the japanese physicist Hideki Yukawa proposed a mathematical potential to represent the nucleon-nucleon interaction. He used the Klein-Gordon equation [1],

[1] Schrödinger was actually the first to write down this equation, but he threw out the idea because it did not give him the right hyperfine structure of Hydrogen. Dirac's comment was: it is more important to have beauty in your equations than to have them fit experiment.

which is the relativistic Schrödinger equation for bosons. The Klein Gordon equation has its origin from the fact that the relativistic energy squared can be written as $E^2 = k^2 + m^2$ in natural units, where m is the rest-mass. Yukawa called these new particles mesons, which were responsible for the strong interaction.

For free mesons we have

$$\left[\frac{\partial^2}{\partial t^2} - \nabla^2 + m^2\right]\phi(\mathbf{r}, t) = 0, \tag{1.162}$$

where ϕ represent the amplitude of the meson field. In the limit $m = 0$, this reduces to the familiar wave equation for electromagnetic fields. If we also include the source of the virtual meson field, which is a nucleon represented by ψ, we will have an additional interaction part of the of the Lagrangian. i.e. $\mathcal{L} = \mathcal{L}_0 + \mathcal{L}'$. We now use the interaction Lagrangian for a scalar meson field given as $\mathcal{L}' = g\bar{\psi}\psi\phi$. From variating the action (see [20]), we obtain the new equation of motion as

$$\left[\frac{\partial^2}{\partial t^2} - \nabla^2 + m^2\right]\phi(\mathbf{r}, t) = g\bar{\psi}(\mathbf{r}, t)\psi(\mathbf{r}, t), \tag{1.163}$$

where g is a dimensionless coupling constant between a scalar meson and the nucleon. In the approximation that the nucleon is infinitely heavy and fixed at $\mathbf{r} = 0$, we have the static relation

$$\left[-\nabla^2 + m^2\right]\phi(\mathbf{r}) = g\delta^3(\mathbf{r}), \tag{1.164}$$

which is satisfied by the "Yukawa potential":

$$\phi(r) = \frac{g}{4\pi}\frac{\exp(-mr)}{r}. \tag{1.165}$$

Here, m can also be recognized as the wave number k and g is the coupling constant representing the strength of the meson field.

In 1960, the accelerators were good enough to produce the first observed meson. This was the lightest π-meson. Today we have found many different mesons. There are for example 15 non-strange mesons with mass less than 1350 MeV. Even though the first meson was not found before 1960 the meson exchange theory was already at that time far developed. Mostly due to the fact that people thought they had discovered a meson in 1937. This was believed to be a meson until just a couple of months before the real π-meson was found.

The potential arising from the strong interactions between two nucleons exchanging the π meson will be

$$\begin{aligned} V_s(r) &= -L_s = -\int_{-\infty}^{\infty} d^3r'\mathcal{L}_s = -\int_{-\infty}^{\infty} d^3r' g\bar{\psi}\psi \\ &= -g\int_{-\infty}^{\infty} d^3r'\delta^3(\mathbf{r}' - \mathbf{r})\psi(\mathbf{r}) \\ &= -\frac{g^2}{4\pi}\frac{\exp(-m_\pi r)}{r}, \end{aligned} \tag{1.166}$$

where m_π is the mass of the pion and g is the coupling constant between the nucleon and the pion. If we include more meson channels, the final potential V will be a sum of all the contributions from these meson exchanges.

Yukawa was able to estimate the pion mass by using the range of the strong forces. From the potential we see that the range x is of the order $x = 1/m_\pi$, or in normal units:

$$x = \frac{\hbar c}{m_\pi c^2} \approx \frac{197}{m_\pi c^2}. \tag{1.167}$$

This agrees with the range prediction from the uncertainty principle $t = \hbar/m_\pi c^2$, where the range of the strong force will be

$$x = ct = \frac{\hbar c}{m_\pi c^2}. \tag{1.168}$$

If we use a range $x = 2$ fm we get a pion with a mass roughly about 100 MeV. This is very close to the pion mass ($m_\pi \approx 138$ MeV).

The correct way to model the NN interactions is to use QCD. Since the quarks have spin-$\frac{1}{2}$ we need to use the Dirac equation. However, a good approximation for the NN system is to assume mesons to be the carriers of the strong force between nucleons. Above we only used scalar meson coupling. There are also other important fields, with different Lagrangians, we have to include if we want to make a better model of the NN interaction.

One also often includes so-called "cutoffs" in the NN potentials for large energies/(small r). In the beginning it was done purely out of a mathematical reason, to avoid divergence in the scattering equations. Today, there is a more physical explanation for the cutoffs. Namely, the fact that quarks are the fundamental particle, not the mesons. The cutoffs are then removing the unphysical part of potential in the high energy region, where mesons behave more like quarks. Including cutoff properties in the Yukawa potential yields

$$V(\mathbf{r}) = \begin{cases} C\,\frac{e^{-\mu r}}{r} & \text{if } |\mathbf{r}| > r_c \\ 0 & \text{else} \end{cases}, \tag{1.169}$$

where the cutoff is represented by r_c.

1.11 Partial wave expansion of Yukawa- and box-potentials

A local 3D-spherical box potential $V(\mathbf{x}, \mathbf{y}, \mathbf{z}) = V(\mathbf{r})$ has a general form

$$V(\mathbf{r}) = \begin{cases} V_0 & \text{if } |\mathbf{r}| \leq a \\ 0 & \text{else} \end{cases}. \tag{1.170}$$

Here a is the range of the potential, and V_0 is a constant that determines the strength of the potential.

The Yukawa potential eq(1.166) is local from definition and was found in the previous section to be

$$V(\mathbf{r}) = C\,\frac{e^{-\mu r}}{r}, \tag{1.171}$$

where C is a constant and μ is the mass of a meson. To transform these local potentials into momentum space we have to solve

$$\langle \mathbf{p}|\hat{V}|\mathbf{k}\rangle = \int_{-\infty}^{\infty} d^3r\; e^{-i\mathbf{pr}}\; V(\mathbf{r})\; e^{i\mathbf{kr}} \tag{1.172}$$

To calculate the phase shifts we need to use a partial wave decomposition of this potential From eq(1.37) we have

$$\langle p|\hat{V}_{ll}|k\rangle = \int_0^{\infty} dr\; r^2 V(r) j_l(pr) j_l(kr). \tag{1.173}$$

In this equation we have used the spherical Bessel functions $j_l(kr)$ defined as.

$$j_l(z) \equiv \sqrt{\frac{\pi}{2z}} J_{l+\frac{1}{2}}(z), \tag{1.174}$$

where $J_{l+\frac{1}{2}}(z)$ is the $\frac{1}{2}$-Besselfuncion:

$$J_{l+\frac{1}{2}}(z) = \sqrt{\frac{2}{\pi}} z^{l+\frac{1}{2}} \left(-\frac{1}{z}\frac{\partial}{\partial z}\right)^l \frac{\sin z}{z}. \tag{1.175}$$

We will now only look at the simplest cases with uncoupled channels and solve $\langle p|\hat{V}_{ll}|k\rangle$ only for $l = 0$. The spherical Bessel function for these S-states reduces to

$$j_0(kr) = \frac{\sin kr}{r}. \tag{1.176}$$

For the box potential we have

$$\begin{aligned}
\langle p|\hat{V}_0^{\text{box}}|k\rangle &= \frac{V_0}{pk}\int_0^a dr\, \sin(pr)\sin(kr) \\
&= \frac{V_0}{2pk}\int_0^a dr\, \left[\cos\big((p-k)r\big) - \cos\big((p+k)r\big)\right] \\
&= \frac{V_0}{2pk}\left[\frac{\sin\big((p-k)a\big)}{p-k}\;\frac{\sin\big((p+k)a\big)}{p+k}\right].
\end{aligned} \tag{1.177}$$

In the special case $p = k$ this reduces to

$$\langle p|\hat{V}_0^{\text{box}}|p\rangle = \frac{V_0}{2p^2}\left[a - \frac{\sin(2pa)}{2p}\right]. \tag{1.178}$$

Fig 1.2 shows the phase shifts calculated from this box potential, where we have used $V_0 = -31.0$ MeV and $a = 2.2$ fm. If we also want to calculate inelasticities, V_0 has to

be a complex number.

For the Yukawa potentials we have

$$\begin{aligned}
\langle p|\hat{V}_0^{\rm Yuk}|k\rangle &= \frac{C}{pk}\int_0^\infty dr\ \frac{e^{-\mu r}}{r}\sin(pr)\sin(kr) \\
&= \frac{C}{2pk}\int_0^\infty dr\ \frac{e^{-\mu r}}{r}[\cos\big((p-k)r\big)-\cos\big((p+k)r\big)] \\
&= \frac{C}{4pk}\int_0^\infty \frac{dr}{r}\left[e^{i(p-k-\mu)r}+e^{-i(p-k+\mu)r}-e^{i(p+k-\mu)r}-e^{-i(p+k+\mu)r}\right] \\
&= \frac{C}{4pk}\ln\left(\frac{(p+k)^2+\mu^2}{(p-k)^2+\mu^2}\right). \qquad (1.179)
\end{aligned}$$

Fig 1.2 shows that three Yukawa potentials can be fitted very accurately with experimental data, where $C_1 = -10.463$ MeV, $C_2 = -1650.6$ MeV and $C_3 = 6484.3$ MeV have been chosen as possible strengths and $\mu_1 = 0.7$ fm, $\mu_2 = 2.8$ fm and $\mu_3 = 4.9$ fm are representing the different meson masses used in the NN interaction. Note that, μ_1 corresponds to a particle with mass: $m \approx 197 \times 0.7$ MeV $= 137.9$ MeV, which is the pion mass. The other mesons we have used in this potential, corresponds to heavier mesons. When C is negative, the NN interactions will be attractive. If C is positive, the NN interactions will be repulsive. Other and more physical potentials, besides this three-scalar-meson exchange potential, will be discussed later.

1.12 Analytical calculations of phase shifts using box potentials

We will here show how to analytically calculate the exact phase shift using the time independent Schrödinger equation for a box potential. With this analytical result, we are able to test the numerical methods used in solving the Lippmann-Schwinger equation. The box potential is a good potential to use for this purpose, since it can be solved both numerical and analytically.

To simplify the problem we will now look at NN scattering at low energies, where we can use non-relativistic energies and the non-relativistic Schrödinger equation. The eigenvalue E obtained from the Schrödinger equation has to be greater than zero, otherwise, we would have a bound state situation.

We now have a two particle system, with masses m_1 and m_2, which are interacting through a local potential V. The classical Hamilton function is for this system given as

$$H(\mathbf{r}_1,\mathbf{r}_2,\mathbf{k}_1,\mathbf{k}_2) = \frac{{\mathbf{k}_1}^2}{2m_1}+\frac{{\mathbf{k}_2}^2}{2m_2}+V(\mathbf{r}_1-\mathbf{r}_2). \qquad (1.180)$$

This two-body system can be reduced into two independent one-particle problems. One due to the moving center of mass, and the other due to the relative NN movements. If we are working in the center of mass system we therefore only need to solve

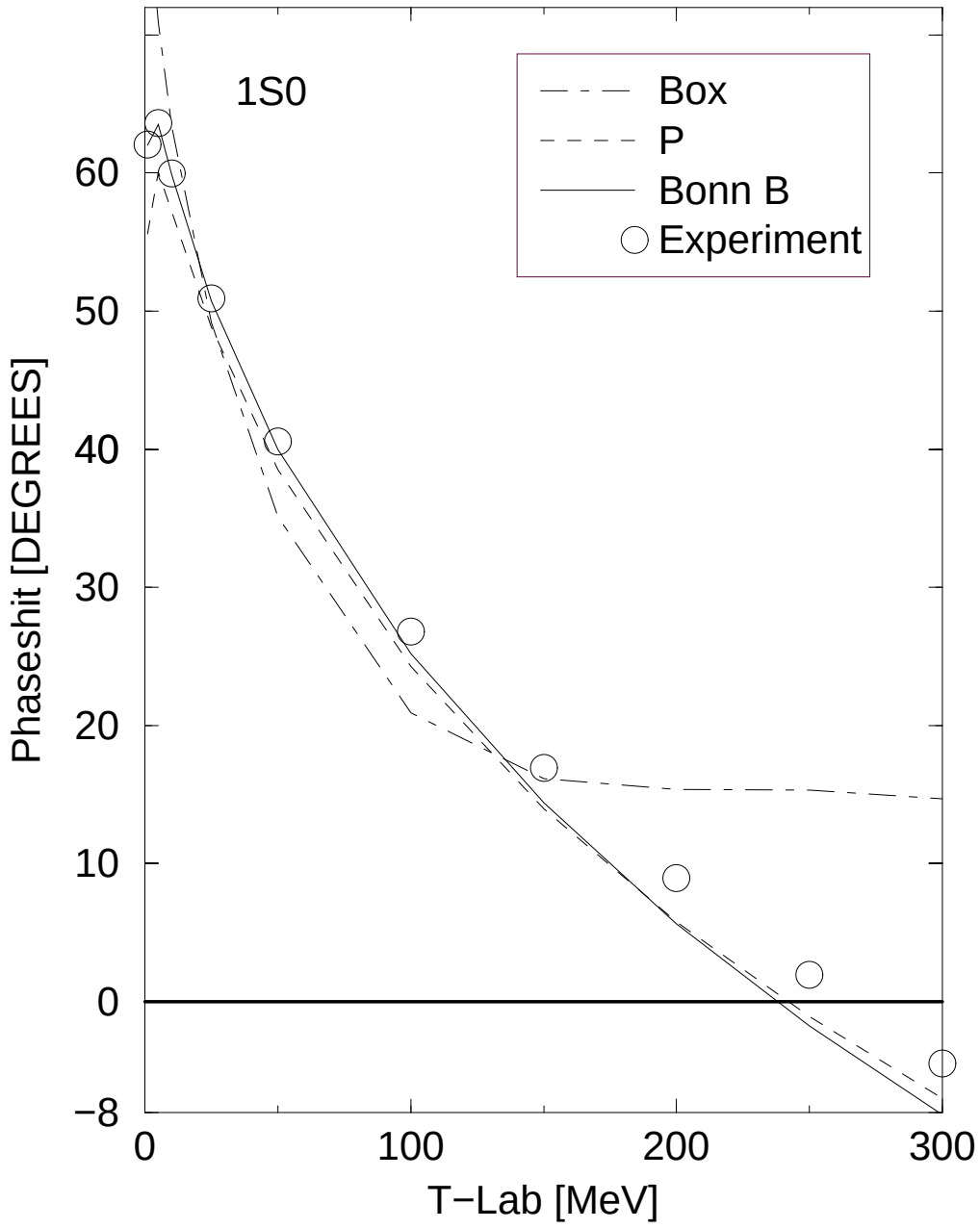

Figure 1.2: ${}^1S_0$ *phase shifts for different potentials. The box Potential* $V(r) = -14.0$ *MeV for* $r \leq 2.7$ *fm and* $V(r) = 0$ *MeV else. "P" denotes a parameterized potential made from three Yukawa potentials:* $V(r) = V_a e^{-ar}/r + V_b e^{-br}/r + V_c e^{-cr}/r$*, where* V_a*,* V_b*,* V_c*,* a*,* b*,* c *are constants fitted to reproduce the experimental data. The Bonn B potential explained in [1] and experimental data from [5]. How these potentials are made will be explained later.*

the one-particle time independent Schrödinger equation with respect to the relative coordinates. Introducing relative coordinates

$$\mathbf{r} = \mathbf{r}_2 - \mathbf{r}_1, \tag{1.181}$$

and the center of mass coordinates

$$\mathbf{R} = \frac{m_1\mathbf{r}_1 - m_2\mathbf{r}_2}{m_1 + m_2}. \tag{1.182}$$

The next step is to find the Hamilton operator with respect to these new coordinates. One way to do this, is to start with the classical Hamilton function ($H = T + V$), and rewrite eq(1.181) and eq(1.182) with respect to the particle coordinates. We find

$$\mathbf{r}_1 = \mathbf{R} - \frac{m_2}{m_1 + m_2}\,\mathbf{r} \tag{1.183}$$

and

$$\mathbf{r}_2 = \mathbf{R} + \frac{m_1}{m_1 + m_2}\,\mathbf{r}. \tag{1.184}$$

The kinetic energy T for the two particles:

$$\begin{aligned} T &= \frac{1}{2}m_1\dot{\mathbf{r}}_1^2 + \frac{1}{2}m_2\dot{\mathbf{r}}_2^2 \\ &= \frac{1}{2}m_1\left[\dot{\mathbf{R}} - \frac{m_2}{m_1 + m_2}\,\dot{\mathbf{r}}\right]^2 + \frac{1}{2}m_2\left[\dot{\mathbf{R}} + \frac{m_1}{m_1 + m_2}\,\dot{\mathbf{r}}\right]^2 \\ &= \frac{1}{2}(m_1 + m_2)\dot{\mathbf{R}}^2 + \frac{1}{2}\frac{m_1 m_2}{m_1 + m_2}\dot{\mathbf{r}}^2. \end{aligned} \tag{1.185}$$

By introducing the reduced mass μ

$$\mu = \frac{m_1 m_2}{m_1 + m_2}, \tag{1.186}$$

we are able to rewrite the Hamilton function eq(1.180) as

$$H = \frac{\mathbf{P}^2}{2(m_1 + m_2)} + \frac{\mathbf{p}^2}{2\mu} + V(\mathbf{r}), \tag{1.187}$$

where $\mathbf{P} = (m_1 + m_2)\dot{\mathbf{R}}$ and $\mathbf{p} = \mu\dot{\mathbf{r}}$. We are going back to quantum mechanics by replacing the momentums with gradient operators. Since $\mathbf{R}$ and $\mathbf{r}$ are independent, we can separate the two orthogonal parts in the wave function as $\psi(\mathbf{R}, \mathbf{r}) = \psi_{mc}(\mathbf{R})\psi_r(\mathbf{r})$. The time independent Schrödinger equation is therefore separable, giving a free particle equation for the moving center of mass system

$$-\frac{1}{2(m_1 + m_2)}\nabla^2_{\mathbf{R}}\psi_{mc}(\mathbf{R}) = E_{mc}\psi_{mc}(\mathbf{R}), \tag{1.188}$$

and another equation, due to the relative momentum between the nucleons, give as

$$\left[-\frac{1}{2\mu}\nabla^2_{\mathbf{r}} + V(\mathbf{r})\right]\psi_r(\mathbf{r}) = E_r\psi_r(\mathbf{r}), \tag{1.189}$$

where the total energy in the laboratory system is $E = E_{mc} + E_r$.

The phase shifts are calculated from eq(1.189). It is therefore natural to find the phase shifts in the center of mass system for both analytically and numerically calculations. The phase shifts will only depend on the radial equation:

$$\left[-\frac{1}{2\mu}\frac{d^2}{dr^2} - \frac{1}{\mu r}\frac{d}{dr} + V(r) + \frac{l(l+1)}{2mr^2} \right] R(r) = E_r R(r), \tag{1.190}$$

where $R(r)$ is the radial part of the wave function. Since we are not interested in solving the general partial wave problem for these simple potentials, we choose the simplest case where the orbital momentum quantum number $l = 0$.

We introduce the definition of a modified radial wave function $u(r) = rR(r)$, and define the box potential as

$$V(r) = \begin{cases} -V_0, & 0 \leq r < a \\ 0, & r > a \end{cases} . \tag{1.191}$$

i.e., the NN interactions, which are approximated with the box potential, are attractive for $V_0 > 0$. Solving eq(1.190) gives

$$\begin{cases} \frac{d^2}{dr^2}u(r) = -k_1^2 u(r), & 0 \leq r < a \\ \\ \frac{d^2}{dr^2}u(r) = -k_2^2 u(r), & r > a \end{cases} , \tag{1.192}$$

where

$$k_1 = \sqrt{2\mu(V_0 + E)} \tag{1.193}$$

and

$$k_2 = \sqrt{2\mu E}. \tag{1.194}$$

The general solution for the radial wave function can then be found from eq(1.192) as

$$u(r) = \begin{cases} A\sin(k_1 r) + B\cos(k_1 r), & 0 \leq r < a \\ C\sin(k_2 r) + D\cos(k_2 r), & r > a \end{cases} , \tag{1.195}$$

where A,B,C and D are constants. In order to proceed any further, we need to take the boundary conditions into account:

- Since the radial wave $R(r)$ is a wave function, it must be finite for all r. That is

$$\lim_{r\to 0} u(r) = \lim_{r\to 0} rR(r) = 0, \tag{1.196}$$

  which means that B=0.

- The wave function $u(r)$ must be continuous

$$\lim_{\epsilon\to 0} u(a+\epsilon) = u \lim_{\epsilon\to 0}(a-\epsilon). \tag{1.197}$$

- The derivate of the wave function $u(r)$ must also be continuous

$$\frac{d}{dr}u(r)\big|_{r\to a_+} = \frac{d}{dr}u(r)\big|_{r\to a_-}. \tag{1.198}$$

Since the wave number k is unchanged between the final and initial state in free NN scattering, it is normal to introduce the phase shifts by rewriting the radial wave function for $r > a$ as

$$F\sin(k_2 r + \delta_0) = C\sin(k_2 r) + D\cos(k_2 r), \tag{1.199}$$

where the phase shift for the S-partial states δ_0 is used ($l = 0$). These equations can now be solved with respect to the boundary conditions, leading to

$$k_1\frac{\cos(k_1 a)}{\sin(k_1 a)} = k_2\frac{\cos(k_2 a + \delta_0)}{\sin(k_1 a + \delta_0)}, \tag{1.200}$$

which is related to the unknown phase shifts δ_0 as

$$\delta_0 = \arctan\left(\frac{k_2}{k_1}\tan(k_1 a)\right) - k_2 a. \tag{1.201}$$

From this expression of the δ_0 phase shift, we see that the radial S wave-function for $r > a$ is

$$u(r) \propto \sin(k_2 r + \delta_0). \tag{1.202}$$

The phase shifts obtained from the attractive box potential are always positive. The physical reason being that the potential will change the wave number k to the effective wave number $k_{eff} = \sqrt{k^2 + V(r)}$ in the region of the potential. From eq(1.193) and eq(1.194) we know that $k_1 > k_2$. The wave function will therefore have a larger frequency and a smaller wave length in the region of the box potential.

We have the same meaning of δ_0 for other more complicated potentials, where both repulsion and attractions between the nucleons are included in the potential. Thus, the phase shifts will only tell about the average of these interactions, and the sign of δ_0 will tell us which one is the most important, since a positive δ tells us that there are more attractions than repulsion between the two nucleons.

The box potential can also be calculated for $l \neq 0$. Instead of setting $l = 0$ we include the l-term. Including this term in an effective potential, we have

$$V_{eff}(r) = V(r) + \frac{l(l+1)}{2mr^2}. \tag{1.203}$$

The δ_l for $l \geq 1$ can be interpreted the same way as δ_0, but the signs of these phase shift now tells if the average V_{eff} is positive or negative.

Note that, we have a $1/r^2$ dependents in $V_{eff}(r)$. This term is always repulsive, and will blow up for small r if $l \neq 0$. In the typical range of nucleus (a couple of Fermi meters), will only the S-states give non-zero δ_l. The centrifugal term therefore prevents states with $l > 0$ to be bound. The δ_0 are positive, corresponding to attractive NN interactions.

Even if the potential is attractive, does not necessarily mean that a S-state is bound. The $^3S_1$ - $^3D_1$ state (deuteron) is the only bound state for the NN system, because the $^1S_0$ state is not attractive enough to bind the two-nucleon system.

Since S-states do not have a centrifugal barrier, they will be the only states which feels the innermost region of the force. i.e, the repulsive core. We have

$$l \approx R_{\text{core}} p = R_{\text{core}} \sqrt{\frac{E_{lab} M}{2}}, \tag{1.204}$$

where R_{core} is (approximately) the range of the repulsive core. From fig 1.2 we see that the $^1S_0$ "Bonn B"-phase shifts turns negative around $E_{lab} = 250$ MeV. If we look at small distances in order of Fermi meters, we can assume that the maximum orbital momentum a state can have is $l = l_{max} \lesssim 1$. Calculating R_{core} gives

$$R_{\text{core}} \lesssim 0.6 \text{ fm}. \tag{1.205}$$

Chapter 2

The One-Boson Exchange Model

Particles can be grouped into three different categories, leptons, baryons and mesons. Leptons are particles like the electron and the neutrino. Baryons are particles with half integer spin like the nucleons, while mesons are particles with integer spin. It is also normal to call the big group of baryons and mesons, which have quarks as the fundamental particles, for hadrons.

The mesons are the carriers of the strong force. They can interact with nucleons through the strong, weak, electromagnetic force. Free mesons can be produced in nucleon-nucleon collisions, but they decay rapidly into lighter mesons, leptons or photons either through strong, weak or electromagnetic interactions. The decay lifetimes are around $10^{-20} - 10^{-23}$ for strong decays, $10^{-16} - 10^{-18}$ for electromagnetic decays and $10^{-8} - 10^{-10}$ for weak decays [7]. Nuclear models are often simplified by neglecting the weak and electromagnetic force, since these forces are relatively small compared to the strong force inside a nuclear.

The OBE model has been very successful in describing the empirical features of the NN force. Both the tensor, spin-orbit and spin-spin forces are accounted for in the meson exchange model. The name of this model is a little misleading, since it gives the impression of a theory dealing with all boson exchanges. We are, however, only dealing with meson exchanges. A better name would therefore be "one-meson exchange model".

2.1 Interaction Lagrangians and OBE amplitudes

The starting point for OBE theory is a phenomenological Lagrangian which describes the interaction between the baryons and meson fields. For the NN interaction at low and intermediate energies the three relevant meson fields are

- the scalar (s) field
- the pseudoscalar (ps) field
- the vector (v) field.

The commonly used interaction Lagrangians that couple these fields to the nucleon are

$$\mathcal{L}_s = g_s\overline{\psi}\psi\phi^{(s)} \tag{2.1}$$

$$\mathcal{L}_{ps} = -g_{ps}\overline{\psi}i\gamma^5\psi\phi^{(ps)} \tag{2.2}$$

$$\mathcal{L}_v = -g_v\overline{\psi}\gamma^\mu\psi\phi^{(v)}_\mu - \frac{f_v}{4M}\overline{\psi}i\sigma^{\mu\nu}\psi\left(\partial_\mu\phi^{(v)}_\nu - \partial_\nu\phi^{(v)}_\mu\right), \tag{2.3}$$

where M is the nucleon mass and ψ is the nucleon Dirac field with its adjoint defined by $\overline{\psi} = \psi\gamma^0$, while $\phi^{(s)}$, $\phi^{(ps)}$ and $\phi^{(v)}$ are the scalar, pseudoscalar and vector meson fields, respectively. Correspondingly, g_s, g_{ps} and g_v are the coupling constants that couple the nucleons to scalar, pseudoscalar and vector mesons, respectively [33]. For isospin 1 mesons, $\phi^{(\alpha)}$ is to be replaced by $\tau\cdot\phi^{(\alpha)}$, where τ is the Pauli matrix vector [1]. In eq(2.3) the first term on the right-hand side is known as vector (v) and the second term the tensor (t) coupling. The tensor force is needed to explain coupled channels, where states with different orbital momentum are interfering. There are two alternative ways to couple pseudoscalar fields to nucleons. The one given above is the pseudoscalar coupling (ps). The so-called gradient coupling or pseudovector (pv) coupling is an effective coupling derived from chiral symmetry [1, 34] and reads

$$\mathcal{L}_{pv} = -\frac{f_{ps}}{m_{ps}}\overline{\psi}i\gamma^5\gamma^\mu\psi\partial_\mu\phi^{(ps)}. \tag{2.4}$$

The ps and the pv coupling are equivalent for on-shell nucleons when the coupling constants are related by $f_{ps} = g_{ps}(m_{ps}/2M)$. The coupling constants may be constrained by nucleon-nucleon scattering data. Empirical information also constrains the ratio of g_v to f_v.

In time-dependent perturbation theory the NN interaction can be considered in terms of so-called Feynman diagrams involving meson-baryon coupling. The Γ operator in the Feynman diagram shown in fig 2.1, can be found from the interaction Lagrangians to yield [2]

$$\Gamma_{ps} = -g_{ps}i\gamma^5 \tag{2.5}$$

$$\Gamma_s = g_s\hat{1} \tag{2.6}$$

$$\Gamma_{pv} = -\frac{f_{ps}}{m_{ps}}\gamma^5\gamma^\mu i(p-p')_\mu \tag{2.7}$$

$$\Gamma_v = -g_v\gamma^\mu + \frac{f_v}{2M}\sigma^{\mu\nu}i(p-p')_\nu \tag{2.8}$$

The field theory was first developed for quantum electrodynamics. When electromagnetic interactions are involved, it is customary to apply perturbation theory,

[1] The Pauli matrices (τ^k) are: $\tau^1 = \begin{pmatrix} 0 & 1 \\ 1 & 0 \end{pmatrix}$, $\tau^2 = \begin{pmatrix} 0 & -i \\ i & 0 \end{pmatrix}$ and $\tau^3 = \begin{pmatrix} 1 & 0 \\ 0 & -1 \end{pmatrix}$

[2] Where $\gamma^0 = \begin{pmatrix} 1 & 0 \\ 0 & -1 \end{pmatrix}$, $\gamma^k = \begin{pmatrix} 0 & \tau^k \\ -\tau^k & 0 \end{pmatrix}$. $\gamma^5 = \gamma_5 = \gamma^1\gamma^2\gamma^3 = \begin{pmatrix} 0 & 1 \\ 1 & 0 \end{pmatrix}$ and $\sigma^{\mu\nu} = \frac{i}{2}[\gamma^\mu, \gamma^\nu]$

which appears quite reasonable for a coupling constant $\alpha \approx 1/137$. Meson-baryon coupling constants originate from the strong interaction and are generally large, up to the order of 10, thus, the perturbation expansion becomes increasingly divergent at shorter distances. For intermediate and long range the diagrammatic expansion can be expected to converge. However, due to the quark structure of the nucleons the meson-exchange model for the NN interaction is not valid at short range. Fortunately, the NN interaction is strongly repulsive at short distances, and presumably the nucleons are kept sufficiently apart from each other to prevent genuine quark-gluon processes between the nucleons. The short range part of the NN interaction can be treated phenomenologically by introducing vertex form factors, which are closely related to the extended quark structure of the hadrons. In the OBE model these form factors are defined as

$$\mathcal{F}_\alpha[(\mathbf{q}' - \mathbf{q})^2] = \left(\frac{\Lambda_\alpha^2 - m_\alpha^2}{\Lambda_\alpha^2 + (\mathbf{q}' - \mathbf{q})^2} \right)^{n_\alpha}, \tag{2.9}$$

where Λ_α is the cutoff mass and n_α indicates the pole of the form factor. It is normal to use different Λ_α and n_α for the different mesons used in the OBE-model.

The form factors suppress the meson exchange at small distances. Taking this into account, the meson theory can be treated in the framework of perturbation theory. The lowest order contribution to the NN scattering are the OBE diagrams.

The one-boson exchange potential (OBEP) is defined as a sum of one-meson exchange amplitudes. Each meson has a certain mass and coupling constant. It is normal in the OBEP to include the five lightest non-strange mesons, and construct one fictive σ-meson. The σ-meson is then supposed to include an effective average of all the other mesons and all the higher order of meson exchange diagrams, where the two-pion exchanges are the most important.

Neglecting mesons with spin $j \geq 1$ in the OBEP, is a good approximation because the mesons are generally heavier as the spin increases (see [29]). The heavier mesons will only contribute to the strong force at short ranges, where the NN interaction is already strongly repulsive. Contributions from heavier mesons to the overall NN interaction can therefor be neglected without to much trouble.

The OBEP is illustrated in fig 2.2, with π and η pseudo-scalar (ps), δ and σ scalar

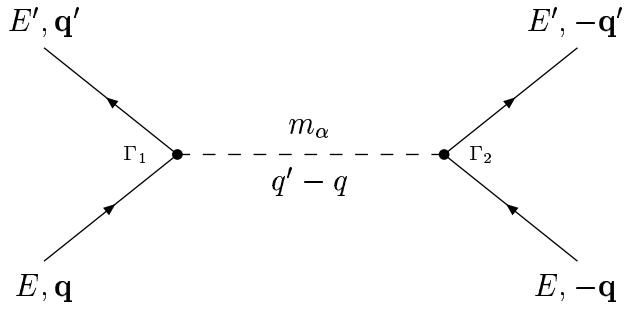

Figure 2.1: *Feynman diagram for a NN-interaction in the center of mass system, where one-meson exchanges are representing the strong force.*

(s) and ρ and ω vector (v) particles. The contributions from the iso-vector mesons π, δ and ρ are similar to the iso-vector mesons, but will contain an additional factor $\tau \cdot \tau$.

The most important mesons which enter the one-boson model are π, σ, ρ, and ω. The heavy vector mesons ρ and ω are important at short distances where the NN interaction becomes strongly repulsive. At intermediate distance attraction is generated mainly by correlated pairs of pions with total spin $J = 0$ and isospin $T = 0$ [35], i.e., the same as we use for the fictive σ meson. The long-range part of the NN interaction is explained by virtual exchanges of the lightest meson, i.e., the pion. This has been well confirmed both theoretically and experimentally, and all realistic NN interactions will include the pion.

The positive energy solutions for the nucleon field ψ in a plane wave basis are written in terms of Dirac spinors as

$$\psi = u(\mathbf{p}, s)e^{ipx}, \tag{2.10}$$

where p is the four-momentum and x is the four-point. The Dirac spinor is defined as

$$u(\mathbf{p}, s) = \sqrt{\frac{E+M}{2M}} \begin{pmatrix} \chi \\ \frac{\sigma \cdot \mathbf{p}}{E+M}\chi \end{pmatrix}, \tag{2.11}$$

or in helicity representation

$$u(\mathbf{p}, \lambda) = \sqrt{\frac{E+M}{2M}} \begin{pmatrix} 1 \\ \frac{2\lambda p}{E+M} \end{pmatrix} |\lambda\rangle, \tag{2.12}$$

where

$$|\lambda = \frac{1}{2}\rangle = \begin{pmatrix} 1 \\ 0 \end{pmatrix} \quad \text{and} \quad |\lambda = -\frac{1}{2}\rangle = \begin{pmatrix} 0 \\ 1 \end{pmatrix} \tag{2.13}$$

The Dirac spinor is normalized covariantly by $\overline{u}(\mathbf{p}, s)u(\mathbf{p}, s) = 1$, where $\overline{u} \equiv u^+\gamma^0$ is the adjoint of u. If we use explicitly antisymmetric NN states, i.e. $(L+S+T)$ is odd, we only have the direct term illustrated in fig 2.1. The meson exchange amplitudes

$$V_{\text{OBEP}} = \sum_{\alpha=\pi,\eta,\rho,\omega,\delta,\sigma} \quad V_\alpha^{\text{OBE}} \quad \equiv$$

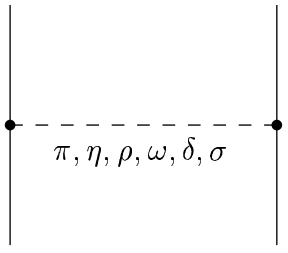

Figure 2.2: *The standard OBE-model, where the five lightest non-strange mesons are included. The σ-meson is artificial constructed to include an average of all the other possible meson exchanges. Solid lines denote nucleons.*

can be found in helicity representation, by using normal Feynman diagram rules, to yield

$$\langle \mathbf{p}'\lambda_1'\lambda_2'|V_\alpha^{\rm OBE}|\mathbf{p}\lambda_1\lambda_2\rangle = \frac{\bar{u}(-\mathbf{p}',\lambda_1')\Gamma_1 u(-\mathbf{p},\lambda_1')\bar{u}(\mathbf{p}',\lambda_2')\Gamma_2 u(\mathbf{p},\lambda_2')}{(p-p')^2-m_\alpha^2} \tag{2.14}$$

There are many important features of the NN interaction, which can be associated with the pion-exchange process and we will now discuss this process in more detail. The contributions from the other mesons can be obtained in similar way. The pion is a pseudoscalar meson and we choose the pseudovector Lagrangian defined by eq(2.4). The pion-exchange process is shown diagrammatically in fig 2.1.

Using pseudovector coupling from eq(2.7), the contribution from one-pion exchange diagram can be written as

$$\begin{aligned} V_\pi &= \frac{f_\pi^2}{m_\pi^2}\frac{\overline{u}(\mathbf{p}_1')\gamma^5\gamma^\mu(p_1-p_1')_\mu u(\mathbf{p}_1)\overline{u}(\mathbf{p}_2')\gamma^5\gamma^\nu(p_2'-p_2)_\nu u(\mathbf{p}_2)}{(p_1-p_1')^2-m_\pi^2} \\ &= -\frac{f_\pi^2}{m_\pi^2}4M^2\frac{\overline{u}(p_1')\gamma_5 u(p_1)\overline{u}(p_2')\gamma^5 u(p_2)}{(p_1-p_1')^2-m_\pi^2}, \end{aligned} \tag{2.15}$$

where the spin indices of the Dirac spinors and the isospin factor $(\tau_1\cdot\tau_2)$ have been suppressed. The four-momentum transfer is $k = p_1 - p_1' = p_2' - p_2$. For the on-shell process the zero component $k_0 = 0$. Hence, $k^2 = (0, -(\mathbf{p}_1 - \mathbf{p}_1'))^2 = -\mathbf{k}^2$. Connections to the empirical features of the NN interaction are most clearly seen in the non-relativistic limit. Approximating the energy by $E \approx M$ in the Dirac spinor (2.11), the above expression can be written in terms of a single momentum, the momentum transfer $\mathbf{k}$

$$\begin{aligned} V_\pi(\mathbf{k}) &= -\frac{f_\pi^2}{m_\pi^2}\frac{(\sigma_1\cdot\mathbf{k})(\sigma_2\cdot\mathbf{k})}{\mathbf{k}^2+m_\pi^2} \\ &= -\frac{f_\pi^2}{m_\pi^2}\frac{1}{3}\Big[\frac{S_{12}(\mathbf{k})}{\mathbf{k}^2+m_\pi^2}+\sigma_1\cdot\sigma_2-\sigma_1\cdot\sigma_2\frac{m_\pi^2}{\mathbf{k}^2+m_\pi^2}\Big], \end{aligned} \tag{2.16}$$

where

$$S_{12}(\mathbf{k}) = 3(\sigma_1\cdot\mathbf{k})(\sigma_2\cdot\mathbf{k}) - (\sigma_1\cdot\sigma_2)\mathbf{k}^2 \tag{2.17}$$

is the tensor operator in momentum space. The second term in eq(2.16) is the spin-spin δ-force and the last term is a spin-spin Yukawa potential. The interaction $V_\pi(\mathbf{k})$ can be Fourier transformed into a local potential $V_\pi(\mathbf{r})$ in coordinate space. This yields

$$\begin{aligned} V_\pi(\mathbf{r}) &= \frac{f_\pi^2}{4\pi}m_\pi\Bigg\{\Big[\frac{1}{(m_\pi r)^3}+\frac{1}{(m_\pi r)^2}+\frac{1}{3m_\pi r}\Big]S_{12}(\hat{\mathbf{r}})e^{-m_\pi r} \\ &\quad -\frac{4\pi}{3m_\pi^3}(\sigma_1\cdot\sigma_2)\delta(\mathbf{r})+(\sigma_1\cdot\sigma_2)\frac{1}{3m_\pi r}e^{-m_\pi r}\Bigg\}, \end{aligned} \tag{2.18}$$

where $r = |\mathbf{r}_1 - \mathbf{r}_2|$ is the distance between the nucleons and

$$S_{12}(\hat{\mathbf{r}}) = 3\frac{(\sigma_1\cdot\mathbf{r})(\sigma_2\cdot\mathbf{r})}{r^2} - (\sigma_1\cdot\sigma_2) \tag{2.19}$$

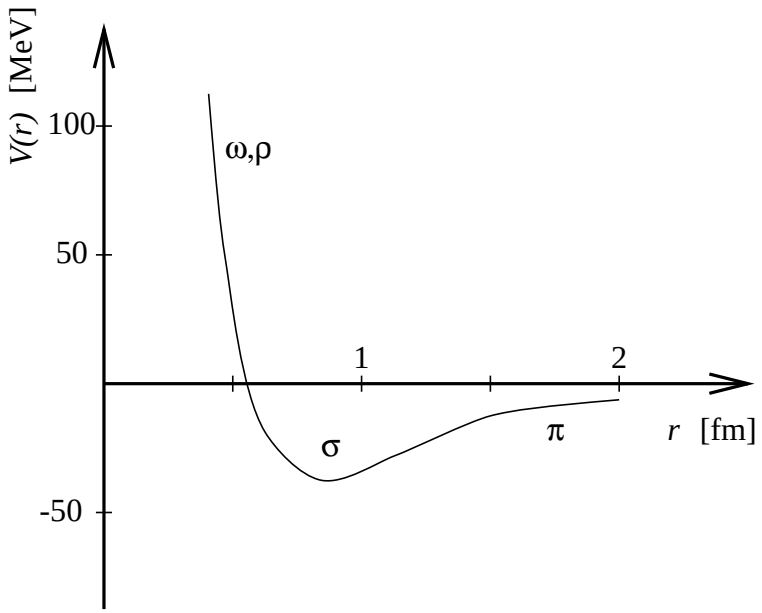

Figure 2.3: *The central part of the NN potential shown schematically as a function of internucleon distance r.*

is the tensor operator in coordinate space. This contribution is modified by vertex form factors, which are determined by cutoff masses. Originally they were introduced to avoid divergences in the scattering equation. The cut-off masses are typically from 1 to 2 GeV. At these energies, quark degrees of freedom are expected to contribute significantly. The form factors suppress the spin-spin δ-force which leads to singularity at zero distance.

The contribution from exchange of scalar and vector mesons can be obtained in a similar way. These mesons also produce the spin-orbit force which is important to reproduce scattering data. For a given spin-isospin partial wave, the NN interaction can be approximated by

$$V(r) = V_c(r) + V_t(r)S_{12} + V_{so}(r)\mathbf{L}\cdot\mathbf{S}, \tag{2.20}$$

where the terms on the right-hand-side are the central, tensor and the spin-orbit force, respectively. An overview of the importance of these terms for the mesons used in the OBE model is shown in table 2.1. We see that the OBE model is strongly spin and isospin dependent. The central potential describes the interactions between the nucleons to lowest order, i.e. only dependent on the internucleon distance r. The central potential is illustrated in fig 2.1. The tensor part of the NN potential explains the quadrupole moment of the ground state of the deuteron, and other coupled states with different orbital momentum l. We see that the tensor part has the necessary $\mathbf{r}$ dependence to explain the non-central force. The spin-orbit term is needed to account for the observed spin-dependent polarization specter we obtain from NN-polarized scattering. Note that $l = \mathbf{r} \times \mathbf{p}$.

Potentials based on the OBE model are usually derived in momentum space. They are non-local by construction. Approximations have to be made to construct inter-

actions which are local in coordinate space. Note that eq(2.16) is a non-relativistic approximation of the general one-pion-exchange contribution. Phenomenological potentials usually contain only local operators and are usually derived in coordinate space.

A convenient way to estimate the different parameters like the cutoff mass Λ and the σ-meson, is to partial wave decompose the potential. In this frame one can fit very accurately the different partial waves with the experimental ones, by variating these parameters. The Bonn B potential is an OBEP, where the unknown cutoff masses have been fitted using the Blankenbecler-Sugar equation and other parameters obtained from experimental data. The Bonn B in-put parameters are shown in table 2.2.

We will later in the in-medium scattering make use of a charge-dependent bonn poten-

Coupling	Mesons (strength of coupling)		Characteristics of predicted forces			
	$T=0$ [1]	$T=1$ $[\tau_1 \cdot \tau_2]$	Central [1]	Spin-Spin $[(\sigma_1 \cdot \sigma_2)]$	Tensor $[S_{12}]$	Spin-Orbit $[\mathbf{L} \cdot \mathbf{S}]$
ps	η (weak)	π (strong)		Weak, coherent with v,t	Strong	
s	σ (strong)	δ (weak)	Strong, attractive			Coherent with v
v	ω (strong)	ρ (weak)	Strong, repulsive	Weak, coherent with ps	Opposite to ps	Strong coherent with s
t	ω (weak)	ρ (strong)		Weak, coherent with ps	Opposite to ps	

Table 2.1: *Various meson-nucleon couplings and their contributions to the nuclear force as obtained from the OBE model in [1]. T denotes the isospin. Isovector ($T=1$) mesons will include the isospin dependent part of the nuclear force.*

	m_α [MeV]	g_α^2	$\frac{f_\alpha}{g_\alpha}$	Λ [MeV]	n_α	J^P	T^G
π	138.03	14.4000	0.00	1700	1	0^-	1^-
ρ	769.00	0.9000	6.10	1850	2	1^-	1^+
η	548.80	3.0000	0.00	1500	1	0^-	0^+
ω	782.60	24.5000	0.00	1850	2	1^-	0^-
δ	983.00	2.4880	0.00	2000	1	0^+	1^-
σ	720.00	18.3773	0.00	2000	1	0^+	0^+

Table 2.2: *Bonn B in-put parameters. Mass (m), width (Λ), coupling constants (f and g), spin (J), parity (P), G-parity (G) and isospin (T).*

tial, which is known as the cdbonn potential (see [15]). The new high energy models also include properties taken from quantum chromodynamics (QCD). Confinement and chiral perturbation are other NN interactions effects that people are focusing on today.

2.2 Partial-wave decompositions

From eq(2.14) we have the OBEP given in helicity amplitudes. These amplitudes can be decomposed into partial waves according to

$$\langle \lambda_1' \lambda_2' | \hat{V}^J(q', q) | \lambda_1 \lambda_2 \rangle = 2\pi \int_{-1}^{1} d(\cos\theta) d^J_{\lambda_1 - \lambda_2, \lambda_1' - \lambda_2'}(\theta) \langle \mathbf{q}' \lambda_1' \lambda_2' | \hat{V}^{\rm OBE}_\alpha | \mathbf{q} \lambda_1 \lambda_2 \rangle, \quad (2.21)$$

where J denotes the total angular momentum of the two nucleons, θ is the angle between $\mathbf{q}'$ and $\mathbf{q}$, and $d^J_{m,m'}(\theta)$ is the conventional reduced rotation matrix, which can be expressed in Legendre polynomials $P_J(\cos\theta)$. Here and throughout the rest of the chapter, momenta denoted by non-bold letters are absolute three-momenta, thus $q = |\mathbf{q}|$.

Ignoring antiparticles, there are $4 \times 4 = 16$ helicity amplitudes for V^J. However, time-reversal invariance, parity conservation, and the fact that we are dealing with two identical fermions imply that only six amplitudes are independent. For these six amplitudes, we choose the following set:

$$\begin{aligned}
\hat{V}^J_1(q', q) &= \langle ++ | \hat{V}^J_{\rm OBEP}(q', q) | ++ \rangle, \\
\hat{V}^J_2(q', q) &= \langle ++ | \hat{V}^J_{\rm OBEP}(q', q) | -- \rangle, \\
\hat{V}^J_3(q', q) &= \langle +- | \hat{V}^J_{\rm OBEP}(q', q) | +- \rangle, \\
\hat{V}^J_4(q', q) &= \langle +- | \hat{V}^J_{\rm OBEP}(q', q) | -+ \rangle, \\
\hat{V}^J_5(q', q) &= \langle ++ | \hat{V}^J_{\rm OBEP}(q', q) | +- \rangle, \\
\hat{V}^J_6(q', q) &= \langle +- | \hat{V}^J_{\rm OBEP}(q', q) | ++ \rangle,
\end{aligned} \quad (2.22)$$

where $\pm$ stands for $\pm\frac{1}{2}$. Notice that

$$\hat{V}^J_5(q', q) = \hat{V}^J_6(q, q'). \quad (2.23)$$

If we use these potentials in helicity representation, the non-relativistic Blankenbecler-Sugar equation (see eq1.136) yields

$$\begin{aligned}
\langle \lambda_1' \lambda_2' | \hat{T}^J(p, k) | \lambda_1 \lambda_2 \rangle \;=\; & \langle \lambda_1' \lambda_2' | \hat{V}^J(p, k) | \lambda_1 \lambda_2 \rangle \\
& + \frac{2m}{\pi} \sum_{h_1, h_2} \left[\int_0^\infty dq\; q^2 \langle \lambda_1' \lambda_2' | \hat{V}^J(p, q) | h_1 h_2 \rangle \; \frac{1}{k^2 - q^2 + i\epsilon} \right. \\
& \left. \times \langle h_1 h_2 | \hat{T}^J(q, k) | \lambda_1 \lambda_2 \rangle \right].
\end{aligned} \quad (2.24)$$

We have six coupled equations, where h_1 and h_2 are the helicities in intermediate states for nucleon 1 and nucleon 2, respectively. To partially decouple this system, it

is useful to introduce the following linear combinations of helicity amplitudes:

$$\begin{aligned}
{}^{0}\hat{V}^{J} &\equiv \hat{V}_{1}^{J} - \hat{V}_{2}^{J}, \\
{}^{1}\hat{V}^{J} &\equiv \hat{V}_{3}^{J} - \hat{V}_{4}^{J}, \\
{}^{12}\hat{V}^{J} &\equiv \hat{V}_{1}^{J} + \hat{V}_{2}^{J}, \\
{}^{34}\hat{V}^{J} &\equiv \hat{V}_{3}^{J} + \hat{V}_{4}^{J}, \\
{}^{55}\hat{V}^{J} &\equiv 2\hat{V}_{5}^{J}, \\
{}^{66}\hat{V}^{J} &\equiv 2\hat{V}_{6}^{J},
\end{aligned} \tag{2.25}$$

where ${}^{0}\hat{V}^{J}$ and ${}^{1}\hat{V}^{J}$ represent two uncoupled T-matrix equations, while the rest will be coupled and result in the coupled triplet T-matrix equation.

In nuclear physics it is more common to use the $|LSJM\rangle$ basis, where S denotes the total spin, L the total orbital momentum, and J the total angular momentum with projection M. We use the short-notation $\hat{V}^{JS}_{L',L} \equiv \langle L'SJM|\hat{V}|LSJM\rangle$. The partial wave expansion of the potential in the LSJ representation can now be obtained by using following unitary transformations:

Spin singlet

$$\hat{V}^{J0}_{J,J} = {}^{0}\hat{V}^{J}. \tag{2.26}$$

Uncoupled spin triplet

$$\hat{V}^{J1}_{J,J} = {}^{1}\hat{V}^{J}. \tag{2.27}$$

Coupled triplet states

$$\hat{V}^{J1}_{J-1,J-1} = \frac{1}{2J+1}\big[(J+1)^{34}\hat{V}^{J} + J^{12}\hat{V}^{J} + \sqrt{J(J+1)}({}^{55}\hat{V}^{J} + {}^{66}\hat{V}^{J})\big], \tag{2.28}$$

$$\hat{V}^{J1}_{J+1,J+1} = \frac{1}{2J+1}\big[(J+1)^{12}\hat{V}^{J} + J^{34}\hat{V}^{J} + \sqrt{J(J+1)}({}^{55}\hat{V}^{J} + {}^{66}\hat{V}^{J})\big], \tag{2.29}$$

$$\hat{V}^{J1}_{J-1,J+1} = \frac{1}{2J+1}\big[(J+1)^{66}\hat{V}^{J} - J^{55}\hat{V}^{J} + \sqrt{J(J+1)}({}^{12}\hat{V}^{J} - {}^{34}\hat{V}^{J})\big], \tag{2.30}$$

$$\hat{V}^{J1}_{J+1,J-1} = \frac{1}{2J+1}\big[(J+1)^{55}\hat{V}^{J} - J^{66}\hat{V}^{J} + \sqrt{J(J+1)}({}^{12}\hat{V}^{J} - {}^{34}\hat{V}^{J})\big]. \tag{2.31}$$

The same LSJ transformations can be done with a T-matrix given in helicity states.

Chapter 3

Experimental Data From Two-Nucleon Systems

3.1 Binding energy of a two nucleon system

There are many methods in receiving the experimental data for the binding energy of nucleon systems. The most accurate way to calculate the deuteron (^{2}H) binding energy, is to measure the energy of the γ-ray photon emitted when a free np system is being bound. With such experiments the binding energy of the deuteron is found to be 2.224589 ± 0.000002 MeV

$$p + n \rightarrow {}^2\mathrm{H} + \gamma \tag{3.1}$$

This binding energy can also be found in the opposite process, where a γ-ray photon breaks apart the deuteron This method is called photodissociation. A third way to measure the binding energy, is by spectroscopy and using the mass doublet method described in [7]. These three methods are all in excellent agreement, but the last two methods are not as accurate as the first one.

3.2 Observables from nucleon-nucleon scattering

Evaluating phase shifts and inelasticities, are on the other hand, a much more complicated process than finding the binding energy. The most important observables in NN scattering are cross sections and spin polarizations. In order to find the phase shifts and inelasticities, one has to do a partial wave decomposition of the scattering amplitude constructed from the observables.

The differential cross section is derived in [47] by Jackson and Blatt. The elastic

	pp isovector phase shifts		np isoscalar phase shifts	
T_{lab}	$^1\text{S}_0$	$^3\text{F}_2$	$^1\text{S}_0$	$^3\text{S}_1$
1 MeV	32.684 ± 0.005	0.000	62.068 ± 0.030	147.747 ± 0.010
100 MeV	24.97 ± 0.08	0.817 ± 0.004	26.78 ± 0.38	43.23 ± 0.14
200 MeV	6.55 ± 0.16	1.424 ± 0.034	8.94 ± 0.39	21.22 ± 0.15
350 MeV	-11.13 ± 0.46	1.04 ± 0.16	-10.59 ± 0.62	0.502 ± 0.32

Table 3.1: *Experimental proton-proton and neutron-neutron phase shifts and their multienergy errors in degrees as obtained in the multienergy analysis [5].*

cross section for proton-proton scattering is e.g.

$$\begin{aligned}\frac{d\sigma}{d\Omega} &= \sum_{l=0}^{\infty}\left(\frac{e^2}{4\pi\epsilon_0}\right)^2\frac{1}{4T^2}\left\{\frac{1}{\sin^4(\theta/2)}+\frac{1}{\cos^4(\theta/2)}-\frac{\cos\left[\beta\ln\tan^2(\theta/2)\right]}{\sin^2(\theta/2)\cos^2(\theta/2)}\right.\\ &\quad -\frac{2}{\beta}\sin\delta_l\left(\frac{\cos\left[\delta_l+\beta\ln\sin^2(\theta/2)\right]}{\sin^2(\theta/2)}+\frac{\cos\left[\delta_l+\beta\ln\cos^2(\theta/2)\right]}{\cos^2(\theta/2)}\right)\\ &\quad \left.+\frac{4}{\beta^2}\sin_l^{\delta}\right\}(2l+1). \qquad (3.2)\end{aligned}$$

Here T is the laboratory kinetic energy of the incident proton (assuming the target nucleon at rest). θ is the scattering angle in the center of mass system and $\beta = \alpha v/c$, where $\alpha \approx 1/137$ is the fine-structure constant and v is the relative velocity of the nucleons.

Note that, δ_l are the only unknowns in eq(3.2). We can measure the differential scattering cross section as a function of angle at different energies. We extract δ_l from the best fit to eq(3.2). This method is far from being as accurate as the method we had to determine the binding energy. also the uncertainties in the phase shifts are getting bigger with higher energies used in the scattering. The accuracy is, however, increasing as new and better experimental data are used.

It is, of course, also possible to go the other way, i.e. to calculate the total cross section from phase shifts and inelasticities. This is for example computed in the program "obs.f", which is written by R. Machleidt.

Converting the observables into phase shifts can be complicated. This is illustrated in R. A. Arndt's phase shifts analysis from 2000 [6], where the difference between experimental and theoretical inelasticities for the $^3\text{D}_1$ can be due to a sign convention (see fig 5.3). Machleidt, strongly believes that Arndt has made a mistake in his sign convention for this state.

How the accuracy in phase shift variates with energy for isoscalar and isovector states, can be seen from phase shifts analysis from 1993 [5]. We see from table 3.1 that the accuracy of phase shifts are better for pp than np scattering. This is due to the fact that it is much easier to handle protons than neutrons. Both giving the nucleons a known initial energy, and observing the nucleons after the scattering are

much more complicated for neutrons than protons. For the same reason, the nn scattering data does not exist. The uncertainty/error in the phase shifts obtained from experiments are generally increasing with energy.

For the $^1S_0$ isoscalar np states, with $T_{\text{lab}} < 350$ MeV, the error estimate of the phase shift is less than 10% of the phase shift. This error is about four times bigger for the isovector np scattering.

The $^3F_2$ state and the $^3S_1$ state, from table 3.1, illustrates smaller phase shifts where the the error estimate is about 50% of the phase shift. In fig 5.3 we have the same problem with the inelasticity in the $^3D_2$ state. In this state the inelasticities are so small, compared with their corresponding uncertainty, that Arndt has set them to zero in his article [6], which includes phase shifts and inelasticities for energies up to 3 GeV.

Phase shifts from NN scattering in nuclear matter scattering are not calculated experimentally and probably never will be, due to the problem of observing scattering data inside heavy nuclei.

Spin polarization experiments for NN scattering are found by polarizing the nucleons spin. Experiments with different spin polarizations will give spin dependent observables, which are needed to explain the spin-orbit and spin-spin parts of the NN interactions.

Chapter 4

Numerical Calculations Of Two-Nucleon Systems Using OBEPs To Describe The Interactions

This chapter is devoted to computational calculations of NN binding energies and phase shifts from free NN scattering. Most of the theory behind the equations used in these calculations are already explained earlier. We will look at numerical methods to calculate bound state energies, and different scattering parameters for two nucleon systems. The potentials, which are used here, are made by R. Machleidt.

Calculations of binding energies can be done both from the Lippmann-Schwinger equation and the Schrödinger equation. Only the eigenvalue method in momentum space will be shown. The phase shifts will be given both in "bar" and Blatt-Biedenharn formalism. These are the most common definitions of phase shift for coupled channels.

Two different methods, derived from the Bethe-Salpeter equation, will be used. Both methods correspond to the Lippmann-Schwinger equation, but have different energies in the propagators. Of these, the Blankenbecler-Sugar method is probably the most commonly used. The other method has been recommended by Thompson because it includes relativistic expressions of the energies in the Lippmann-Schwinger equation. These methods will have slightly different parameters when they are fitted with experimental data.

Computers were slow when one first started with numerical calculations of the NN system, this led to the use of the R-matrix. The R-matrix is an elastic scattering reduction of the T-matrix. The R-matrix makes the computer program run faster, and works well for low energy problems where non-complex potentials can be used.

Kowalski recommended a new method to solve the Blankenbecler-Sugar equation numerically. He published this method in 1965 [2]. In the "Kowalski method", the Blankenbecler-Sugar equation is rewritten to yield an identical analytical equation, but not numerically equivalent, since the singularity in the propagator is introduced later in the numerical calculations.

Note that, it is often recommended to do a quick dimensional check of the equations before using them in a computer program. This way one can detect errors in an early phase, and save time.

4.1 Nucleon-nucleon binding energies

For a bound state $|\psi_B\rangle$ we have $E < 0$. The binding energies, can be found from the eigenvalues of the Schrödinger equation in the center of mass system. From eq(1.189) we have

$$\left[-\frac{1}{2\mu}\nabla^2 + V(\mathbf{r}) \right] \psi(\mathbf{r}) = E\psi(\mathbf{r}), \tag{4.1}$$

or written in momentum space as

$$\frac{k^2}{2\mu}\psi(k) + \frac{2}{\pi}\int_0^\infty dp\; p^2 V_l(k,p)\psi(p) = E\psi(k), \tag{4.2}$$

where we also have used partial wave decompositions of the potential. This integral can be calculated numerically by using Gaussian quadrature. In this approach we introduce N, which is the number of fixed lattice points. The integral can then be approximated by N weights ω_i and N mesh points x_i as

$$\frac{k^2}{2\mu}\psi(k) + \frac{2}{\pi}\sum_{i=1}^{N} \omega_i\; p_i^2 V(k,p_i)\psi(p_i) = E\psi(k). \tag{4.3}$$

Theoretically one would expect an error in this equation to be smaller if N is increased. Numerically this is not necessary the case, since the sum can create round-off error that blows up if large numbers in the sum cancel each other.

If we choose $k = p_j$, we have N equations and N unknown eigenvalues. We can therefore rewrite the problem as a matrix equation

$$H\Psi = E\Psi, \tag{4.4}$$

where

$$\Psi = \begin{pmatrix} \psi(p_1) \\ \psi(p_2) \\ \vdots \\ \psi(p_N) \end{pmatrix} \tag{4.5}$$

and

$$H_{ij} = \frac{p_j^2}{2\mu} + \frac{2}{\pi}\sum_{i=1}^{N} \omega_i\; p_i^2 V(p_j,p_i)\psi(p_i). \tag{4.6}$$

From eq(4.4) we will get N eigenvalues, but only the negative values will be eigenvalues of bound states. i.e. binding energies.

This integral can be solved with the Gauss-Legendre method. This function gives weights w_i and mesh points x_i, where x_i will be in the interval $[-1,1]$. Since the integral goes from 0 to ∞, we need to map these weights and mesh points. This mapping can be done with the tan function

$$p_i = C \tan\left(\frac{\pi}{4}(1+x_i)\right). \tag{4.7}$$

If we derivate p_i with respect to p_i and multiply it with the old weights, we get the new sett of weights as

$$\omega_i = C\frac{\pi}{4}\frac{w_i}{\cos^2\left(\frac{\pi}{4}(1+x_i)\right)}, \tag{4.8}$$

where C is a constant. In our case $C = 1000$ is a good choice, since only the mesons with mass less than 1000 MeV are included in the OBE-models.

The eigenvalues are calculated using an IMSL function called DEVLCG. This returns the eigenvalues in decreasing order for a general Hermitian matrix. These eigenvalues are then only some of the eigenvalues of the NN system. If we insert a complete set of states for both positive and negative energies in the Lippmann-Schwinger equation, the Green operator then becomes

$$\sum_i \frac{|i\rangle\langle i|}{E - \hat{H} \pm i\epsilon} = \sum_n \frac{|\varphi_n\rangle\langle\varphi_n|}{E - E_n} + \frac{1}{(2\pi)^3}\int_{-\infty}^{\infty} d^3q \frac{|\varphi_q\rangle\langle\varphi_q|}{E - E_q \pm i\epsilon}, \tag{4.9}$$

where the regulator for the bond states has been removed, since there are no poles for negative energies ($E < 0$), and E_n represents different binding energies. The other eigenvalues we find with this method are different E_q's from the continuous specter with $E > 0$.

In coupled channels the potentials are defined as a 2×2 matrix. In the potential codes written by R. Machleidt, this potential is usually defined as

$$V = \begin{pmatrix} V(3) & V(5) \\ V(6) & V(4) \end{pmatrix} = \begin{pmatrix} \langle l = j+1|V|l' = j+1\rangle & \langle l = j+1|V|l' = j-1\rangle \\ \langle l = j-1|V|l' = j+1\rangle & \langle l = j-1|V|l' = j-1\rangle \end{pmatrix}, \tag{4.10}$$

where $V(i)$ is the potential returned from the OBEP-routines (like the Bonn B and nna13).

We only get one bound state using the Bonn B potential. This is for the coupled $^3S_1$ - $^3D_1$ state where one of the eigenenergies is -2.2246 MeV. This state is only possible for a proton-neutron system, and the bound state is known as the deuteron. The experimental value of the binding energy is 2.224575 MeV [23] , which is almost exactly the same as the OBE-models give.

4.2 Solving the Blankenbecler-Sugar equation numerically

The "Minimal Relativity" equation is a version of of the Blankenbecler-Sugar equation, and has the same form as the non-relativistic Lippmann-Schwingerequation. To solve the "Minimal Relativity" equation we need the relation between the energy in the laboratory system $E_{\rm lab}$ and the one particle momentum k in the center of mass system. This is given as

$$E_{\rm lab} = \frac{k_{\rm lab}^2}{2m} = \frac{2k^2}{m} = \frac{1}{2}E_{\rm cm}. \tag{4.11}$$

The Minimal Relativity equation in the center of mass system was found in eq(1.136) to yield

$$\begin{aligned}\langle p|\hat{T}_{l'l}(E_k)|k\rangle &= \langle p|\hat{V}_{l'l}|k\rangle + \frac{2m}{\pi}\sum_{l''}\left[\mathcal{P}\int_0^\infty dq\; q^2\langle p|\hat{V}_{l'l''}|q\rangle\;\frac{1}{k^2-q^2}\;\langle q|\hat{T}_{l''l}(E_k)\;|k\rangle\right.\\ &\left. -ikm\langle p|\hat{V}_{l'l''}|k\rangle\langle k|\;\langle k|\hat{T}_{l''l}(E_k)\;|k\rangle\right].\end{aligned} \tag{4.12}$$

To solve the integral, we need a way to remove the singularity. Noting that

$$\int_{-\infty}^{\infty}\frac{dq}{k-q} = 0, \tag{4.13}$$

which can be rewritten as

$$\int_{-\infty}^{\infty}\frac{dq}{k-q} = \int_0^\infty\frac{dq}{k-q} + \int_{-\infty}^0\frac{dq}{k-q} = 2k\int_0^\infty\frac{dq}{k^2-q^2} = 0. \tag{4.14}$$

We can therefor remove the singularity in eq(4.12) by adding the zero term given as

$$-\frac{2m}{\pi}\;k^2\langle p|\hat{V}_{l'l''}|k\rangle\langle k|\hat{T}_{l''l}(E_k)\;|k\rangle\;\int_0^\infty\frac{dq}{k^2-q^2} = 0, \tag{4.15}$$

and when we don't any singularities in the integral, we can as well remove $\mathcal{P}$. We have

$$\begin{aligned}\langle p|\hat{T}_{l'l}|k\rangle &= \langle p|\hat{V}_{l'l}|k\rangle + \frac{2m}{\pi}\sum_{l''}\left[\int_0^\infty dq\frac{1}{k^2-q^2}\left(q^2\langle p|\hat{V}_{l'l''}|q\rangle\langle q|\hat{T}_{l''l}|k\rangle\right.\right.\\ &\left.\left. -k^2\langle p|\hat{V}_{l'l''}|k\rangle\langle k|\hat{T}_{l''l}|k\rangle\right) - ikm\langle p|\hat{V}_{l'l''}|k\rangle\langle k|\hat{T}_{l''l}|k\rangle\right],\end{aligned} \tag{4.16}$$

which is now a smooth integral. The integral can be calculated just like we did in the last section, where we used the Gauss-Legendre method with a remapping of the mesh points into the new interval $[0,\infty]$. The remapped mesh points are

$$q_i = C\tan\left(\frac{\pi}{4}(1+x_i)\right) \tag{4.17}$$

and their weights are

$$\omega_i = C\frac{\pi}{4}\frac{w_i}{\cos^2\left(\frac{\pi}{4}(1+x_i)\right)}, \tag{4.18}$$

where x_i and w_i are respectively the mesh points and the weights from Gauss-Legendre, and C is a constant, which should be chosen around 1000 MeV. Since half the mesh points will be less than C, and the integrand vary most in the region of the meson masses. Note that, all the mesons included in the OBE-model have masses in the region [0MeV, 1000MeV]. We can now rewrite eq(4.16) as

$$\begin{aligned}\langle p|\hat{V}_{l'l}|k\rangle &= \langle p|\hat{T}_{l'l}|k\rangle - \frac{2m}{\pi}\sum_{l''}\Bigg[\sum_{j=1}^{N}\frac{\omega_j q_j^2}{k^2-q_j^2}\langle p|\hat{V}_{l'l''}|q_j\rangle\langle q_j|\hat{T}_{l''l}|k\rangle \\ &\quad + \frac{2m}{\pi}\langle p|\hat{V}_{l'l''}|k\rangle\langle k|\hat{T}_{l''l}|k\rangle\sum_{j=1}^{N}\frac{\omega_j k^2}{k^2-q_j^2} \\ &\quad - ikm\langle p|\hat{V_{l'l''}}|k\rangle\langle k|\hat{T}_{l''l}|k\rangle\Bigg].\end{aligned} \tag{4.19}$$

Let us first look at the uncoupled states, and deal with the coupled states later.

4.2.1 Uncoupled states

The spin singlet and uncoupled spin triplet states have $N+1$ unknowns N from $\langle q_i|\hat{T}_l|k\rangle$ and one from $\langle k|\hat{T}_l|k\rangle$), where we have used the simplified notation $\hat{T}_l = \hat{T}_{ll}$ for uncoupled states. To solve this problem we therefor need $N+1$ equations. We define $q_{N+1} = k$, where k is the on-shell momentum. Eq(4.19) can now be solved, by letting p have all the values of q_i, e.i., $1 \leq i \leq (N+1)$. Eq(4.19) can then be rewritten, where we only have to solve the matrix equation

$$AT = V. \tag{4.20}$$

Here, A is a $(N+1)\times(N+1)$ matrix defined as

$$A_{i,j} = \delta_{i,j} - \langle q_i|\hat{V}_l|q_j\rangle u_j, \tag{4.21}$$

where δ is the Kronecker delta, and u is a $(N+1)$ vector defined as

$$u_j = \frac{2m}{\pi}\frac{\omega_j q_j^2}{q_{N+1}^2 - q_j^2} \qquad \text{for } 1 \leq j \leq N \tag{4.22}$$

and

$$u_{N+1} = -\frac{2m}{\pi}\sum_{j=1}^{N}\frac{\omega_j q_{N+1}^2}{q_{N+1}^2 - q_j^2} + imq_{N+1}. \tag{4.23}$$

If V is known, then A can ce calculated from V. From eq(4.20) we then have all we need to calculate the unknown T. Multiplying the inverse A-matrix (A^{-1}) from the left hand side of eq(4.20), we have

$$T = A^{-1}V. \tag{4.24}$$

To calculate the inverse of a matrix [1] I use a standard routine from the IMSL library called DLINCG. This function returns the inverse matrix of any complex matrix.

When the on-shell element of the T-matrix is known, the S-matrix can be calculated. From eq(1.137) we have

$$S_l = 1 - 2imk\, T^l_{N+1,N+1}. \tag{4.25}$$

The S-matrix relations to the phase shifts and inelasticities was found in eq(1.78) as

$$\eta_l\, e^{2i\delta_l} = S_l = |S_l|\, \exp\left(i\, \tan^{-1}\left[\frac{\mathcal{I}m\{S_l\}}{\mathcal{R}e\{S_l\}}\right]\right). \tag{4.26}$$

Separating the phase shifts and inelasticities yields

$$\eta_l = |S_l| \tag{4.27}$$

and

$$\delta_l = \frac{1}{2}\tan^{-1}\left(\frac{\mathcal{I}m\{S_l\}}{\mathcal{R}e\{S_l\}}\right). \tag{4.28}$$

4.2.2 Coupled states

For couplet channels we have to do things a little bit differently, since the S-matrix is given from the four unknowns $\langle k|\hat{T}_{ll}|k\rangle$, $\langle k|\hat{T}_{l'l}|k\rangle$, $\langle k|\hat{T}_{ll'}|k\rangle$ and $\langle k|\hat{T}_{l'l'}|k\rangle$, where we have used the short-notation "+" for $l = j+1$, and "−" for $l = j-1$. In this notation $V_{l,l'}$ can for example be written as $V_{+-} = \langle l = j+1|V|l' = j-1\rangle$.

First of all, we define a new $2(N+1)\times 2(N+1)$ potential matrix V_c as

$$V_c = \begin{pmatrix} \langle q_i|V_{++}|q_j\rangle & \langle q_i|V_{+-}|q_j\rangle \\ \langle q_i|V_{-+}|q_j\rangle & \langle q_i|V_{--}|q_j\rangle \end{pmatrix}. \tag{4.29}$$

The coupled $2(N+1)\times 2(N+1)$ matrix A_c will then be

$$A_c = \begin{pmatrix} \delta_{i,j} - \langle q_i|V_{++}|q_j\rangle u_j & -\langle q_i|V_{+-}|q_j\rangle u_j \\ -\langle q_i|V_{-+}|q_j\rangle u_j & \delta_{i,j} - \langle q_i|V_{--}|q_j\rangle u_j \end{pmatrix}, \tag{4.30}$$

where u_j and q_j are defined as before. By taking the inverse of A_c, we can determine the $2(N+1)\times 2(N+1)$ T-matrix. Since the S-matrix is calculated from the on-shell elements of the T-matrix, we only need to calculate the 2×2-matrix

$$\begin{pmatrix} \hat{S}^{J1}_{++} & \hat{S}^{J1}_{+-} \\ \hat{S}^{J1}_{-+} & \hat{S}^{J1}_{--} \end{pmatrix} = \begin{pmatrix} 1 & 0 \\ 0 & 1 \end{pmatrix} - imk \begin{pmatrix} \langle q_{N+1}|T_{++}|q_{N+1}\rangle & \langle q_{N+1}|T_{+-}|q_{N+1}\rangle \\ \langle q_{N+1}|T_{-+}|q_{N+1}\rangle & \langle q_{N+1}|T_{--}|q_{N+1}\rangle \end{pmatrix}. \tag{4.31}$$

[1] Computations of the inverse of a matrix, A, is a often needed in numerical calculations. This is usually done by LU factorization $A = LU$, where L is a lower triangular matrix and U is an upper triangular matrix. The inverse of U is a new upper triangular matrix and the inverse of L is a new lower triangular matrix. Both these inverses can be found straight forward. Finally $A^{-1} = U^{-1}L^{-1}$. Since we are using a dense matrix, we need to solve the general problem. This will involve N^3 numerical operations.

Finding phase shifts, inelasticities and the mixing factor in "Blatt-Biedenharn" or "bar" formalism are straight forward. All the formulas needed are given in eq(1.107)-eq(1.119).

If we calculate the phase shifts with these numerical methods and use the Bonn B potential, the results will be identical to the ones Machleidt published in [16]. Except for the $^3P_0$ state at 300 MeV, where a minus-sign has been lost. The right isoscalar np phase shift at 300 MeV with the Bonn B potential is -11.48 degrees. The first phase shifts and inelasticities calculated with the nna13 potential, are shown in fig 5.3.

The numerical method shown in this section can cause trouble if some of the mesh points are close to the on-shell momentum q_{N+1}. Because of numerical errors entering when we add and subtract large numbers which cancel each other. In this case the zero term (used to remove the singularity) will cancel the term from the propagator close to the singularity. Since both these terms will grow large for mesh points close to q_{N+1}, we will probably loose numerical precision. To avoid this problem I have implemented a function in my program that can determine when mesh points are close to q_{N+1}. Statistically the number of "bad" mesh points will grow with the number of mesh points. The numerical errors can be reduced by using the Kowalski method, where the singularity is removed later in the calculations. However, even for $N = 600$ the difference in phase shifts between these methods are of order 10^{-12} when using double precision. Since the singularity does not seem to be of much importance in numerically calculations of NN scattering, the standard method, derived in this section, can be used.

4.3 Solving the Thompson equation numerically

Technically, the only difference between solving the Thompson equation and the Blankenbecler-Sugar equation numerically, as done in last section, will be in the u_j and in the relation between S_l and T_l. The potential V will also be different. The two methods are based upon different approaches, and their OBEP parameters have been fitted differently to experimental data. The Thompson and Blankenbecler-Sugar equation are two different approximations of the Bethe-Salpeter equation. These two approaches are Lippmann-Schwinger equations with different propagators. This will again lead to different relations between the S- and T-matrix in these two cases. Also the zero term added to remove the singularity in the integral will be affected.

The u_j in eq(4.22) - eq(4.23) will, if we solve the Thompson equation, be replaced with

$$u_j = \frac{\omega_j q_j^2}{\pi} \left(\frac{\sqrt{q_j^2 + m^2} + \sqrt{q_{N+1}^2 + m^2}}{q_{N+1}^2 - q_j^2} \right) \qquad \text{for } 1 \leq j \leq N \tag{4.32}$$

and

$$u_{N+1} = -\frac{2}{\pi}\sum_{j=1}^{N}\frac{\omega_j q_{N+1}^2\sqrt{q_{N+1}^2+m^2}}{q_{N+1}^2-q_j^2} + iq_{N+1}\sqrt{q_{N+1}^2+m^2}. \tag{4.33}$$

The S-matrix from eq(4.25) will for uncoupled channels read

$$S_l = 1 - i2q_{N+1}\sqrt{q_{N+1}^2+m^2}\,T_{N+1,N+1}. \tag{4.34}$$

For coupled channels, a similar S-matrix equation yields

$$\begin{pmatrix} \hat{S}_{++}^{J1} & \hat{S}_{+-}^{J1} \\ \hat{S}_{-+}^{J1} & \hat{S}_{--}^{J1} \end{pmatrix} = \begin{pmatrix} 1 & 0 \\ 0 & 1 \end{pmatrix} - iq_{N+1}\sqrt{q_{N+1}^2+m^2}\begin{pmatrix} T_{++} & T_{+-} \\ T_{-+} & T_{--} \end{pmatrix}, \tag{4.35}$$

which will replace eq(4.31).

Solving the Thompson equation with the Kowalski method is done in a similar way as for the Blankenbecler-Sugar equation.

The phase shifts we find with the Thompson method can be fitted to reproduce the experimental in the same accuracy as we had for Blankenbecler-Sugar equation.

4.4 The R-matrix

Sometimes it is preferable to calculate the R-matrix, also known as the "K-matrix" instead of using the T-matrix. We are interested in defining a practical $\hat{R}$ which is real, but still obey some of the similar relations as $\hat{T}$. In operational form the T-matrix is defined as

$$\hat{T} = \hat{V} + \hat{V}\frac{1}{E-\hat{H}_0+i\varepsilon}\hat{T}. \tag{4.36}$$

A corresponding expression for the real R-matrix is defined as

$$\hat{R} = \hat{V} + \hat{V}\mathcal{P}\left\{\frac{1}{E-\hat{H}_0+i\varepsilon}\right\}\hat{R}. \tag{4.37}$$

The relations between T and R can be found by eliminating V in the two equations above. The complex transition matrix T can now be expressed as

$$\hat{T} \equiv \hat{R} - i\pi\hat{R}\delta(E-\hat{H}_0)\hat{T}. \tag{4.38}$$

The R-matrix will make the program much faster, since all the matrix equations are now real instead of complex. The R-matrix has been widely used, but since an accurate calculation of the on-shell T-matrix is done within seconds, it's not a "must" anymore. For example, the Bonn B potential, going from T-matrix to R-matrix calculations, will not even make the computer-program twice as fast.

The rate in which we save time by using the R-matrix is also dependent on the potential we use. The time to make the potential matrix $V_{l'l}(p,k)$ will be of order

$N \times N \times$"number of operations done in the potential", while computing the inverse of a $N \times N$ matrix, needed to calculate the T-matrix from the potential, will be of order N^3. We see that if the potential includes more than N operations, the potential routine will become the most time consuming part of the phase shifts calculations. Today the low energy region, where we can use the R-matrix, is very well simulated, while the higher energy potentials are still to be developed. Some of these high energy potentials are complex, because they include inelastic processes in the intermediate states, i.e., we have to use the T-matrix.

Like we had the minimal relativity equation eq(4.12) for the complex T-matrix, we now find a similar equation for the real R-matrix. From the definition eq(4.37), the R-matrix elements in the Blankenbecler-Sugar equation reads

$$\langle p|\hat{R}_{l'l}|k\rangle = \langle p|\hat{V}_{l'l}|k\rangle + \frac{2m}{\pi}\sum_{l''}\mathcal{P}\int_0^\infty dq\, q^2\langle p|\hat{V}_{l'l''}|q\rangle\,\frac{1}{k^2-q^2}\langle q|\hat{R}_{l''l}|k\rangle. \quad (4.39)$$

To find the phase shifts from the on-shell the Blankenbecler-Sugar R-matrix elements we rewrite the eq(4.38) in partial waves. For uncoupled channels we have

$$\langle k|\hat{R}_l\ |k\rangle = \langle k|\hat{T}_l\ |k\rangle + imk\langle k|\hat{R}_l\ |k\rangle\langle k|\hat{T}_l\ |k\rangle, \quad (4.40)$$

where we used the short notation $l = ll$. If we also make use of the relation for elastic scattering found in eq(1.137)

$$2imk\ \langle k|\hat{T}_l\ |k\rangle = 1 - e^{2i\delta_l} = e^{i\delta_l}\Big(e^{-i\delta_l} - e^{i\delta_l}\Big), \quad (4.41)$$

the phase shifts δ for the uncoupled states can be found straight forward by rewriting eq(4.40) as

$$\begin{aligned}\langle k|\hat{R}_l\ |k\rangle &= \frac{\langle k|\hat{T}_l\ |k\rangle}{1 - imk\langle k|\hat{T}_l\ |k\rangle} \\ &= \frac{\frac{1}{2imk}(1 - e^{2i\delta_l})}{\frac{1}{2}(1 + e^{2i\delta_l})} \\ &= -\frac{1}{mk}\tan\delta_l, \end{aligned} \quad (4.42)$$

where we used eq(4.41). The phase shifts will for the spin singlet states be

$$\tan\Big[\ {}^0\delta^J(\mathrm{E_{lab}})\Big] = -\ km\ {}^0R^J(k,k), \quad (4.43)$$

and for the uncoupled spin triplet states it will be

$$\tan\Big[\ {}^1\delta^J(\mathrm{E_{lab}})\Big] = -\ km\ {}^1R^J(k,k). \quad (4.44)$$

If we use the Blatt and Biedenharn convention for the coupled states, we similarly find

$$\tan \bar{\delta}^J_{\mp}(\mathrm{E_{lab}}) = -\frac{1}{2}km\left[R^J_{--} + R^J_{++} \pm \frac{R^J_{--} + R^J_{++}}{\cos(2\bar{\epsilon}_J)}\right] \tag{4.45}$$

and

$$\tan\left(2\bar{\epsilon}_J(\mathrm{E_{lab}})\right) = \frac{2R^J_{+-}}{R^J_{--} - R^J_{++}}, \tag{4.46}$$

where $\bar{\epsilon}$ is the mixing factor. The R-matrix from the Thompson equation can can be calculated in the same way.

4.5 The Kowalski method

The Kowalski method [2] is an alternative to the standard method used earlier to calculate the T-matrix numerically. In the Kowalski method we rewrite the Lippmann-Schwinger equation, so that the singularity will appear later in the numerical calculations. This method can be used for the minimal relativity equation from eq(4.12). For uncoupled channels, using the simplified notation $T_l = T_{ll}$ and $V_l = V_{ll}$, we have

$$\langle p|\hat{T}_l|k\rangle = \langle p|\hat{V}_l|k\rangle + \frac{2m}{\pi}\mathcal{P}\int_0^\infty dq\; q^2 \frac{\langle p|\hat{V}_l|q\rangle}{k^2 - q^2}\langle q|\hat{T}_l|k\rangle - ikm\langle p|\hat{V}_l|k\rangle\langle k|\hat{T}_l|k\rangle. \tag{4.47}$$

If we use $p = k$ in eq(4.47) and multiply it with $\frac{\langle p|\hat{V}_l|k\rangle}{\langle k|\hat{V}_l|k\rangle}$, we get

$$\begin{aligned}\frac{\langle p|\hat{V}_l|k\rangle}{\langle k|\hat{V}_l|k\rangle}\langle k|\hat{T}_l|k\rangle &= \langle p|\hat{V}_l|k\rangle + \frac{2m}{\pi}\mathcal{P}\int_0^\infty dq\; q^2 \frac{\langle p|\hat{V}_l|k\rangle\langle k|\hat{V}_l|q\rangle}{\langle k|\hat{V}_l|k\rangle}\frac{1}{k^2 - q^2}\langle q|\hat{T}_l|k\rangle \\ &\quad -ikm\langle p|\hat{V}_l|k\rangle\langle k|\hat{T}_l|k\rangle. \end{aligned}\tag{4.48}$$

By subtracting eq(4.48) from eq(4.47) we obtain

$$\begin{aligned}\langle p|\hat{T}_l(E)|k\rangle &= \frac{\langle p|\hat{V}_l|k\rangle}{\langle k|\hat{V}_l|k\rangle}\langle k|\hat{T}_l(E)|k\rangle \\ &\quad +\frac{2}{\pi}\int_0^\infty dq\; q^2\left[\langle p|\hat{V}_l|q\rangle - \frac{\langle p|\hat{V}_l|k\rangle\langle k|\hat{V}_l|q\rangle}{\langle k|\hat{V}_l|k\rangle}\right]\frac{1}{k^2 - q^2}\langle q|\;\hat{T}_l(E)\;|k\rangle,\end{aligned}\tag{4.49}$$

where we have removed the principal value $\mathcal{P}$, since there are no singularities in this integrand. The integral is calculated by using a remapping of the Gauss-Legendre mesh points to the interval $[0, \infty]$. We let p have all the values q_i for $1 \le i \le N$:

$$\begin{aligned}\langle q_i|\hat{T}_l(E)|k\rangle &= \frac{\langle q_i|\hat{V}_l|k\rangle}{\langle k|\hat{V}_l|k\rangle}\langle k|\hat{T}_l(E)|k\rangle + \frac{2m}{\pi}\sum_{j=1}^N \omega_j q_j^2\Bigg[\langle q_i|\hat{V}_l|q_j\rangle \\ &\quad -\frac{\langle q_i|\hat{V}_l|k\rangle\langle k|\hat{V}_l|q_j\rangle}{\langle k|\hat{V}_l|k\rangle}\Bigg]\frac{1}{k^2 - {q^2}_j}\langle q_j|\;\hat{T}_l(E)\;|k\rangle.\end{aligned}\tag{4.50}$$

We have now $N+1$ unknowns and N equations. To solve these equations, we divide eq(4.50) by $\langle k|\hat{T}_l(E)|k\rangle$. We will then only have N unknowns with respect to $\langle q_i|\hat{T}_l(E)|k\rangle/\langle k|\hat{T}_l(E)|k\rangle$, which yields

$$\begin{aligned}\frac{\langle q_i|\hat{T}_l(E)|k\rangle}{\langle k|\hat{T}_l(E)|k\rangle} &= \frac{\langle q_i|\hat{V}_l|k\rangle}{\langle k|\hat{V}_l|k\rangle} + \frac{2m}{\pi}\sum_{j=1}^{N}\frac{\omega_j q_j^2}{(k^2-q_j^2)}\Bigg[\langle q_i|\hat{V}_l|q_j\rangle \\ &\quad - \frac{\langle q_i|\hat{V}_l|k\rangle\langle k|\hat{V}_l|q_j\rangle}{\langle k|\hat{V}_l|k\rangle}\Bigg]\frac{\langle q_j|\ \hat{T}_l(E)\ |k\rangle}{\langle k|\hat{T}_l(E)|k\rangle}. \end{aligned} \tag{4.51}$$

The unknown $\langle k|\hat{T}_l(E)|k\rangle$ can be determined by eq(4.47), and substituting

$$\langle q_i|\hat{T}_l(E)|k\rangle = \frac{\langle q_i|\hat{T}_l(E)|k\rangle}{\langle k|\hat{T}_l(E)|k\rangle}\langle k|\hat{T}_l(E)|k\rangle \tag{4.52}$$

in the minimal relativity equation from eq(4.47). By doing this, the singularity will enter the equations again. This singularity can be handled as before, where we added the zero term from eq(4.15), which will remove the singularity in the integrand. Finally, we let $p=k$, and the unknown $\langle k|\hat{T}_l|k\rangle$ can be calculated from

$$\langle k|\hat{T}_l|k\rangle = \frac{\langle k|\hat{V}_l|k\rangle}{1-\frac{2m}{\pi}\sum_{j=1}^{N}\frac{\omega_j}{k^2-q_j^2}\left[q_j^2\langle k|\hat{V}_l|q_j\rangle\frac{\langle q_j|\hat{T}_l|k\rangle}{\langle k|\hat{T}_l|k\rangle} - k^2\langle k|\hat{V}_l|k\rangle\right] + ikm\langle k|\hat{V}_l|k\rangle}. \tag{4.53}$$

This equation has two terms with singularities in the sum. These terms will be large when a mesh point q_j is close to k. This can cause a numerical loss in precision in the sum. The numerical error will generally increase with N, because more mesh points will be nearer to the singularity. A good guess however, is that this method will be better than the standard method for large N, since numerical errors are more likely to grow if they are introduced early in calculations.

To calculate eq(4.51), we can build up a matrix equation

$$T = B^{-1}U, \tag{4.54}$$

where B is a $N\times N$ matrix. Both T and U are vectors of length N. We define the off-shell T-matrix elements as

$$T_i = \frac{\langle q_i|\hat{T}_l|k\rangle}{\langle k|\hat{T}_l|k\rangle}, \tag{4.55}$$

which is calculated from eq(4.54) using

$$U_i = \frac{\langle q_i|\hat{V}_l|k\rangle}{\langle k|\hat{V}_l|k\rangle} \tag{4.56}$$

and

$$B_{i,j} = \delta_{i,j} - \Big[\langle q_i|\hat{V}_l|q_j\rangle - U_i\langle k|\hat{V}_l|q_j\rangle\Big]q_j^2 s_j, \tag{4.57}$$

where

$$s_j = \frac{2m}{\pi}\frac{\omega_j}{k^2 - q_j^2} \qquad \text{for } 1 \le j \le N \tag{4.58}$$

The on-shell T-matrix is then found from eq(4.53) to yield

$$\langle k|\hat{T}_l|k\rangle = \frac{\langle k|\hat{V}_l|k\rangle}{1 + \sum_{j=1}^{N}\left[q_j^2\langle k|\hat{V}_l|q_j\rangle T_j - k^2\langle k|\hat{V}_l|k\rangle\right]s_j + ikm\langle k|\hat{V}_l|k\rangle} \tag{4.59}$$

This equation can be solved straight-forwardly. Note that, we can use the same methods as before to calculate phase shifts and inelasticities from the known $\langle k|\hat{T}_l|k\rangle$.

The Kowalski method is similar for coupled channels, but instead of using the numbers $\langle k|\hat{V}_l|k\rangle$ and $\langle k|\hat{T}_l|k\rangle$, we have to use the 2×2 matrices $\langle k|\hat{V}_{l'l}|k\rangle$ and $\langle k|\hat{T}_{l'l}|k\rangle$. This implies that we need to calculate the inverse of matrices, instead of the inverse of numbers as we did above.

Comparing the Kowalski method with the standard method used in [3], we find the numerical results to be almost identical. It turns out that for my code the standard method is only about 1% faster than the Kowalski method. This difference is too small to recommend one method over the other.

The similarities between the two methods can be seen in table 4.1. Where the $^1S_0$ phase shifts are shown for the Bonn B potential, at 25 MeV in the laboratory system, using the minimal relativity equations. The phase shifts are given with 14 digits after comma. This high precision is interesting when analyzing numerical methods, but doesn't make physical sense. Since, the Bonn B potential is based on theories and parameters of much less precision.

In table 4.1 "A" is the number of mesh points q_i in the region $q_{N+1} \pm$ 5.0E-2 MeV, "B" is the number of mesh points in the region $q_{N+1} \pm$ 5.0E-3 MeV and "C" is the number of mesh points in the region $q_{N+1} \pm$ 5.0E-4 MeV.

"Time" is the amount of time used to run the program which calculates the phase shifts for 15 different lab energies.

"*" denotes the cases where the S-matrix is not exactly unitary for the standard method. The Kowalski method on the other hand, is unitary in those cases. However, this can also happen for the Kowalski method. These errors are small. Biggest inelasticity error observed was 5.0E-14.

"s" denotes that N (the number of mesh points) where specially selected due to its interesting configuration of mesh points close to q_{N+1}.

If we assume that the numerical errors in phase shifts calculations are totally random, we see from table 4.1 that 50.7167474578 is a good estimate of the phase shift, i.e., we have 12 counting digits. With this in mind, the number of correct reproduced digits, of the phase shifts in table 4.1, have bin plotted in fig 4.1.

N	(A)(B)(C)	Kowalski		Brown and Jackson		Difference
		Phase shift	time	Phase shift	time	Phase shift
3	(0)(0)(0)	71.62345689430250	0.04s	71.62345689430260	0.04s	1.0E-13
5	(0)(0)(0)	41.46263918236210	0.05s	41.46263918236210	0.05s	0
10	(0)(0)(0)	51.08156285146330	0.17s	51.08156285146330	0.15s	0
25	(1)(0)(0)	50.71696055173802	0.90s	50.71696055173803	0.89s	1.0E-14
50	(0)(0)(0)	50.71674962783273	3.09s	50.71674962783273	3.09s	0
75	(0)(0)(0)	50.71674749296322	7.11s	50.71674749296330	7.00s	8.0E-14
100	(0)(0)(0)	50.71674746062610	14.32s	50.71674746062610	13.55s	0
150	(2)(0)(0)	50.71674746145212	–	50.71674746145210	–	2.0E-14
200	(0)(0)(0)	50.71674745769040	–	50.71674745769050	–	1.0E-13
250	(0)(0)(0)	50.71674745807750	–	50.71674745807711	–	3.9E-13
300	(1)(0)(0)	50.71674745539690	–	50.71674745539662	–	2.8E-13
350	(1)(0)(0)	50.71674745671981	–	50.71674745671972	–	1.1E-13
400	(1)(0)(0)	50.71674746084243	–	50.71674746084244	–	1.0E-14
450	(2)(0)(0)	50.71674745973450	–	50.71674745973450	–	0
500	(1)(0)(0)	50.71674745780814	–	50.71674745780800	–	1.4E-13
550	(1)(0)(0)	50.71674745755723	–	50.71674745755700	–	2.3E-13
600	(3)(0)(0)*	50.71674745788354	1266s	50.71674745788430	1257s	7.6E-13
650	(0)(0)(0)	50.71674745747293	–	50.71674745747272	–	2.1E-13
700	(3)(0)(0)*	50.71674745725370	–	50.71674745725340	–	3.0E-13
750	(1)(0)(0)	50.71674745849564	–	50.71674745849570	–	6.0E-14
800	(0)(0)(0)	50.71674745901132	–	50.71674745783083	–	1.2E-9
850	(1)(0)(0)	50.71674745774120	–	50.71674745774120	–	0
789	s(3)(1)(1)	50.71674745784843	2727s	50.71674745784860	2624s	1.7E-13
801	(1)(0)(0)	50.71674745781930	–	50.71674745781930	–	0
802	(2)(0)(0)	50.71674745762290	–	50.71674745762272	–	2.8E-13
803	(2)(0)(0)	50.71674745783440	–	50.71674745783370	–	7.0E-13
821	s(0)(0)(0)	50.71674745783100	3352s	50.71674745783083	3182s	1.7E-13
843	s(3)(2)(0)*	50.71674746936084	–	50.71674747021500	–	8.5E-10

Table 4.1: *Accuracy and computer running time using two different numerical methods, with double precision and the Bonn B potential, to calculate the* $^1S_0$ *phase shifts from isoscalar np scattering using the minimal relativity equation.*

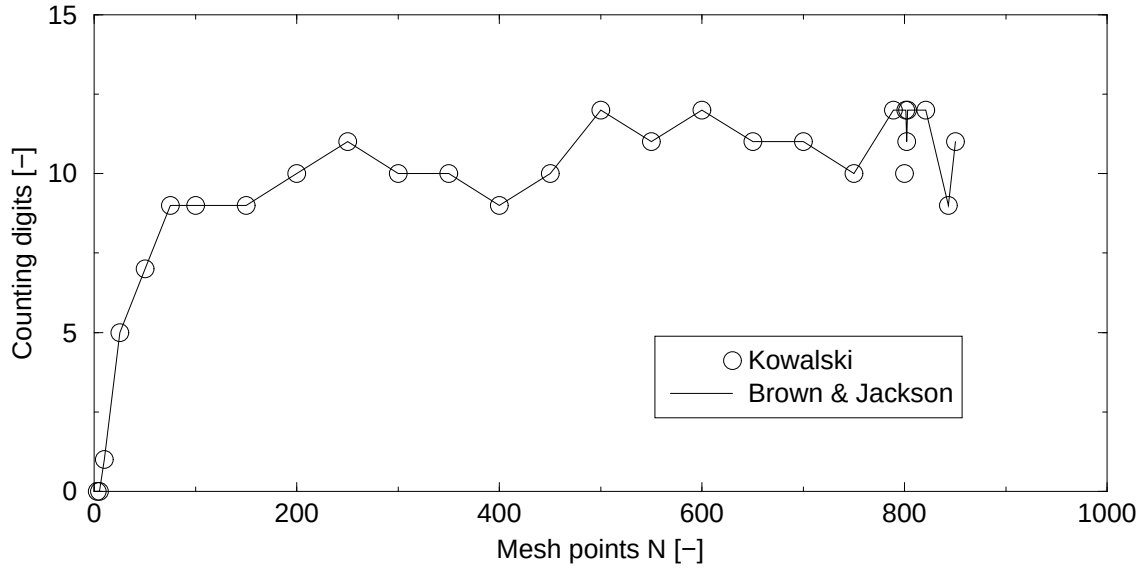

Figure 4.1: *Phase shifts in table 4.1 are compared with a 12 digit phase shift, which is believed to be numerically correct.*

With mesh points less than 30, it seems that the difference between the phase shifts for the two methods is less than 1.0E-13. It appears that the difference is slowly increasing with the number of mesh points. This is probably due to more numerical errors, since the number of calculations done are increasing rapidly with N ($\sim N^3$). For calculations with 600 mesh points the difference was found to be less than 1.0E-12. With N=843 the difference was in the order of 1.0E-7.

Numerical errors can be divided into two parts. One due to the to the accuracy in the integral calculation. This error will usually be less as N increase, and will depend on the potential. The other part is due to the numerical round-off errors. This type of error will be dependent of the singularity in the integrand, but more or less independent of the potential. Statistically will the numerical round-off errors increase with N, since more mesh points are lying close to the singularity.

If we assume that the two methods generate independent errors, then the difference in the phase shifts will give us information about the size of the numerical round-off errors arising from the singularity in the integral.

In the cases where the difference is 0, we clearly see that the assumption that the two methods produces independent round-off errors isn't always very good. For some numerical reason the phase shifts will often turn out to be identical down to the last digit, even at large N. To get the best estimate of the size of the numerical error one should therefore study each N at many energy samples. In table 4.1, the first obvious round-off errors accrues in the Kowalski method for N=800, where we have no mesh points close to (q_{N+1}). This is therefore not the situation the Kowalski method was created for. The standard method gives very good results in this case, and we clearly see the numerical round-off errors accrues in the phase shifts. For N=843 both methods involve large round-off errors. In this case there are two mesh points in the range of $(q_{N+1})\pm$5.0E-3. This is a situation Kowalski had in mind when

he recommended his method, and it is interesting to see that Kowalski was the best method in this case.

These errors don't always become big. Statistically it seems like if something goes wrong, then a lot more will go wrong. For $800 \leq N \leq 850$, about 25% where such cases where the round-off errors are relative large.

At N=789 there was one mesh point in the range of q_{N+1}±5.0E-4. This is the "worst" mesh point for $600 < N < 850$. The Kowalski method handle this situation very well, but so did the standard method. Both managed to reproduce the 12 first digits of the phase shift. So the importance of a mesh point hitting close to the singularity seems to be small.

In summary, the phase shifts in table 4.1 and fig 4.1 illustrates the facts:

- These methods are not only analytically equivalent, they are almost numerical identical too. With the Bonn B potential, one can trust about 7 digits after the comma using mesh point between 200 and 600. But N=60 is good enough compared with the accuracy in the Bonn B potential.

- One should be careful using a large N (especially for N larger than 700), since this can reproduce large numerical errors. If one needs to calculate higher precisions the phase shifts, one can look at an average of many samples with different N, or choose variables with better precision in the computer program, i.e., better than double precision.

- Mesh points ending up as close as 5.0E-4 MeV to the singularity in the propagator seems to be of less importance for the phase shift precision.

- The two methods use almost the same time to calculate the T-matrix.

These methods are almost numerical identical, and it is really hard to recommend one method over the other. Looks like Kowalski was a little bit too worried about the numerical errors. The same can be said about Brown and Jackson. In their book "Nucleon-Nucleon interaction" they also recommend the Kowalski method. Kowalski developed this method in 1965. But, even when Brown and Jackson recommended it in their book written in 1976, computers that could handle more than 100 mesh points didn't exist. And they wouldn't know if the problem was relevant for more accurate calculations.

Chapter 5

Nucleon-Nucleon Scattering Up To 1 GeV In Free Space

For NN scattering at low-energies, the only inelastic processes possible are due to Bremsstrahlung ($N + N \rightarrow N + N + \gamma$). Such inelasticities are relatively small compared with the contribution arising from processes involving strong coupling constants, which are possible above 300 MeV in the laboratory system. At this energy the nucleons have enough energy to create a free pion ($N + N \rightarrow N + N + \pi$). At even higher energies other mesons can also be created in the process. At 600 MeV creation of two free pions are possible, but, at this energy we also have enough energy to excitate one of the nucleons into a $\triangle(1232)$. The isobar excitations of nucleons, as we will discussed later, can be used to explain the most decisive inelastic signature to the elastic and inelastic scattering parameters.

From fig 5 we see how the inelastic cross section is dependent on the NN scattering energies. There exist four $\triangle$-barions (isobars) and they come from the spin-

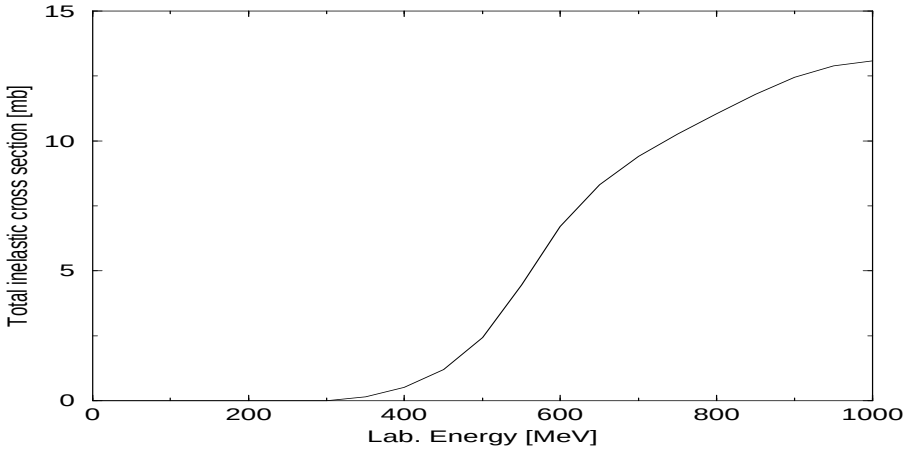

Figure 5.1: *The inelastic cross section for isoscalar np scattering as calculated from the nna13 potential.*

$\frac{3}{2}$ and isospin-$\frac{3}{2}$ barion group. These isobars can be expressed in terms of quarks as $\triangle^- = \mathrm{ddd}(T_3 = -3/2)$, $\triangle^- = \mathrm{udd}(T_3 = -1/2)$, $\triangle^- = \mathrm{uud}(T_3 = 1/2)$ and

$\triangle^{++} = \mathrm{uuu}(T_3 = 3/2)$. Where T_3 is the isospin projection, and is related to the isobars electrical charge. In the isospin-$\frac{1}{2}$ barion doublet we have $n(T_3 = -1/2)$ and $p(T_3 = 1/2)$.

Due to isospin addition rules, the process, $N + N \to N + \triangle$ is only possible for two-nucleon states with isospin $T = 1$. Above 1.2 GeV in the laboratory system, both the nucleons can be excited, i.e. $(N + N \to \triangle + \triangle)$, which will be possible for NN states with both $T = 0$ and $T = 1$. The isobar is a highly unstable particle with a natural width $\Gamma_\triangle \approx 120$ MeV, which is much larger than the spacing between nuclear levels. It is therefore unclear whether the isobar should be treated as an elementary fermion, a three-quark cluster or as a pion-nucleon resonance.

If we include the isobar degrees of freedom in the intermediate states in NN scattering, the isobar width can be used to explain most of the inelasticities up to 1 GeV through dibarion resonances.

5.1 Including isobar degrees of freedom

To build a meson theory, which will work well at laboratory energies above 300 MeV, one should include isobar degrees of freedom in the intermediate states. The isobar is here treated as a nuclear constituent in the same way as protons and neutrons. Since the isobars are carriers of spin and isospin $\frac{3}{2}$ and the nucleons have spin and isospin $\frac{1}{2}$, the only mesons which can couple nucleons and isobars (included in the OBE model), are the π- and ρ-mesons.

The new isobar degrees of freedom will yield the coupled non-relativistic T-matrix equation:

$$\begin{aligned} T_{NN,NN} = V_{NN,NN} &- \int_{-\infty}^{\infty} d^3k \frac{V_{NN,NN} T_{NN,NN}}{\varepsilon_{NN} - \varepsilon^0_{NN} + i\epsilon} - \int_{-\infty}^{\infty} d^3k \frac{V_{NN,N\triangle} T_{N\triangle,NN}}{\varepsilon_{N\triangle} - \varepsilon^0_{NN} + i\epsilon} \\ &- \int_{-\infty}^{\infty} d^3k \frac{V_{NN,\triangle\triangle} T_{\triangle\triangle,NN}}{\varepsilon_{\triangle\triangle} - \varepsilon^0_{NN} + i\epsilon}. \end{aligned} \tag{5.1}$$

Note that, the equation above includes both direct and exchange terms. To calculate $T_{NN,NN}$ exact, we need to evaluate the unknown $T_{N\triangle,NN}$ and $T_{\triangle\triangle,NN}$, which can be found in a similar way as

$$\begin{aligned} T_{N\triangle,NN} = V_{N\triangle,NN} &- \int_{-\infty}^{\infty} d^3k \frac{V_{N\triangle,NN} T_{NN,NN}}{\varepsilon_{NN} - \varepsilon^0_{NN} + i\epsilon} - \int_{-\infty}^{\infty} d^3k \frac{V_{N\triangle,N\triangle} T_{N\triangle,NN}}{\varepsilon_{N\triangle} - \varepsilon^0_{NN} + i\epsilon} \\ &- \int_{-\infty}^{\infty} d^3k \frac{V_{N\triangle,\triangle\triangle} T_{\triangle\triangle,NN}}{\varepsilon_{\triangle\triangle} - \varepsilon^0_{NN} + i\epsilon} \end{aligned} \tag{5.2}$$

and

$$\begin{aligned} T_{\triangle\triangle,NN} = V_{\triangle\triangle,NN} &- \int_{-\infty}^{\infty} d^3k \frac{V_{\triangle\triangle,NN} T_{NN,NN}}{\varepsilon_{NN} - \varepsilon^0_{NN} + i\epsilon} - \int_{-\infty}^{\infty} d^3k \frac{V_{\triangle\triangle,N\triangle} T_{N\triangle,NN}}{\varepsilon_{N\triangle} - \varepsilon^0_{NN} + i\epsilon} \\ &- \int_{-\infty}^{\infty} d^3k \frac{V_{\triangle\triangle,\triangle\triangle} T_{\triangle\triangle,NN}}{\varepsilon_{\triangle\triangle} - \varepsilon^0_{NN} + i\epsilon}, \end{aligned} \tag{5.3}$$

where

$$\varepsilon_{NN} = 2E_{\rm N}, \tag{5.4}$$

$$\varepsilon_{N\triangle} = E_{\rm N} + E_{\triangle}, \tag{5.5}$$

$$\varepsilon_{\triangle\triangle} = 2E_{\triangle}, \tag{5.6}$$

$$\mathrm{E}_{\triangle} = \frac{k^2}{2m_{\triangle}} + m_{\triangle} \tag{5.7}$$

and

$$\mathrm{E}_{\rm N} = \frac{k^2}{2m_{\rm N}} + m_{\rm N}, \tag{5.8}$$

where we have included the particles masses in the single particle energies. This is done to account for the kinetic energy lost in excitations of nucleons to isobars. The isobar mass is $m_{\triangle} = 1232$ MeV, and the on-shell energy is given as

$$\varepsilon^0_{NN} = 2\left(\frac{q_0^2}{2m_{\rm N}} + m_{\rm N}\right). \tag{5.9}$$

We can not solve these equations exact, since we don't know much about the interaction Lagrangians including isobars in both the initial and the final state. Thus, we can't construct the transition potentials $V_{N\triangle,\triangle N}$, $V_{N\triangle,\triangle\triangle}$ and $V_{\triangle\triangle,\triangle\triangle}$. For interactions where the $N\triangle$ vertexes involve mesons, which can be either the π- or the ρ-meson, one obtains the following interaction Lagrangians [24, 25]:

$$\mathcal{L}_{N\triangle\pi} = -\frac{f_{N\triangle\pi}}{m_\pi}\bar{\psi}\mathbf{T}\psi\partial_\mu\phi^{(\pi)} + \mathrm{H.}c. \tag{5.10}$$

and

$$\mathcal{L}_{N\triangle\rho} = i\frac{f_{N\triangle\rho}}{m_\rho}\bar{\psi}\ \gamma^5\gamma^\mu\ \mathbf{T}\psi^\nu(\partial_\mu\phi^{(\rho)}_\nu - \partial_\nu\phi^{(\rho)}_\mu) + \mathrm{H.}c., \tag{5.11}$$

where $\mathbf{T}$ is the isospin transition operator, ψ_μ is the Rarita-Schwinger field [26] describing the spin-$\frac{3}{2}$ $\triangle$ particle and H.c. stands for the Hermitian conjugate. The coupling constant for the π-meson is given by a relation obtained from the non-relativistic quark model [36] as

$$f_{N\triangle\pi} = \frac{6}{5}\sqrt{2}f_{NN\pi} = \frac{6}{5}\sqrt{2}g_{NN\pi}\frac{m_\pi}{2m_N}, \tag{5.12}$$

and similar for the ρ-meson we have

$$f^2_{N\triangle\rho} = \frac{f^2_{N\triangle\pi}}{f^2_{NN\pi}}g^2_{NN\rho}\frac{m^2_\rho}{4m^2_N}\left(1 + \frac{f_{NN\rho}}{g_{NN\rho}}\right)^2, \tag{5.13}$$

with

$$f_{NN\rho} = \sqrt{4\pi}g_{NN\rho}\frac{m_\rho}{m_N}\left(1 + \frac{f_{NN\rho}}{g_{NN\rho}}\right), \tag{5.14}$$

which is predicted from the quark model (see [1]). Implying $g_{NN\rho} = 0.95$ and $f_{NN\rho}/g_{NN\rho} = 6.1$. The relation $f_{N\triangle\rho}/f_{NN\pi} = 1.7$ is too small compared to the

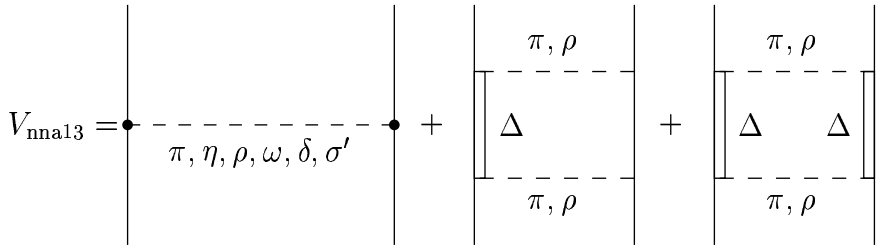

Figure 5.2: *The nna13 potential, which includes the most important diagrams for isovector NN scattering below 1 GeV. The nna13 potential includes the charge dependent OBEP called the cdbonn potential. The first diagram on the right-hand-side is a redefined OBEP (cdbonn), the rest are two-meson exchange diagrams involving intermediate isobars. For isoscalar np scattering the second diagram on the right-hand-side is not allowed.*

experimental values of the isobar width, which gives $f_{N\triangle\rho}/f_{NN\pi} = 2.15$. A monopole form factor, given in eq(2.9), is included at each vertex to regularize the meson propagators occurring in the new potentials involving isobars.

The contributions to the total NN interactions from e.g. $V_{N\triangle,N\triangle}$ is found to be rather small [37]. If we assume that the unknown transition potentials can be neglected in the total NN interactions, the coupled set of equations transition matrix in eq(5.1) and eq(5.3) can be rewritten as

$$T_{N\triangle,NN} \approx V_{N\triangle,NN} - \int_{-\infty}^{\infty} d^3k \frac{V_{N\triangle,NN} T_{NN,NN}}{\varepsilon_{NN} - \varepsilon^0_{NN} + i\epsilon} \tag{5.15}$$

and

$$T_{\triangle\triangle,NN} \approx V_{\triangle\triangle,NN} - \int_{-\infty}^{\infty} d^3k \frac{V_{\triangle\triangle,NN} T_{NN,NN}}{\varepsilon_{NN} - \varepsilon^0_{NN} + i\epsilon}. \tag{5.16}$$

With these approximations we are able to solve eq(5.1) with respect to $T_{NN,NN}$, however, these equations can not be solved with the same numerical methods as used in the low-energy scattering. An alternative approach with a potential including isobar channels in the intermediate states has been made. This is done by moving the isobar channels from the minimal relativity equation and into the potential. The nna13 potential is such a potential.

5.2 The nna13 potential

The nna13 potential is defined as

$$V_{\text{nna13}} = V'_{\text{cdbonn}} - \int_{-\infty}^{\infty} d^3k \frac{V_{NN,N\triangle} V_{N\triangle,NN}}{\varepsilon_{N\triangle} - \varepsilon^0_{NN}} - \int_{-\infty}^{\infty} d^3k \frac{V_{NN,\triangle\triangle} V_{\triangle\triangle,NN}}{\varepsilon_{\triangle\triangle} - \varepsilon^0_{NN}}, \tag{5.17}$$

which uses an OBEP part (cdbonn) and two box diagram parts from the two-meson exchanges involving isobars. This is illustrated schematically in fig 5.2.

We see that the nna13 potential is energy dependent, due to the ε^0_{NN} term in eq(5.17) From the ε^0_{NN} dependence of the nna13 potential we see that this potential will be energy dependent. The cdbonn potential part uses a redefined σ'-meson, since we have separated some of the two-meson exchange diagrams (including isobars) from the fictive σ-meson (see fig 2.2). The nna13 potential will therefore yield the minimal relativity equation, and we have

$$T_{NN,NN} = V_{nna13} - \int_0^\infty dk\ k^2 \frac{V_{nna13} T_{NN,NN}}{\varepsilon_{NN} - \varepsilon^0_{NN} + i\epsilon}, \tag{5.18}$$

which can be calculated the same way as in the lower energy scattering region, except that we will also need inelasticities along with the phase shifts to describe each partial wave. The nna13 potential can reproduce NN scattering data up to 1 GeV. Note that, V_{nna13} and $T_{NN,NN}$ will be complex numbers.

The first phase shifts and inelasticities, with the nna13 potential, are plotted in 5.3. From this, one can calculate the total cross section. The total cross section will be dependent on all the partial waves. The importance of the phase shifts and inelasticities as J increases are shown in tab 5.1 and tab 5.2. We see that the cross section calculated from the phase shifts converges, and we don't need to include more than the first 20 partial wave states in the calculations.

	$\sigma_{NN-elastic}\ [mb]$				
T_{lab}	$J_{max} = 3$	$J_{max} = 10$	$J_{max} = 20$	$J_{max} = 80$	Experimental
200 MeV	40.254595	41.849377	41.851221	41.851221	42.78
400 MeV	29.286240	32.212076	32.228529	32.228552	32.40
600 MeV	24.781240	28.080876	28.120242	28.120412	29.54
800 MeV	21.486933	24.551982	24.614851	24.615376	26.25
1000 MeV	20.521614	23.093538	23.177359	23.178458	23.29

Table 5.1: *Total elastic cross section from isoscalar np scattering obtained with the nna13 potential including all partial waves up to J_{max}. Experimental values from [6] are also included.*

	$\sigma_{NN-inelastic}\ [mb]$				
T_{lab}	$J_{max} = 3$	$J_{max} = 10$	$J_{max} = 20$	$J_{max} = 80$	Experimental
200 MeV	0.000000	0.000000	0.000000	0.000000	0.0000
400 MeV	0.477711	0.518062	0.518062	0.518062	0.6947
600 MeV	6.036612	6.706089	6.707221	6.707221	6.479
800 MeV	8.879003	11.032602	11.040103	11.040103	12.37
1000 MeV	9.815736	13.053151	13.074315	13.074315	15.45

Table 5.2: *Total inelastic cross section from isoscalar np scattering obtained with the nna13 potential including all partial waves up to J_{max}. Experimental values from [6] are also included.*

At NN scattering above 1 GeV in the laboratory system one also needs to include other resonances. Of these, the Roper resonance (N*) is probably the most important [46].

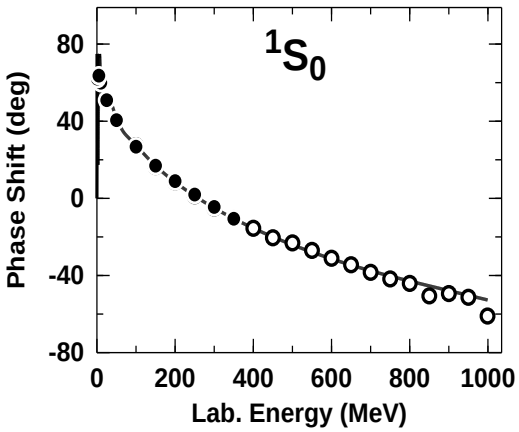
$^1S_0$
Phase Shift (deg)
Lab. Energy (MeV)

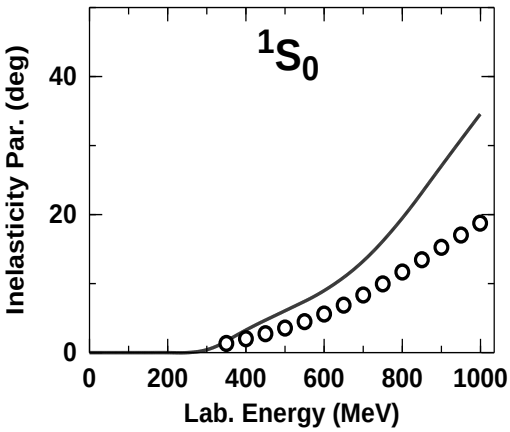
$^1S_0$
Inelasticity Par. (deg)
Lab. Energy (MeV)

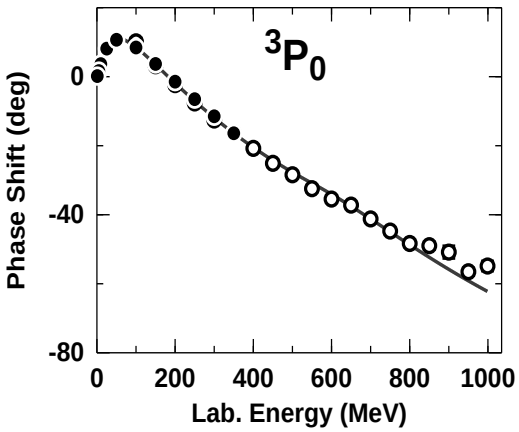
$^3P_0$
Phase Shift (deg)
Lab. Energy (MeV)

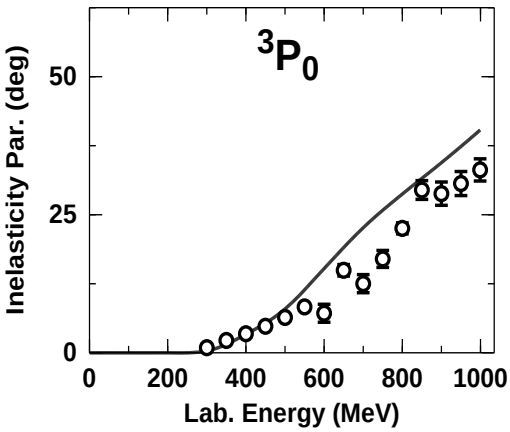
$^3P_0$
Inelasticity Par. (deg)
Lab. Energy (MeV)

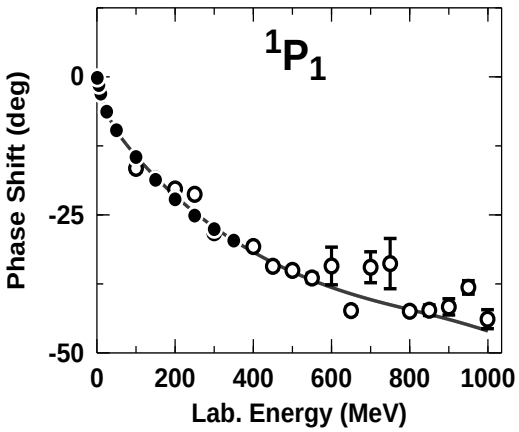
$^1P_1$
Phase Shift (deg)
Lab. Energy (MeV)

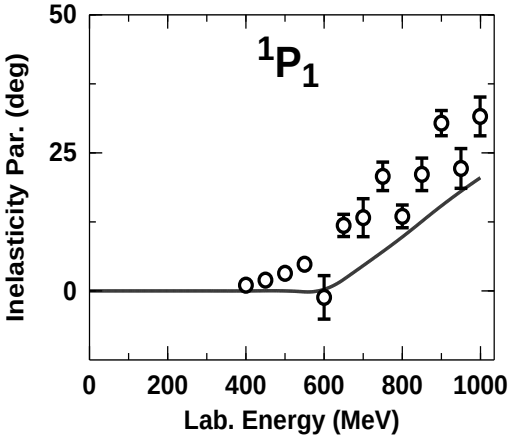
$^1P_1$
Inelasticity Par. (deg)
Lab. Energy (MeV)

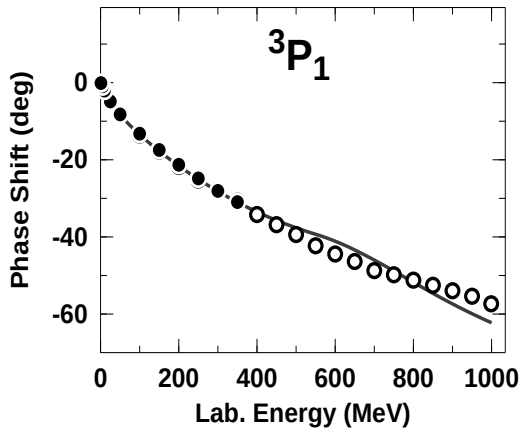
$^3P_1$
Phase Shift (deg)
0
-20
-40
-60
0
200
400
600
800
1000
Lab. Energy (MeV)

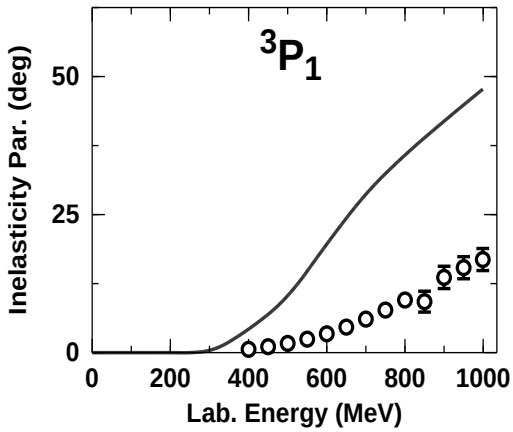
$^3P_1$
Inelasticity Par. (deg)
50
25
0
0
200
400
600
800
1000
Lab. Energy (MeV)

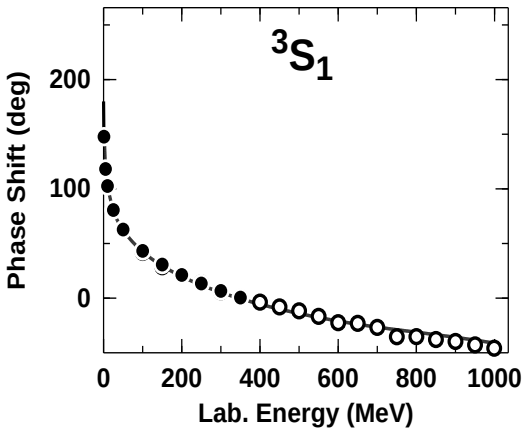
$^3S_1$
Phase Shift (deg)
200
100
0
0
200
400
600
800
1000
Lab. Energy (MeV)

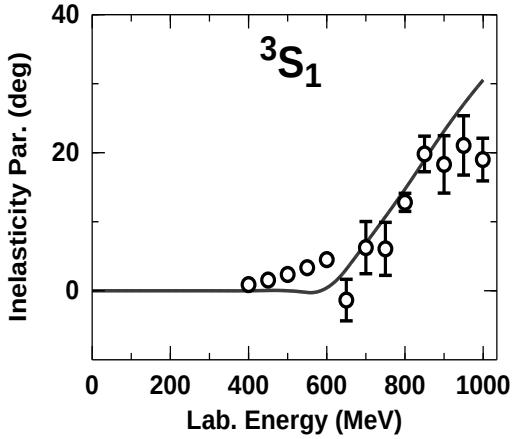
$^3S_1$
Inelasticity Par. (deg)
40
20
0
0
200
400
600
800
1000
Lab. Energy (MeV)

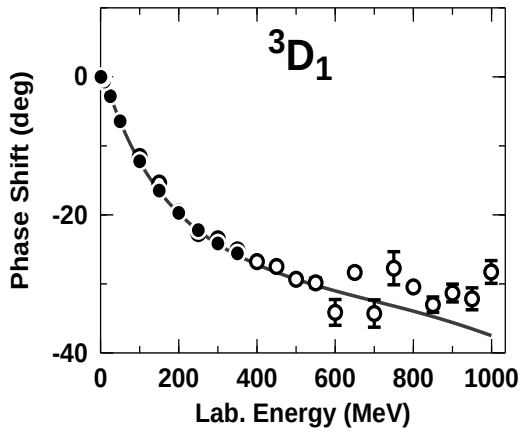
$^3D_1$
Phase Shift (deg)
0
-20
-40
0
200
400
600
800
1000
Lab. Energy (MeV)

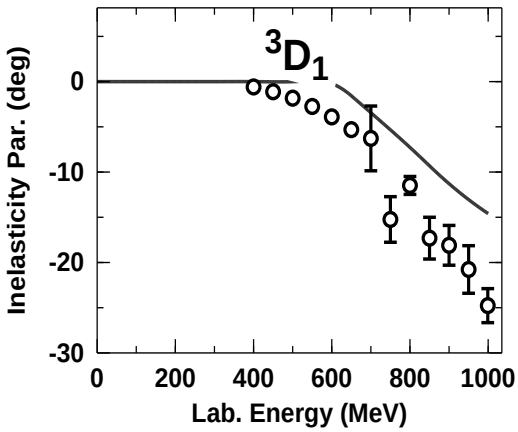
$^3D_1$
Inelasticity Par. (deg)
0
-10
-20
-30
0
200
400
600
800
1000
Lab. Energy (MeV)

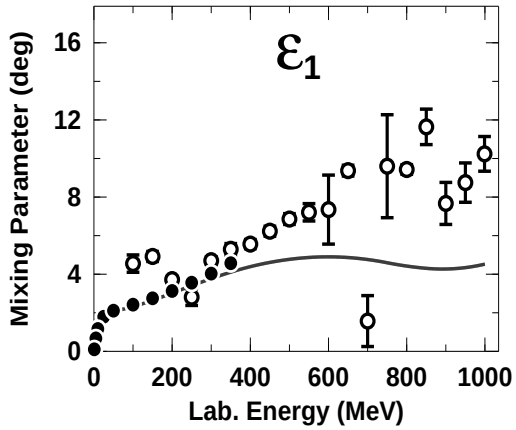
ε1
Mixing Parameter (deg)
Lab. Energy (MeV)

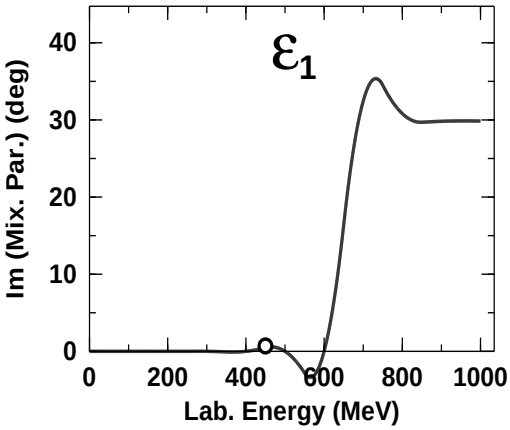
ε1
Im (Mix. Par.) (deg)
Lab. Energy (MeV)

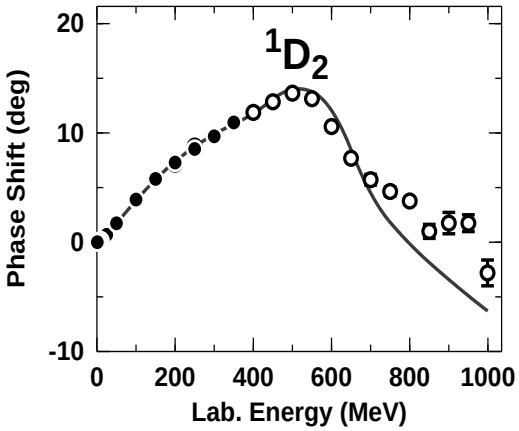
1D2
Phase Shift (deg)
Lab. Energy (MeV)

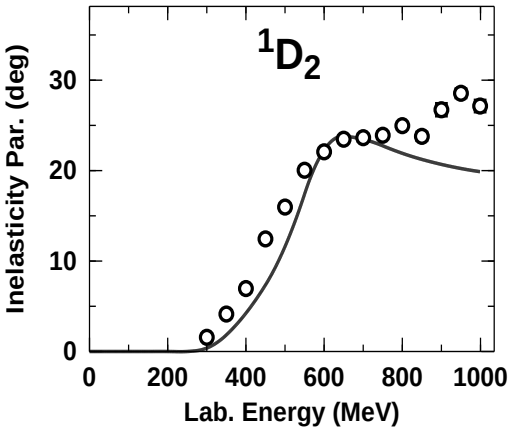
1D2
Inelasticity Par. (deg)
Lab. Energy (MeV)

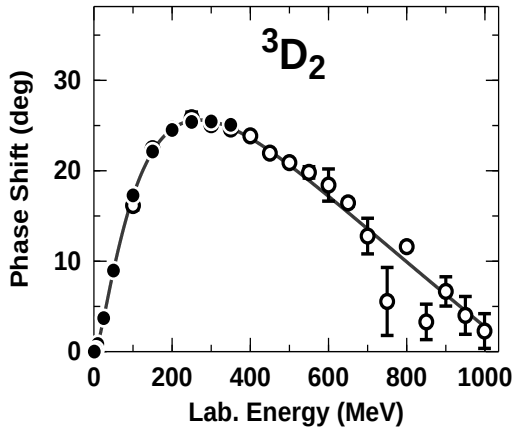
3D2
Phase Shift (deg)
Lab. Energy (MeV)

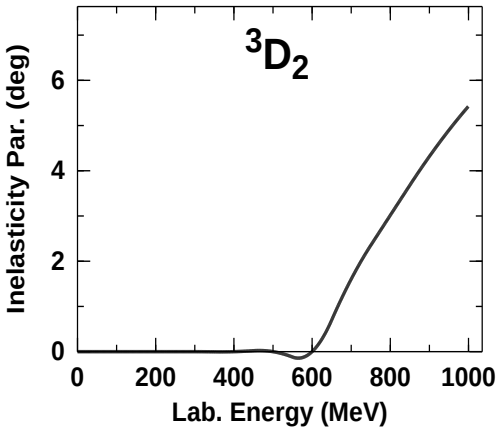
3D2
Inelasticity Par. (deg)
Lab. Energy (MeV)

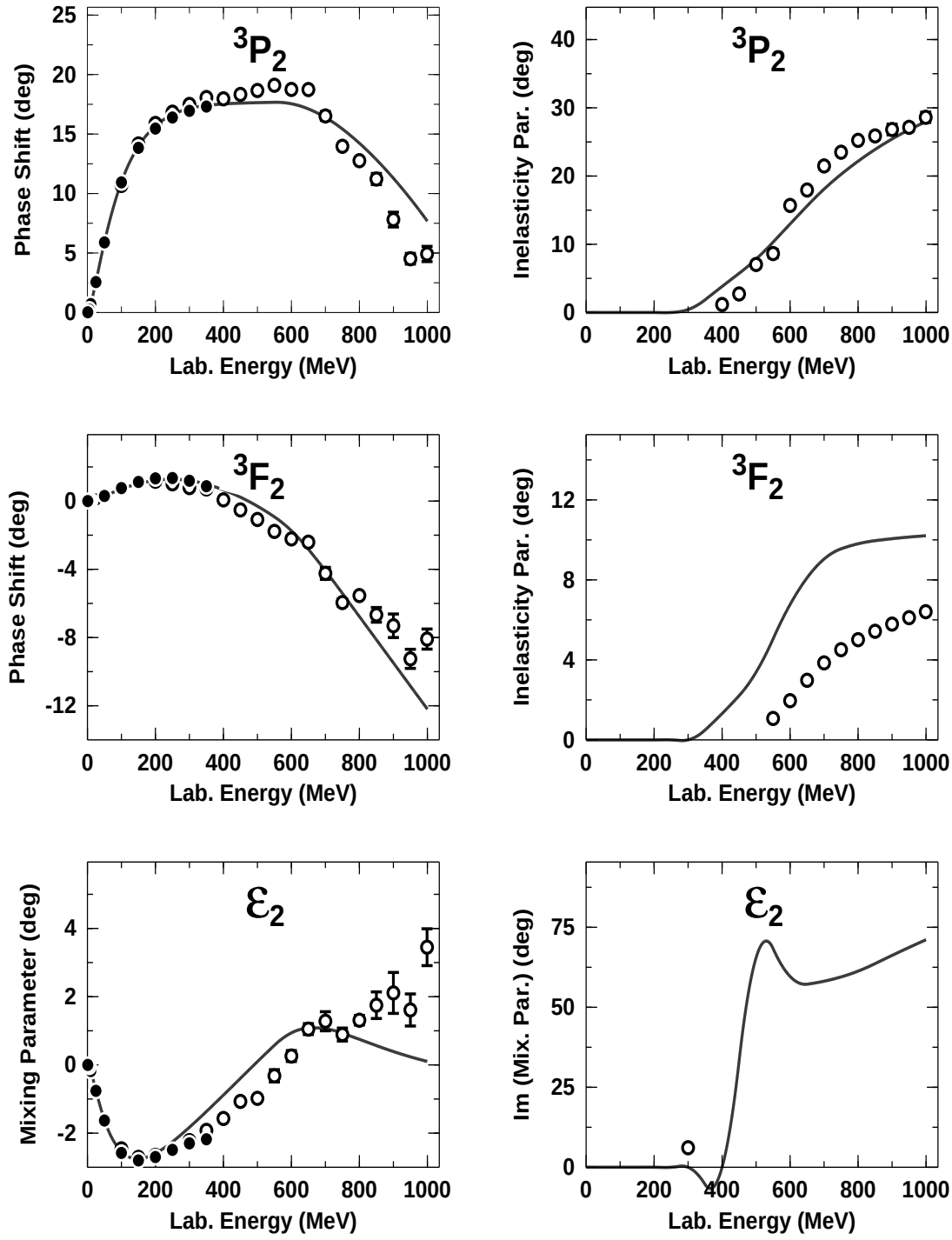

Figure 5.3: Theoretical isoscalar np phase shifts and inelasticities from calculations with the "Minimal Relativity" using the nna13 potential. The dots are experimental data. Where the black dots are taken from [5], and the white dots from [6].

Chapter 6

In-Medium Scattering

So far only NN scattering in free space has been considered. Since the strong force is a three body force, we will experience a different interaction between two nucleons in free space and two nucleons in a nuclei with three or more nucleons. However, much of the many-body theory today is based on approaches where we can make use of the potentials designed for the free NN systems.

Because of the spherical geometry and the boundary conditions of a nucleus, it is difficult to construct a mathematical model of the nuclear force. A commonly used simplification to the problem, is to introduce the theoretical "nuclear matter" model. This model is an approximation to the homogeneous situation we have in the interior of heavy nuclei. Nucleons in the boundary of a nucleus will behave slightly different, and their interactions are more difficult describe mathematically. The nuclear matter approximation will be better the closer we are to the center of a heavy nucleus.

In order to describe the many particle system one has to include properties from many particle theory. From Brueckner-Bethe-Goldstone (BBG) theory we can calculate the reaction matrix (G-matrix), which is a many particle version of the T-matrix found in free NN scattering. The G-matrix will include properties like the Pauli principal and the dispersion effect. From the on-shell G-matrix elements one can extract in-medium phase shifts and inelasticities.

6.1 Nuclear matter

Nuclear matter in definition, is an infinite uniform system of Z protons and N neutrons, where the nucleons are only interacting through the strong force. i.e., the Coulomb interaction is turned off. In the limit of the nuclear matter model, both the number of particles $A = N + Z \to \infty$ and volume $\Omega \to \infty$. The nucleon density is $n = (N + Z)/\Omega$. In the special case where $N = Z$, known as symmetric nuclear matter, the nucleon density is related to the Fermi moment k_F by $n = 2k_F^3/(3\pi^2)$. The average binding energy per nucleon in symmetric nuclear matter at equilibrium density can be extracted from the Bethe-Weizsäcker mass formula:

$$\frac{E}{A} = -a_\nu + a_s A^{-1/3} + a_c Z(Z-1)A^{-4/3} + a_{\text{sym}}\frac{(N-Z)^2}{A} \tag{6.1}$$

where $a_\nu = 16 \pm 1$ MeV is the volume term, a_c is the surface term, a_c is the contribution arising from the Coulomb force and a_{sym} is the symmetry term favoring symmetric nuclei. The three last terms in eq(6.1) can be removed by neglecting the Coulomb force, setting $N = Z$ and letting $A \to \infty$. The average binding energy per particle (see [27]) is then

$$\left(\frac{E}{A}\right)_{n=n_0} = -16 \pm 1 \quad \text{MeV}. \tag{6.2}$$

From the charge distribution of heavy nuclei, which is determined in electron scattering, the saturation density can be found by taking into account corrections due to the Coulomb repulsion and the surface tension [28], which yields

$$n_0 = 0.17 \pm 0.02 \quad \text{nucleons/fm}^3. \tag{6.3}$$

This is equivalent to a Fermi momentum of

$$k_F = 1.35 \pm 0.05 \quad \text{fm}^{-1}, \tag{6.4}$$

with a corresponding mass density $\rho_0 \approx 2.8\text{E}14$ g/cm^3. The Fermi momentum is an important factor in phase shift analysis, and is a result of the Pauli effect in a medium consisting of fermions.

The non relativistic Hamiltonian of an interacting many-particle system is

$$\begin{aligned} \hat{H} &= \hat{T} + \hat{V} \\ &= \hat{T} + \hat{U} + \hat{W} \\ &= \sum_{i=1}^{N} \frac{\mathbf{p}_i^2}{2m} + \sum_{i=1}^{N} u(\mathbf{r}_i) + \sum_{i<j}^{N} w(\mathbf{r}_i, \mathbf{r}_j), \end{aligned} \tag{6.5}$$

where N is the number of particles in the system. Here, $\hat{T}$ is the kinetic energy operator and $\hat{U}$ is an effective single-particle (sp) potential operator extracted from the two-body potential operator $\hat{V}$ leaving the remaining interactions in $\hat{W}$ For a general translational invariant system we must have

$$u(\mathbf{r}) = \text{constant}. \tag{6.6}$$

The nuclear matter model has been constructed to be such a uniform many-body system, where the potential from the nucleons position in the nuclear matter is the same for all the nucleons because there are not any boundary effects and the nuclear matter is symmetric.

For a translational invariant system we will have momentum conservation, which will lead to eliminations of certain classes of diagrams. Also the single-particle waves for a translational invariant system can be expressed as plane waves instead of self-consistent Hartree-Fock wave functions, which is the solution obtained from solving the exact wave function for heavy nuclei.

6.2 The Goldstone expansion

We wish to calculate the ground state properties of a system containing $A = N + Z$ nucleons interacting via a realistic NN interaction. Within a non-relativistic framework the exact ground state Ψ_0 is given by the Schrödinger equation

$$\hat{H}|\Psi_0\rangle = E_0|\Psi_0\rangle, \tag{6.7}$$

where the Hamiltonian is given as

$$\hat{H} = \hat{T} + \hat{V}. \tag{6.8}$$

This equation cannot be solved exactly and we seek approximate solutions using perturbation techniques.

BBG theory is based on the Rayleigh-Schrödinger perturbation expansion of the ground state energy, where the Hamilton operator is rewritten as

$$\hat{H} = \hat{H}_0 + \hat{H}_I, \tag{6.9}$$

with the unperturbed part only including sp operators

$$\hat{H}_0 = \hat{T} + \hat{U}, \tag{6.10}$$

and the perturbated part

$$\hat{H}_I = \hat{V} - \hat{U}. \tag{6.11}$$

The total Hamilton operator $\hat{H}$ does not involve the sp potential operator $\hat{U}$. The final result should therefore in principle be independent of $\hat{U}$. However, the energy is calculated using a perturbation series, and the convergence of that series will depend on the choice of U. It is therefore important to choose $\hat{U}$ such that the energy expansion converges rapidly enough to be useful in our calculations.

The unperturbed ground state satisfies the Schrödinger equation

$$\hat{H}_0|\Phi_0\rangle = W_0|\Phi_0\rangle. \tag{6.12}$$

Since $\hat{H}_0 = \hat{T} + \hat{U}$ consists of one-body terms, we will only need to solve the one-body Schrödinger equation

$$(\hat{T} + \hat{U})|\alpha_i\rangle = \epsilon_i|\alpha_i\rangle. \tag{6.13}$$

The unperturbed ground state of the nucleon system will be a Slater determinants formed by putting particles into the A one-particle states with the lowest energy states available

$$|\Phi_0\rangle = |\alpha_1\alpha_2\cdots\alpha_A\rangle. \tag{6.14}$$

These occupied states are known as Fermi sea, but can also corresponds to the particle-hole vacuum defined in Goldstone theory. If we use $\langle\Phi_0|\Psi_0\rangle = 1$, the ground state energy is given as

$$\langle\Phi_0|\hat{H}|\Psi_0\rangle = E_0 = W_0 + \Delta E_0, \tag{6.15}$$

where ΔE_0 is the ground state energy shift. Rayleigh-Schrödinger perturbation theory gives the formal expression for the energy shift as

$$\Delta E_0 = \sum_{n=0}^{\infty} \langle \Phi_0 | \hat{H}_I \left\{ \frac{\hat{Q}}{W_0 - \hat{H}_0} (\hat{H}_I - \Delta E_0) \right\}^n | \Phi_0 \rangle, \tag{6.16}$$

where

$$\hat{Q} = \mathbf{1} - |\Phi_0\rangle\langle\Phi_0|, \tag{6.17}$$

is the Pauli exclusion operator. It ensures that $|\Phi_0\rangle$ does not occur as an intermediate state, i.e. in the intermediate states at least one particle has to be excited.

By iterating eq(6.16), we find ΔE_0 up to third order in $\hat{H}_I$ as

$$\begin{aligned} \Delta E_0 &= \langle \Phi_0 | \hat{H}_I | \Phi_0 \rangle + \langle \Phi_0 | \hat{H}_I \frac{\hat{Q}}{W_0 - \hat{H}_0} \hat{H}_I | \Phi_0 \rangle \\ &+ \langle \Phi_0 | \hat{H}_I \frac{\hat{Q}}{W_0 - \hat{H}_0} \hat{H}_I \frac{\hat{Q}}{W_0 - \hat{H}_0} \hat{H}_I | \Phi_0 \rangle \\ &+ \langle \Phi_0 | \hat{H}_I | \Phi_0 \rangle \langle \Phi_0 | \hat{H}_I \frac{\hat{Q}}{(W_0 - \hat{H}_0)^2} \hat{H}_I | \Phi_0 \rangle. \end{aligned} \tag{6.18}$$

This expansion can be expressed in terms of linked diagrams, the so-called Goldstone diagrams. The intermediate state $|\alpha_k \alpha_l\rangle$ contains two particles in sp states above the Fermi level corresponding to the upward going lines (particle lines) and consequently two sp states in the Fermi sea α_i and α_j are left unoccupied corresponding to downward going lines (hole lines). Note that these two diagrams depend on $\hat{U}$ through the energy denominator.

The first order diagrams, with respect to $\hat{H}_I = \hat{V} - \hat{U}$, that contribute to ΔE_0 are shown in fig 6.1. The contribution from these diagrams is

$$\Delta E_0^{(1)} = \frac{1}{2} \sum_{i,j<A} \langle \alpha_i \alpha_j | \hat{V} | \alpha_i \alpha_j - \alpha_j \alpha_i \rangle - \sum_{i<A} \langle \alpha_i | \hat{U} | \alpha_i \rangle, \tag{6.19}$$

where we have introduced the short-hand notation

$$\langle \alpha_i \alpha_j | \hat{V} | \alpha_i \alpha_j - \alpha_j \alpha_i \rangle \equiv \langle \alpha_i \alpha_j | \hat{V} | \alpha_i \alpha_j \rangle - \langle \alpha_i \alpha_j | \hat{V} | \alpha_j \alpha_i \rangle. \tag{6.20}$$

The last term in eq(6.19) cancels the potential energy contribution from $\hat{H}_0$. The first term on the right hand side corresponds to the contributions from two-independent hole line diagrams (2h), which we rewrite as

$$\Delta^{2h} E_0^{(1)} = \frac{1}{2} \sum_{i,j<A} \langle \alpha_i \alpha_j | \hat{V} | \alpha_i \alpha_j - \alpha_j \alpha_i \rangle. \tag{6.21}$$

The only second-order diagrams contributing in nuclear matter are the diagram shown in fig 6.2a and the corresponding exchange diagram in fig 6.2b. Using the

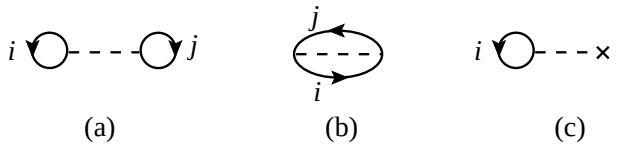

Figure 6.1: *The first-order Goldstone diagrams appearing in the linked cluster expansion.*

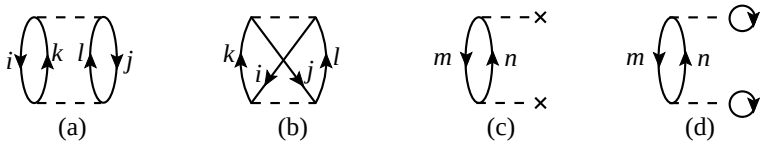

Figure 6.2: *Second-order Goldstone diagrams. Only diagram (a) and (b) contribute in nuclear matter.*

above shorthand notation, the contribution the second-order of Goldstone diagrams involving two-independent hole line in nuclear matter can be written as

$$\Delta^{2h}E_0^{(2)} = \frac{1}{2}\sum_{i,j<A}\sum_{k,l>A}\frac{\langle\alpha_i\alpha_j|\hat{V}|\alpha_k\alpha_l\rangle\langle\alpha_k\alpha_l|\hat{V}|\alpha_i\alpha_j-\alpha_j\alpha_i\rangle}{\epsilon_i+\epsilon_j-\epsilon_k-\epsilon_l}. \tag{6.22}$$

Since the sp in nuclear matter are plane waves, the sp state α_i is uniquely characterized by its momentum $\mathbf{k}_i$ together with the spin s_i and isospin t_i. The sp states are eigenstates of the unperturbed Hamilton operator $\hat{H}_0 = \hat{T} + \hat{U}$, which will be diagonal in the plane wave basis. The operator $\hat{U}$ can therefore not change the total momentum of a many-particle state, This total momentum conservation will remove certain types of diagrams like those shown in fig 6.2c and fig 6.2d, which contain only one particle and one hole in an intermediate state. This is because the total momentum in the intermediate state $\mathbf{k}_p - \mathbf{k}_h$ has to be different from zero since $|\mathbf{k}_h| < k_F$ and $|\mathbf{k}_p| > k_F$.

6.3 The reaction matrix and single-particle energies

Because of the strong short-range repulsive core in the NN interaction, the two-body matrix elements of $\hat{V}$ are very large and the perturbation series does not converge. A solution to this problem is provided by the well-known Brueckner theory, where the two-particle correlations are summed into infinite order. We see that E_0 will be independent on the sp potential U, since the U term in W_0 will cancel the U term $\Delta E_0^{(1)}$, which is illustrated in fig 6.1 c. The $\hat{U}$ dependence will, however, enter in the two-hole line contribution through the propagators of the second- and higher-order Goldstone diagrams.

The Goldstone expansion for the two-independent hole line, found for the first- and second-order in the previous section, can be rewritten in terms of the reaction matrix G to infinite order of interactions as

$$E_0 = \langle\Phi_0|\hat{H}|\Psi_0\rangle = \langle\Phi_0|(\hat{T}+\frac{1}{2}\hat{V})|\Psi_0\rangle \simeq W_0 + \Delta^{2h}E_0 = \langle\Phi_0|(\hat{T}+\frac{1}{2}\hat{G})|\Phi_0\rangle, \quad (6.23)$$

which is known as the first-order approximation of the ground state energy in the BBG expansion. In eq(6.23) we used $\hat{G}|\Phi_0\rangle = \hat{V}|\Psi_0\rangle$ and $\langle\Phi_0|\hat{T}|\Psi_0\rangle = \langle\Phi_0|\hat{T}|\Phi_0\rangle$. The $\frac{1}{2}$ factor appears in front of $\hat{V}$ because of double counting of particle pairs. This factor is from the definition of the G-matrix transferred over to $\hat{G}$. i.e., both the direct and exchange contributions of the infinite sum of ladder diagrams are included in the antisymmetric $\hat{G}$ operator.

The G-matrix equation yields on operator form

$$\hat{G}(\omega) = \hat{V} + \hat{V}\frac{\hat{Q}}{\omega - \hat{H}_0}\hat{G}(\omega), \quad (6.24)$$

which is also known as the BBG integral equation. The G-matrix is usually represented by a wavy line vertex as shown diagrammatically in fig 6.3. This equation

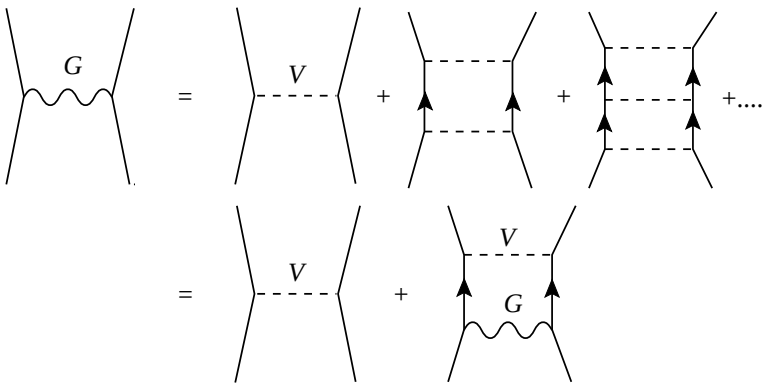

Figure 6.3: *Diagrammatic representation of the reaction matrix G as a sum of ladder diagrams. The last line represent the Brueckner-Bethe-Goldstone equation.*

is similar to the Lippmann-Schwinger equation which defines the scattering matrix, and we can use the on-shell elements of the G-matrix to calculate phase shifts. Note that, in free space the term $\hat{Q}/(\omega - \hat{H}_0)$ will be equivalent to the one used in the Lippmann-Schwinger equation, and the G-matrix will be reduced to the familiar T-matrix. The BBG equation contains a Pauli exclusion operator $\hat{Q}$ which prevents scattering into occupied states. In the unperturbed basis it reads

$$\hat{Q} = \sum_{m,n>A} |\alpha_m\alpha_n\rangle\langle\alpha_m\alpha_n|. \quad (6.25)$$

When the unperturbed Hamiltonian $\hat{H}_0$ is acting on an intermediate state $|\alpha_m\alpha_n\rangle$ it gives a contribution $(\varepsilon_m + \varepsilon_n)$ to the energy denominator. Hence, the energy

denominator involves medium-dependent sp energies. These medium-dependent sp energies will from now on be denoted $(\widetilde{\varepsilon}_m + \widetilde{\varepsilon}_n)$. In addition, the energy denominator contains a general energy variable ω, the so-called starting energy, which is equal to the initial in medium energy for an on-shell G-matrix.

The first-order BBG diagrams are illustrated in fig 6.4. Higher-order expansion will also contribute. Some of the second-order diagrams are shown in 6.5, where the wavy line vertex represent the G-matrix.

It is not given that series which are grouped according to the number of G-vertexes, will converge. In Brueckner theory this problem is circumvented by recasting the Goldstone expansion into series ordered according to the number of independent hole lines (BBG expansion). Formal arguments for the convergence of the hole line expansion have been given by Brandow [42]. He estimated that the contribution to the energy of a diagram with i independent hole lines is proportional to κ^{i-1}, where the so-called wound integral κ is essentially the probability to have an unoccupied state below the Fermi sphere. This dimensionless quantity provides a measure of the convergence rate of the hole-line expansion. At the empirical saturation density the wound integral has been to be about 0.2. This has later been confirmed by Day in [43], where all hole-lines diagrams up to third order have been calculated.

The lowest order contribution, the one containing two independent hole lines, corresponds to the diagrams in fig 6.4.

Figure 6.4: *The first-order (two-independent hole line) contributions to the ground state energy in the BBG expansion.*

The energy per nucleon obtained from lowest order of the BBG expansion, can now be rewritten in terms of the sp potential

$$\begin{aligned}
\frac{E_0}{A} &= \langle\Phi_0|(\hat{T}+\frac{1}{2}\hat{V})|\Phi_0\rangle \\
&= \frac{1}{A}\sum_{i\leq A}\langle\alpha_i|\hat{T}|\alpha_i\rangle + \frac{1}{2A}\sum_{i,j\leq A}\langle\alpha_i\alpha_j|\hat{G}(\omega=\widetilde{\epsilon}_i+\widetilde{\epsilon}_j)|\alpha_i\alpha_j-\alpha_j\alpha_i\rangle \\
&= \frac{1}{A}\sum_{i\leq A}\langle\alpha_i|\hat{T}+\frac{1}{2}\hat{U}|\alpha_i\rangle, \qquad (6.26)
\end{aligned}$$

where we in the last step used the sp potential definition of $U(i)$ known as the *standard choice* suggested in [44] as

$$\langle\alpha_i|\hat{U}|\alpha_i\rangle = \begin{cases} \sum_{j\leq A}\langle\alpha_i\alpha_j|\hat{G}(\omega=\widetilde{\epsilon}_i+\widetilde{\epsilon}_j)|\alpha_i\alpha_j-\alpha_j\alpha_i\rangle, & i\leq A \\ 0, & i>A \end{cases}$$

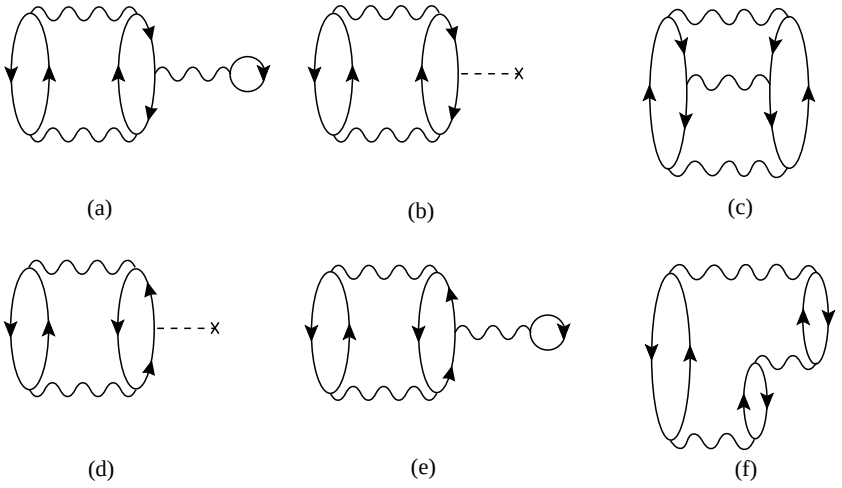

Figure 6.5: *The simplest diagrams that contribute to second-order in the BBG expansion. The diagrams (a), (c), (e), and (f) involve three-independent hole lines.*

which produces a gap at the Fermi surface. Alternatively, a *continuous choice* for U can be made(see [45]) for a complex G-matrix by defining

$$\langle\alpha_i|\hat{U}|\alpha_i\rangle = \mathcal{R}\mathrm{e}\Big\{\sum_{j\leq A}\langle\alpha_i\alpha_j|\hat{G}(\omega=\widetilde{\varepsilon}_i+\widetilde{\varepsilon}_j)|\alpha_i\alpha_j-\alpha_j\alpha_i\rangle\Big\}, \tag{6.27}$$

for all states α_i below and above the Fermi surface.

The G-matrix defined in eq(6.24) will be a function of sp energies. If two interacting particles have momenta $k_1=|\mathbf{k_1}|$ and $k_2=|\mathbf{k_1}|$, the non-relativistic sp energies $\widetilde{\varepsilon}$ in the nuclear matter are

$$\widetilde{\varepsilon}(k_1) = T(k_1)+U(k_1) = (k_1^2/2m)+\langle k_1|\hat{U}|k_1\rangle. \tag{6.28}$$

The sp energy will be dependent on the interaction of each nucleon with all the other nucleons in the Fermi sea. The sp energy part U can now be found by choosing an adequate initial U. Which will, when inserted in the G-matrix eq(6.24), reproduce a new U. This process is done until self-consistence is achieved. Finally the self-consistent U can be used to calculate the average energy per nucleon, which can be compared with the one obtained from the Bethe-Weizsäcker mass formula in eq(6.2).

The two particle propagator in nuclear matter includes the Pauli principle projection operator $\hat{Q}$, which projects out states with two nucleons above the Fermi sea, can be rewritten as

$$\frac{\hat{Q}}{\omega-\hat{H}_0+i\epsilon}|\mathbf{k_1k_2}\rangle = \frac{\theta(k_1-k_F)\theta(k_2-k_F)}{\omega-\widetilde{\varepsilon}(k_1)-\widetilde{\varepsilon}(k_2)}|\mathbf{k_1k_2}\rangle, \tag{6.29}$$

The reaction matrix is often evaluated in terms of relative and center-of-mass momenta defined by

$$\mathbf{q}=\frac{\mathbf{k}_i-\mathbf{k}_j}{2} \quad \text{and} \quad \mathbf{K}=\mathbf{k}_i+\mathbf{k}_j, \tag{6.30}$$

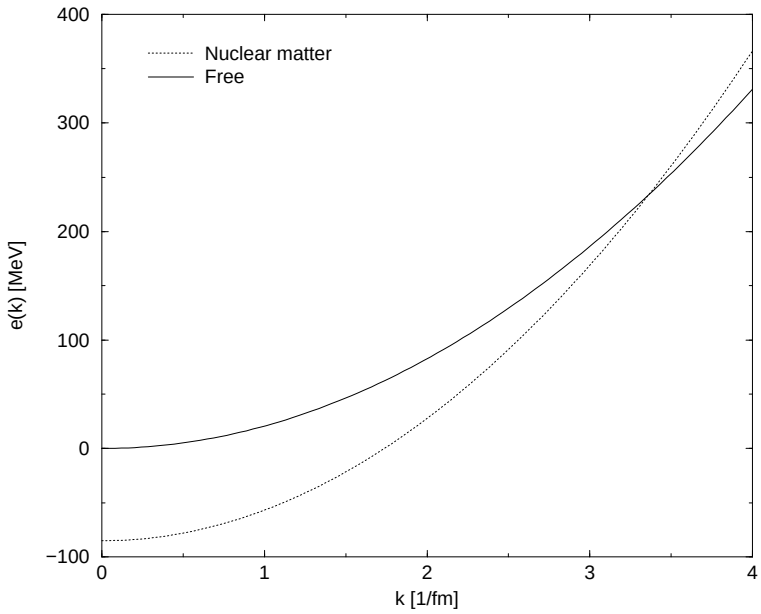

Figure 6.6: *The sp energy in free NN scattering, and in nuclear matter NN scattering obtained from the effective mass approximation where* $m^* = 688$ *MeV and* $U_0 = 89$ *MeV.*

respectively. Note that, the Pauli operator $\hat{Q}$ is not diagonal in the above representation. It will depend on the angle between $\mathbf{q}$ and $\mathbf{K}$. This angle dependence causes $\hat{Q}$ to couple states with different angular momentum J. A partial wave decomposition of eq(6.24) therefore becomes rather difficult. The angular dependence of the Pauli operator can be eliminated by introducing the angle-average Pauli operator, where one replaces the exact Pauli operator $\hat{Q}(k, K)$ by its average over all angles between the relative and the center-of-mass momentum. However, this problem can be avoided in the zero center of mass system $\mathbf{K} = 0$, where the propagator in eq(6.29) will be reduced to

$$\frac{\hat{Q}}{\omega - H_0 + i\epsilon}|\mathbf{q}\rangle = \frac{\theta(q - k_F)}{\omega - \widetilde{\varepsilon}(q) - \widetilde{\varepsilon}(q)}|\mathbf{q}\rangle. \tag{6.31}$$

In eq(6.28) the in-medium sp energies are given as

$$\widetilde{\varepsilon}(q) = T(q) + U(q). \tag{6.32}$$

With the so-called effective mass approximation of the sp energy, we obtain

$$\widetilde{\varepsilon}(q) \approx \frac{q^2}{2m^*} - U_0, \tag{6.33}$$

It is very practical to use such a simple sp energy function, since it will allow us to calculate the phase shifts in nuclear matter in a similar way as before. Calculating a real G-matrix from the cdbonn potential in symmetric nuclear matter, we reach

self-consistence with $k_F = 1.35$ fm^{-1} for $m^* \approx 688$ MeV and $U_0 \approx 89$ MeV. This sp energy is shown in fig 6.6. For more accurate sp energies and how they are calculated see [40], [41] and [39].

The sp potential energy term $U(k)$ arises because the nucleons interact with the nuclear matter through a three-body force. From the sp energies in fig 6.6 we see that the non relativistic effective mass approximation becomes unphysical for large k. The sp energy in free space should always be greater than in a medium, since the NN system can lose energy to the nuclear matter, but the nuclear matter, which by definition is occupying the lowest energy states possible, can not give away energy to the NN system. At large energies we expect to see

$$\lim_{k\to\infty} \sqrt{k^2 + m^{*2}} \lesssim \lim_{k\to\infty} \sqrt{k^2 + m^2} \lesssim k, \tag{6.34}$$

which is of course the relativistic effective mass approximation. We will assume that the nuclear matter approximation is as good as the non-relativistic approximations done in the nna13 potential, i.e. good for $\epsilon(\bar{q}) < 1$ or equivalent $k < 2.5$ fm^{-1}.

6.4 The energy dependent nna13 potential in nuclear matter

The nna13 potential was defined in eq(5.17). In nuclear matter it reads

$$V_{\text{nna13}} = V'_{\text{cdbonn}} - \int_0^\infty dk\ k^2 \frac{V_{\text{NN,N}\Delta} V_{\text{N}\Delta,\text{NN}}}{\widetilde{\varepsilon}_{\text{N}\Delta} - \widetilde{\varepsilon}^0_{\text{NN}}} \int_0^\infty dk\ k^2 \frac{V_{\text{NN},\Delta\Delta} V_{\Delta\Delta,\text{NN}}}{\widetilde{\varepsilon}_{\Delta\Delta} - \widetilde{\varepsilon}^0_{\text{NN}}}, \tag{6.35}$$

where only the sp energies will be different than the free space definition of V_{nna13}. The nna13 potential uses an OBEP part (cdbonn) and two box diagram parts from the two-meson exchanges involving intermediate isobars. This is illustrated schematically in fig 5.2. The box diagram parts of the nna13 potential are energy dependent, and the nna13 potential will therefore be different in NN scattering in a free space system than in a nuclear matter system. In single-particle energy representation, the nucleon $\widetilde{\varepsilon}_N$ and the isobar $\widetilde{\varepsilon}_\Delta$, If we use the effective mass approximation for the sp energy for a nucleon in nuclear matter obtained in eq(6.33), we have

$$\widetilde{\varepsilon}_{\text{N}}(k) = \frac{k^2}{2m^*_{\text{N}}} - U_0, \tag{6.36}$$

The sp energy for a isobar will be the same as for free NN scattering, since we have neglected the in-medium effects of isobars in the nuclear matter model. However, we need to include an additional term $\widetilde{\varepsilon}_{\text{N}}(k=0)$ to account for the additional kinetic energy gained from exciting a nucleon to an isobar. We have

$$\begin{aligned} \widetilde{\varepsilon}_\Delta(k) = \varepsilon_\Delta(k) &= \frac{k^2}{2m_\Delta} + (m_\Delta - m_{\text{N}} + \widetilde{\varepsilon}_{\text{N}}(k=0)) \\ &= \frac{k^2}{2m_\Delta} + (m_\Delta - m_{\text{N}} - U_0), \end{aligned} \tag{6.37}$$

With these sp energies we can rewrite the propagators in eq(6.35) as

$$\frac{1}{\widetilde{\varepsilon}_{N\Delta} - \widetilde{\varepsilon}^0_{\rm NN}} = \frac{1}{\widetilde{\varepsilon}_N(k) + \widetilde{\varepsilon}_\Delta(k) - 2\widetilde{\varepsilon}_{\rm N}(k_0)} = \frac{1}{\frac{k^2}{2m^*_{\rm N}} + \frac{k^2}{2m_\Delta} - \frac{k_0^2}{m^*_{\rm N}}} \tag{6.38}$$

and

$$\frac{1}{\widetilde{\varepsilon}_{\Delta\Delta} - \widetilde{\varepsilon}^0_{\rm NN}} = \frac{1}{2\widetilde{\varepsilon}_\Delta - 2\widetilde{\varepsilon}^0_{\rm N}} = \frac{1}{\frac{k^2}{m_\Delta} - \frac{k^2}{m^*_{\rm N}}}. \tag{6.39}$$

Note that, we have chosen to work with the effective mass sp approximation obtained from a non-complex OBE-potential. One should in principle have used the energy dependent nna13 potential when the sp energy was found from evaluating the G-matrix until the sp potential is self-consistent. This process is more difficult to do with the nna13 potential, since nna13 is energy-dependent and complex. i.e., the sp energies obtained with nna13 will be complex.

An in-nuclear matter version of the nna13 potential has been written by R. Machleidt in 2002. This is called the nna13in potential. The nna13in potential is using the effective mass $m^* = 688$ MeV in the propagators obtained in eq(6.38) and eq(6.39).

6.5 Nucleon-nucleon scattering in symmetric nuclear matter

To calculate phase shifts and inelasticities from NN scattering in nuclear matter, we need to calculate the G-matrix. Since we are using a complex potential, we need to redefine eq(6.24) to yield a complex G-matrix. If we use the particle basis not involving antiparticles, we need to solve

$$\hat{G}(\omega) = \hat{V} + \hat{V}\frac{\hat{Q}}{\omega - \hat{H}_0 + i\epsilon}\hat{G}(\omega). \tag{6.40}$$

The Pauli projection operator $\hat{Q}$ will, as obtained in eq(6.31) in a system where the nuclear matter is immobile and $\mathbf{K} = \mathbf{k_1} + \mathbf{k_2} = 0$, will be given as

$$Q(k, K = 0) = \begin{cases} 1, & k > k_{\rm F}, \\ 0, & \text{else} \end{cases}. \tag{6.41}$$

If we want to use the laboratory system for the two scattered particles, like we used for NN scattering in free space, we can look at the equivalent situation in a system where the nuclear matter is moving with the center of mass system of the two scattering particles. If we use non-relativistic energies, we have $E_{\rm cm} = E_{\rm lab}/2$. The more general problem, e.g. where the nuclear matter is immobile in the laboratory system, can be solved by using an angle average $\hat{Q}$-operator.

For simplicity, we choose to work with immobile nuclear matter in the center of mass system of the two scattering particles, where we can use eq(6.41). The

partial wave decomposition of the Blankenbecler-Sugar G-matrix equation for coupled channels will then yield

$$\begin{aligned}\langle p|\hat{G}_{l'l}(k_0)|k\rangle &= \langle p|\hat{V}_{l'l}(k_0)|k\rangle \\ &+\frac{2}{\pi}\sum_{l''}\int_{k_F}^{\infty} dq\; q^2\langle p|\hat{V}_{l'l''}(k_0)|q\rangle\;\frac{1}{2\widetilde{\varepsilon}(k_0)-2\widetilde{\varepsilon}(q)+i\epsilon}\;\langle q|\hat{G}_{l''l}(k_0)|k\rangle,\end{aligned} \tag{6.42}$$

where $\widetilde{\varepsilon}(k_0)$ is the on-shell sp energy in the center of mass system. Note that, we use the energy dependent nna13in potential to calculate $V_{l'l}(k_0)$. The single-particle energies $\widetilde{\varepsilon}(k)$ are in the non-relativistic Blankenbecler-Sugar approach given as

$$\widetilde{\varepsilon}(k) = \frac{k^2}{2m_N} + U(k). \tag{6.43}$$

If we apply the effective mass approximation, we have

$$\widetilde{\varepsilon}(k) = \frac{k^2}{2m_N^*} - U_0, \tag{6.44}$$

where $m^* = 688$ MeV is the effective mass, as obtained from the symmetric nuclear matter model we use. The propagator term in eq(6.42) will only be dependent on the difference between $\widetilde{\varepsilon}(k)$ and $\widetilde{\varepsilon}(q)$, which is

$$2\widetilde{\varepsilon}(k_0) - 2\widetilde{\varepsilon}(q) = \frac{k_0^2}{m_N^*} - \frac{q^2}{m_N^*}. \tag{6.45}$$

Eq(6.42) can therefore be rewritten as

$$\begin{aligned}\langle p|\hat{G}_{l'l}(k_0)|k\rangle &= \langle p|\hat{V}_{l'l}(k_0)|k\rangle \\ &+\frac{2m_N^*}{\pi}\sum_{l''}\Bigg[\mathcal{P}\int_{k_F}^{\infty} dq\; q^2\langle p|\hat{V}_{l'l''}(k_0)|q\rangle\frac{1}{k_0^2-q^2}\langle q|\hat{G}_{l''l}(k_0)|k\rangle \\ &-ik_0m_N^*\langle p|\hat{V_{l'l''}}(k_0)|k\rangle\;\langle k|\hat{G}_{l''l}(k_0)|k\rangle\Bigg].\end{aligned} \tag{6.46}$$

The relation between the on-shell momentum k_0 in the center of mass system and the kinetic lab energy T_{lab} is the same as before. Namely,

$$k_0 = \sqrt{\frac{m_N T_{lab}}{2}}, \tag{6.47}$$

where m_N is the nucleon mass in free space. The G- and T-matrices are based on a different perturbations. The S-matrix will be related to the G-matrix as

$$S_{ll'}(p,k) = \delta_{ll'}\delta(p-k) - 2im^*k\;G_{ll'}(p,k). \tag{6.48}$$

We can therefore still use the formula for phase shifts and inelasticities found in eq(1.78) for NN scattering in free space. However, we can not have $k_{cm} < k_F \simeq 1.35$

fm^{-1} in nuclear matter NN scattering. i.e. the kinetic energy $T_{\mathrm{cm}} \lesssim 80$ MeV or $T_{\mathrm{lab}} \lesssim 160$ MeV. This region is forbidden because all the energy states of such a system are already, by definition of k_{F}, occupied by nucleons from the nuclear matter.

Note that, the whole energy specter can be used if we define a new vacuum and use particle-hole formalism to study the situation where two holes or two particles are scattered. In such calculations the in-medium propagator, also known as the Galitski-Feynman propagator $\Gamma(k_1, k_2, \omega)$, is given as [41]

$$\Gamma(k_1, k_2, \omega) = \frac{\theta(k_1 - k_F)\theta(k_2 - k_F)}{\omega - \varepsilon(k_1) - \varepsilon(k_2) + i\epsilon} - \frac{\theta(k_F - k_1)\theta(k_F - k_2)}{\omega - \varepsilon(k_1) - \varepsilon(k_2) - i\epsilon}, \tag{6.49}$$

using the sp momenta k_1 and k_2. The first term on the right hand side represent the particle, and the second term is the antiparticle, i.e. a hole in a particle-hole basis.

6.6 Numerical calculations of isoscalar np scattering in nuclear matter

In this section we will only look at uncoupled states. The coupled channels can be calculated similar as done for the T-matrix, but, where we also need include the in-medium effects discussed below. The dispersion effect is included in the computer program if all the Nucleon masses m are replaced with the effective mass m^*, except in the calculation of the on-shell momentum $k_{\mathrm{N+1}}$ in the center of mass system.

We will here work in the laboratory system, where the target nucleon is not in motion before the interaction and the nuclear matter is immobile in the center of mass system. This way we can continue to use the laboratory system and the simplified $\hat{Q}$ operator (with $K = 0$) for the in-nuclear matter scattering. Note that, it is easy to convert laboratory energies to center of mass energies between the systems with $\hat{Q}(K = 0)$, since

$$E_{\mathrm{cm}} = E_{\mathrm{lab}}/2. \tag{6.50}$$

The Pauli effect is included by changing the integral from $(0, \infty) \to (k_{\mathrm{F}}, \infty)$. Numerically this can be done by adding k_{F} to all the mesh points

$$q_i = q_i + k_{\mathrm{F}}, \qquad for \quad i \leq N, \tag{6.51}$$

where N is the number of mesh points. The on-shell momentum $k_{\mathrm{N+1}}$ will be unchanged. When we are changing the integral limits, we also need to change the integral limits in the term which numerically removes the singularity in the integrand. The term in eq(4.15) is now replaced with

$$-\frac{2m^*}{\pi}\, k^2 \langle p|\hat{V}_l|k\rangle \langle k|\hat{G}_l\ |k\rangle \int_{k_{\mathrm{F}}}^{\infty} \frac{dq}{k^2 - q^2} \neq 0, \tag{6.52}$$

which is no longer zero. One can therefore not use it to remove the singularity in eq(6.46). However, if we also add

$$-\frac{2m^*}{\pi}\, k^2 \langle p|\hat{V}_l|k\rangle \langle k|\hat{G}_l\ |k\rangle \int_{0}^{k_{\mathrm{F}}} \frac{dq}{k^2 - q^2} \tag{6.53}$$

to eq(6.52), the two terms will together be zero. Eq(6.53) can be calculated analytically to yield

$$-\frac{2m^*}{\pi}\, k^2\langle p|\hat{V}_l|k\rangle\langle k|\hat{G}_l|k\rangle \int_0^{k_{\rm F}} \frac{dq}{k^2-q^2} = -\frac{m^*k}{\pi}\langle p|\hat{V}_l|k\rangle\langle k|\hat{G}_l|k\rangle \log\left|\frac{k_{\rm F}+k}{k_{\rm F}-k}\right|. \quad (6.54)$$

The numerical equations we get from eq(6.52) is therefore

$$\begin{aligned}\langle p|\hat{V}_l|k\rangle &= \langle p|\hat{G}_l|k\rangle - \frac{2m^*}{\pi}\sum_{j=1}^{N}\frac{\omega_j q_j^2}{k^2-q_j^2}\langle p|\hat{V}_l|q_j\rangle\langle q_j|\hat{G}_l|k\rangle \\ &\quad +\frac{2m^*}{\pi}\langle p|\hat{V}_l|k\rangle\langle k|\hat{G}_l|k\rangle\sum_{j=1}^{N}\frac{\omega_j k^2}{k^2-q_j^2} \\ &\quad -m^*k\left(i+\frac{1}{\pi}\log\left|\frac{k_{\rm F}+k}{k_{\rm F}-k}\right|\right)\langle p|\hat{V}_l|k\rangle\langle k|\hat{G}_l|k\rangle. \quad (6.55)\end{aligned}$$

Comparing this equation with eq(4.19), we see that this will only change the $u(\mathrm{N}+1)$ vector given in eq(4.23). The $u_i = u(q_i)$ elements will be the same as before, except the nucleon mass m which will be replaced with the effective mass m^*. The $u_{\mathrm{N}+1}$ vector element will be given as

$$u_{N+1} = -\frac{2m^*}{\pi}\sum_{j=1}^{N}\frac{\omega_j q_{N+1}^2}{q_{N+1}^2-q_j^2} + im^*q_{N+1} + \frac{m^*q_{N+1}}{\pi}\log\left|\frac{k_{\rm F}+q_{N+1}}{k_{\rm F}-q_{N+1}}\right|. \quad (6.56)$$

The Thompson method in nuclear matter can be calculated in a similar way, but we will then need a new potential analogous to the nna13in potential with relativistic energies.

6.7 Results

The first phase shifts and inelasticities from in-nuclear matter scattering, are shown in fig 6.8 and fig 6.10. The in-medium cross sections are shown in fig 6.8. To illustrate the importance of the different in-medium effects, both fig 6.8 and fig 6.8 contains unphysical plots containing only parts of the in-medium theory. The Pauli principal is one effect, and effective mass is another. The effective mass is important both in the computation of the G-matrix (here with the Blankenbecler-Sugar equation) and in the high energy nna13 potential constructed from box diagrams.

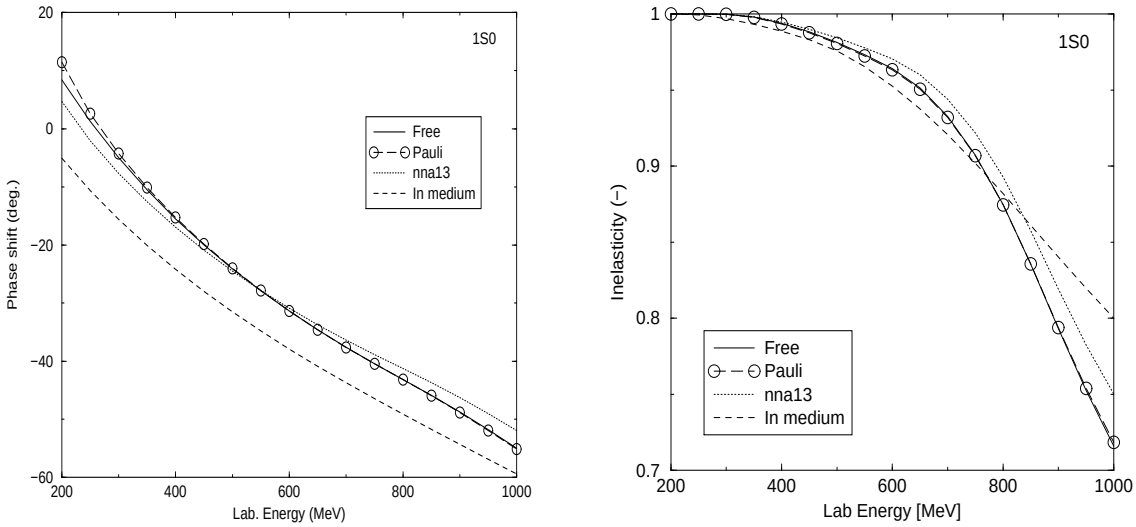

Figure 6.7: *Free space and in nuclear matter isoscalar np phase shifts and inelasticities for the partial* $^1S_0$ *-state as a function of kinetic energy in the laboratory system. The nuclear matter is immobile in center of mass system. Includes free space scattering. "Pauli" includes only the in-medium Pauli effect. "nna13" has additionally been included effective mass, but uses the nna13 potential. "In medium" is the final nuclear matter calculations, which also includes the nna13in potential.*

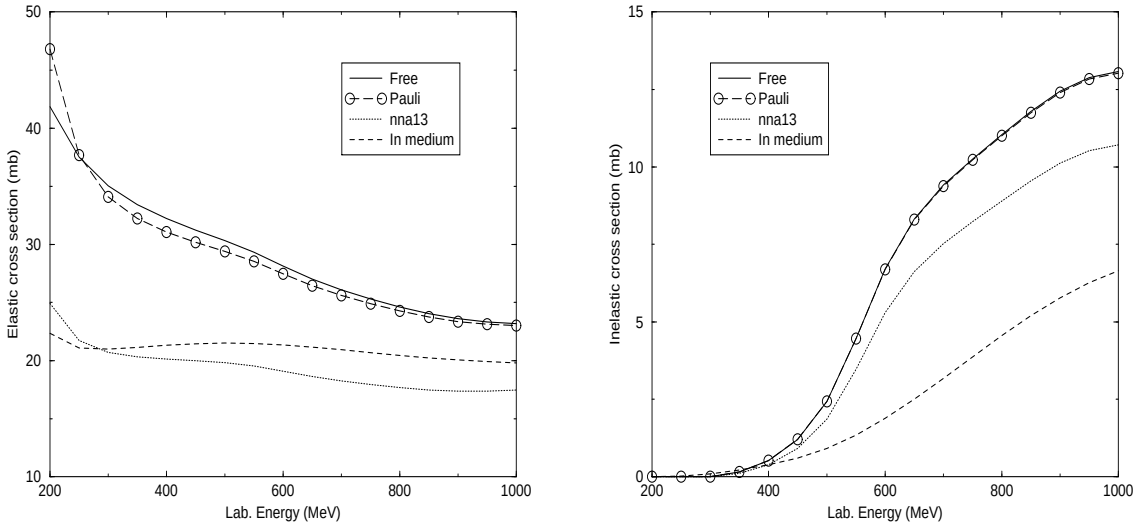

Figure 6.8: *Free space and in nuclear matter cross sections obtained from isoscalar np scattering as a function of kinetic energy in the laboratory system. The nuclear matter is immobile in center of mass system. Includes free space scattering. "Pauli" includes only the in-medium Pauli effect. "nna13" has additionally been included effective mass, but uses the nna13 potential. "In medium" is the final nuclear matter calculations, which also includes the nna13in potential.*

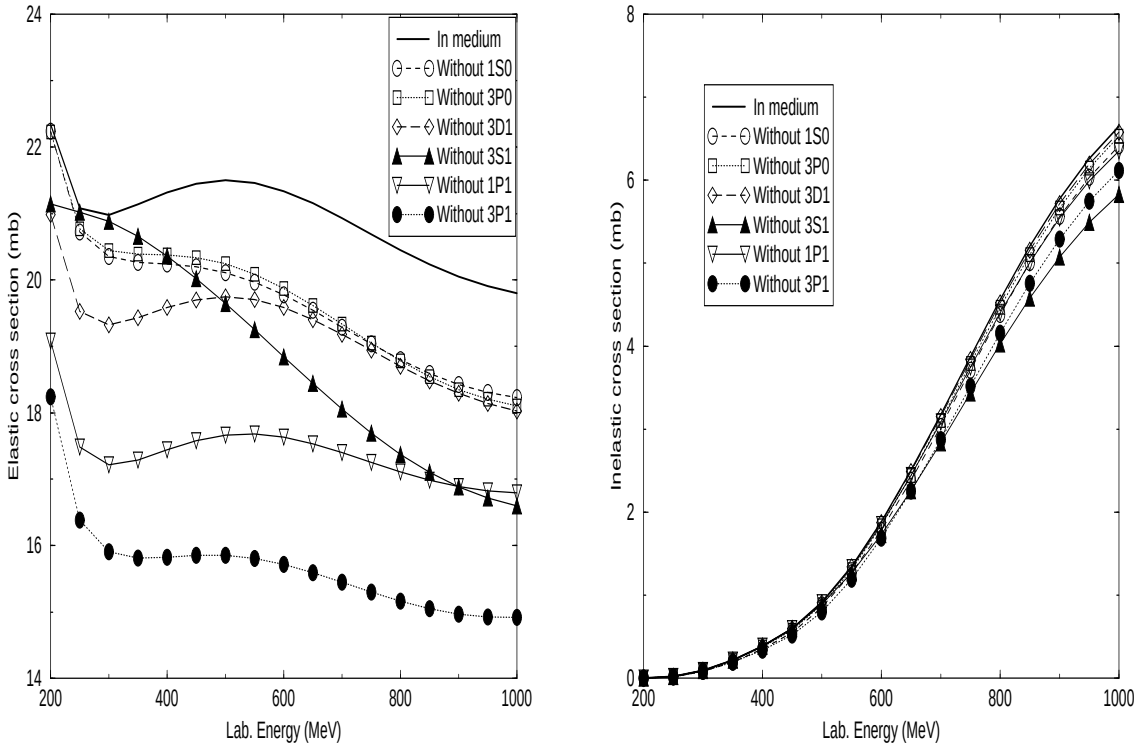

Figure 6.9: *In nuclear matter cross sections obtained from isoscalar np scattering as a function of kinetic energy in the laboratory system.*

6.8 A short summary of our in-medium-scattering system

We look at isoscalar np scattering in a system already occupied by symmetric nuclear matter, which is immobile in the center-of-mass system of the two scattering particles. The two nucleons being scattered have states orthogonal to the states occupied by nucleons from the nuclear matter. The nuclear matter will therefore remove all the states with momentum less than the Fermi momentum from the separated np system. The two nucleons are initially given the same energy as in free space. The two nucleons are then entering the nuclear matter without experience any boundary conditions. Remember that the nuclear matter is defined without a boundary, which simulates the situation inside a heavy nucleus. The incoming nucleons will then interact with the other nucleons in the nuclear matter. The scattering nucleons will, because of the symmetry of the nuclear matter, not be accelerated from such interactions. However, the scattered nucleons will experience a different interaction between each other than they would have in free space, due to the three-body nature of the strong force. The Pauli principal will at the same time forbid intermediate states with momentum less than the Fermi momentum. Note that the three-body force between the nucleons can be explained by the Pauli principal, since it will remove parts of the NN interactions arising from virtual meson exchanges of forbidden nucleon states. These many-body effects will have a large effect on the scattering.

It is commonly known in nuclear physics that the attractions between nucleons increase with the number of neighboring nucleons. We also know that the Pauli principal will work against this attraction, causing an effective repulsion by removing intermediate states which will give an attractive contribution to the total NN interaction. In nuclear matter are these two effects balancing each other (the nuclear matter is saturated by definition). The nucleons can therefore not create a bound state with the nuclear matter. When we now introduce two new particles in the medium, the Pauli principal will remove more attractive NN interaction parts than the three body force will increase their strength. The S-states, which feels the innermost region (the Pauli principle forbidden part), will due to less attraction produce phase shift less than in free space. We can see this in both $^1S_0$ (fig 6.10) and in $^3S_1$ (fig 6.7). Since also repulsive contributions are removed by the Pauli principle, we will expect to see that the cross sections will be less than in free space scattering.

In the BBG theory we define a new system, where the nuclear matter is a constant background field (often redefined as new vacuum states). In this system we are able to calculate the in-medium sp energies, which are needed when we are evaluating the energy operators in the scattering equations (due to the new in-medium particle states).

We have here started the calculations of the scattering data at 200 MeV in the laboratory system. The particle formalism is in theory valid already at 160 MeV, we will however expect more uncertainties in this region from e.g. not using a diffuse Fermi momentum. This will be more important if a particular system has few states to occupy. Note that, all our calculations are done with a sharp Fermi momentum, but this is perhaps not totally compatible with physical nuclei.

6.9 Conclusion

Fig 6.8 clearly illustrates that the elastic cross section is dramatically less than in free space scattering. From phase shifts plotted in fig 6.8 and fig 6.10, we see that e.g. the $^1S_0$, $^3S_1$, $^3D_1$, $^1P_1$ and $^3P_2$ are among the partial waves responsible for the smaller (in-medium) elastic cross section.

The shape of the elastic in-medium cross section is is perhaps better illustrated in fig 6.9. Where we clearly see that the elastic cross section has a minimum at about 250 MeV and a maximum at about 500 MeV in the laboratory system. The shape of this elastic cross section, as a function of energy, is very different to the one obtained in free space. The main reason for these extreme points we obtain, are the in-medium Pauli effect and the $^3S_1$ state. From fig 6.10 we have that the $^3S_1$ phase shift is equal to zero at 250 MeV. Since the elastic cross section is proportional to the phase shifts squared (see eq(1.81)), will the contributions from the $^3S_1$ state at 250 MeV be zero. The elastic cross section around the zero point will be positive, creating a minimum point. This is illustrated in fig 6.9. The maximum point arrives mainly because of the special Pauli effect on the $^3S_1$, since the elastic cross section will increase with energies in the region between 250 MeV and 1GeV. At about 500 MeV will the con-

tribution to the elastic cross section from all the other partial wave states decrease more rapidly with energy than the $^3S_1$ contribution will increase. From the S-waves we see that repulsive core defined in eq(1.204) will increase to $R_{\text{core}} \approx 0.7$.

Fig 6.9 illustrates that the inelastic cross section in nuclear matter, which we see from fig 6.8 will be larger than in free space scattering until about 350 MeV in the laboratory system. At higher energies it will be less than half of the obtained inelastic cross section in free space. From fig 6.8 we also see that the Pauli operator will have a minimal effect on the inelastic cross section (obtained from free space scattering). This is not surprising, since the inelastic cross section is identical to zero in the forbidden region, i.e. the on-shell momentum in center-of-mass system is less than k_{F}.

The larger inelastic cross section at lower energies, and non-zero even at less energies than pion mass, can be traced back to $^1S_0$ (see fig 6.7). This is possible if a pion, created from an inelastic process, is interacting with the nuclear matter and can be associated with an effective mass. Then a pion can be created with less energy than the free pion mass. A mesons bound to the nuclear matter theory is however unphysical, since nuclei only consists of neutrons and protons, which are fermions and therefore are orthogonal to meson states. i.e. mesons cannot form bound states with nucleons.We must therefore assume that this effect arrives from all the approximations and simplified theories we have use obtaining our in-medium scattering parameters.

If we look at energies above 350 MeV, the inelastic cross section obtained in nuclear matter is less than in free space. In fig 6.8 we see that there is a dramatic change in the inelastic nuclear matter cross section in the region between 400 MeV and 600 MeV. Fig 6.10 shows that much of this behavior can be traced back to e.g. $^3P_0$, $^3P_1$ and $^1D_2$. From fig 6.9 and fig 6.10, we see that partial states contributing the most to the inelastic cross section in nuclear matter scattering are the $^3S_1$ and $^3P_1$.

Fig 6.8 shows how important it is to include the dispersion relation in the energy dependent nna13 potential.

The reduction of the cross section in-medium scattering compared to in-free space scattering must be due to NN interaction with shorter range or/and of less strength.

To make a better in-medium model, one can include effects like the interaction between the isobar particles and the nuclear matter, which will also contain isobars. More important is however the Dirac effect. The Dirac effect is derived by using the Dirac-Bruckner approach and let the effective mass enter the picture already in Dirac spinors obtained from solutions of the Dirac equation. note that, a relativistic potential will be different from the nna13in potential, which is derived from non-relativistic energies. More about Dirac-Bruckner approach can be found in [10].

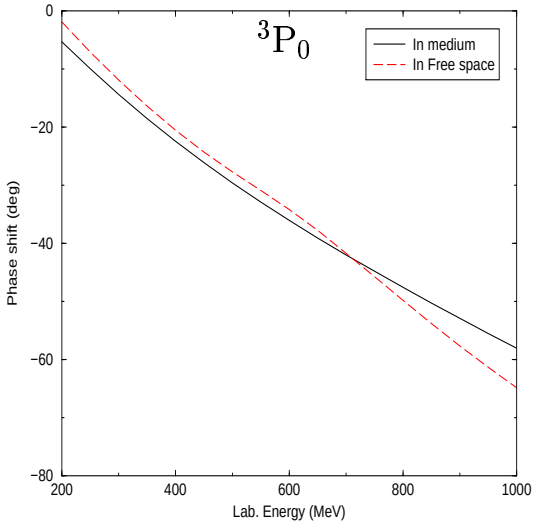
$^3P_0$
In medium
In Free space
Phase shift (deg)
Lab. Energy (MeV)

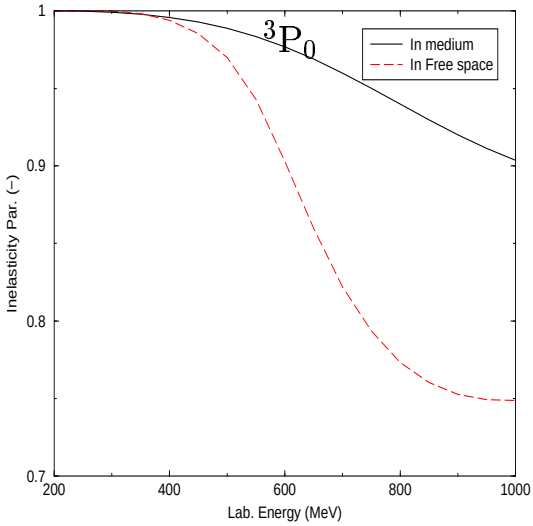
$^3P_0$
In medium
In Free space
Inelasticity Par. (–)
Lab. Energy (MeV)

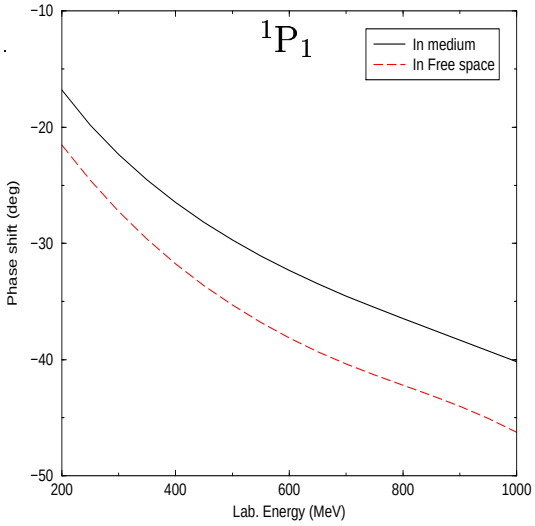
$^1P_1$
In medium
In Free space
Phase shift (deg)
Lab. Energy (MeV)

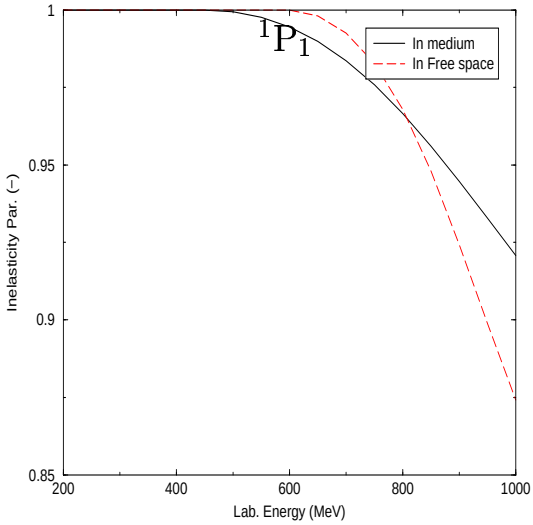
$^1P_1$
In medium
In Free space
Inelasticity Par. (–)
Lab. Energy (MeV)

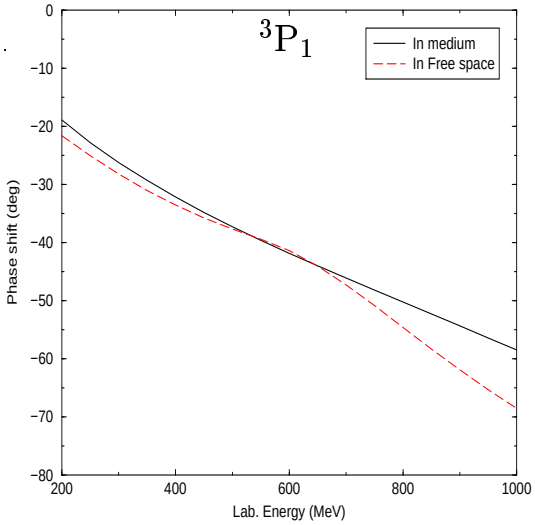
$^3P_1$
In medium
In Free space
Phase shift (deg)
Lab. Energy (MeV)

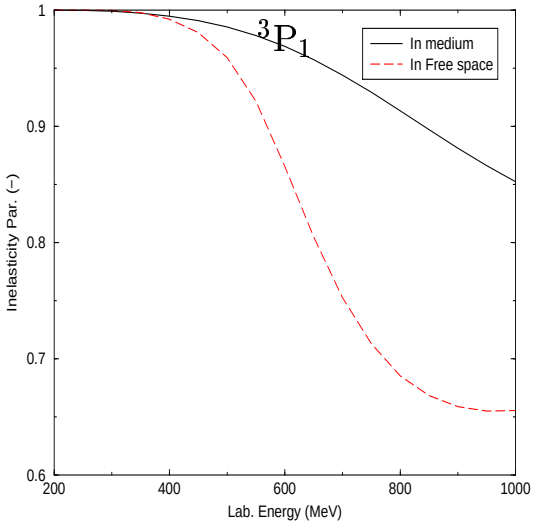
$^3P_1$
In medium
In Free space
Inelasticity Par. (–)
Lab. Energy (MeV)

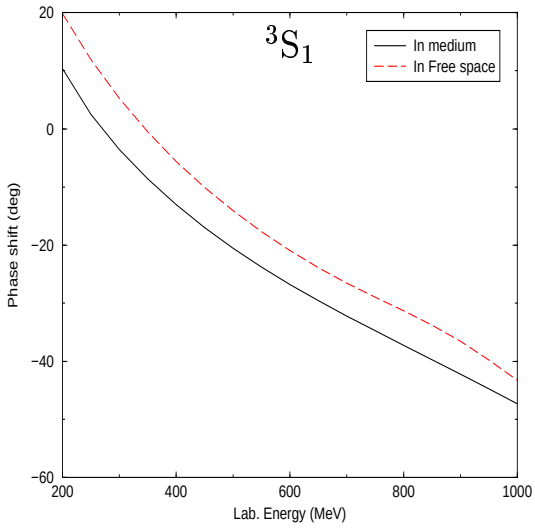
$^3S_1$
In medium
In Free space
Phase shift (deg)
Lab. Energy (MeV)

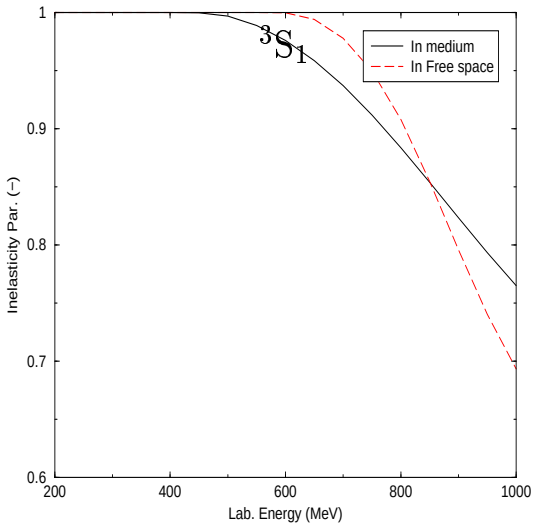
$^3S_1$
In medium
In Free space
Inelasticity Par. (–)
Lab. Energy (MeV)

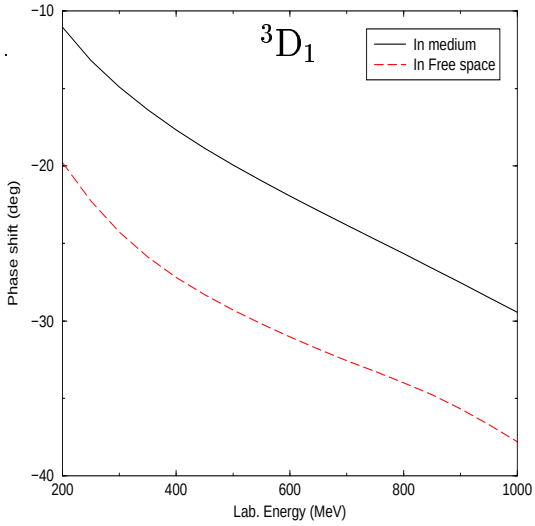
$^3D_1$
In medium
In Free space
Phase shift (deg)
Lab. Energy (MeV)

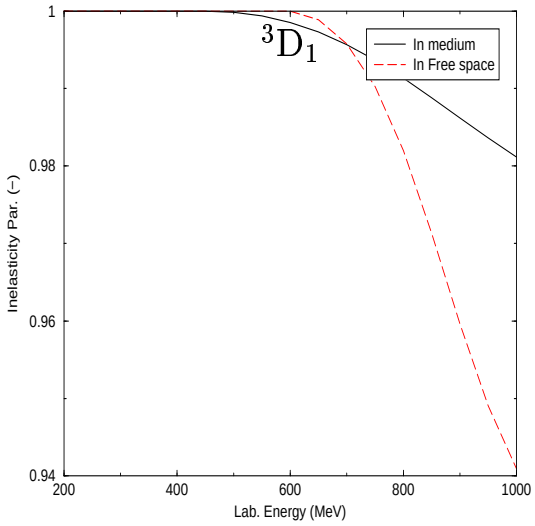
$^3D_1$
In medium
In Free space
Inelasticity Par. (–)
Lab. Energy (MeV)

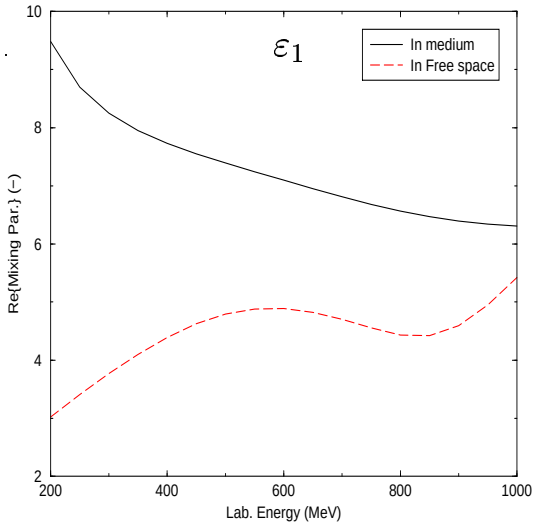
ε_1
In medium
In Free space
Re{Mixing Par.} (–)
Lab. Energy (MeV)

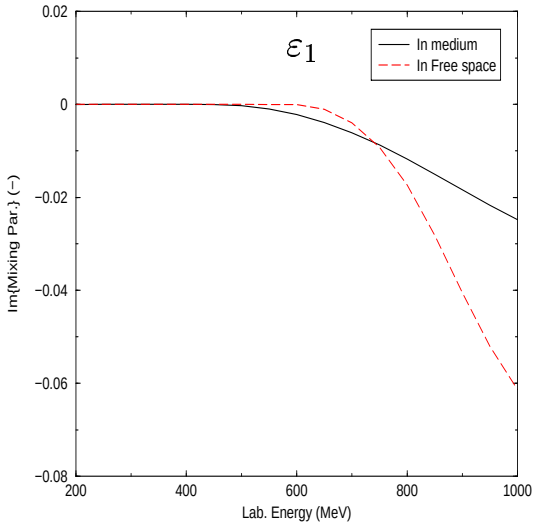
ε_1
In medium
In Free space
Im{Mixing Par.} (–)
Lab. Energy (MeV)

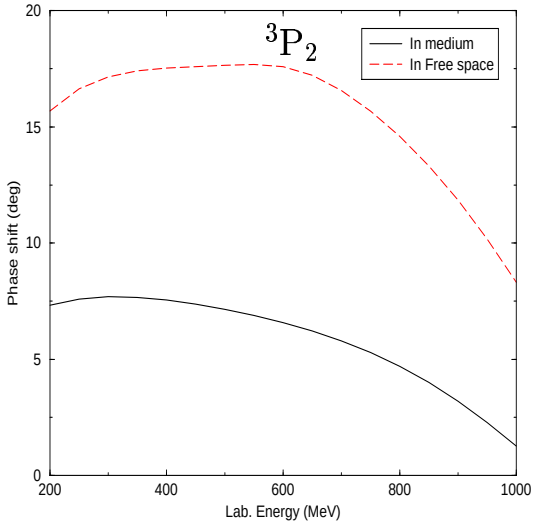
$^3P_2$
In medium
In Free space
Phase shift (deg)
Lab. Energy (MeV)

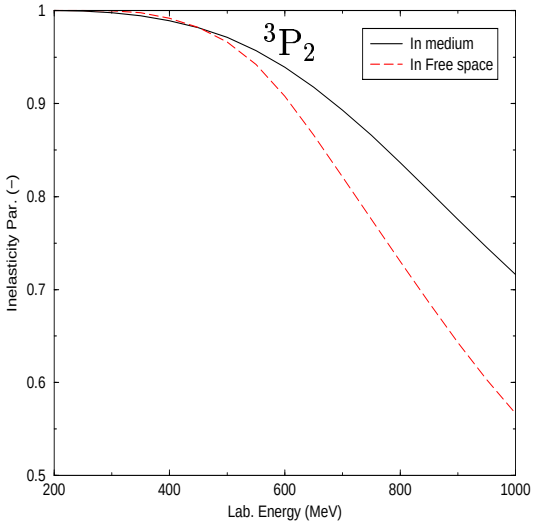
$^3P_2$
In medium
In Free space
Inelasticity Par. (–)
Lab. Energy (MeV)

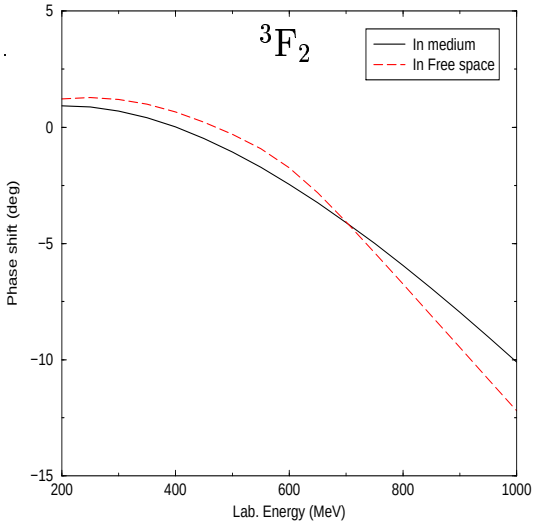
$^3F_2$
In medium
In Free space
Phase shift (deg)
Lab. Energy (MeV)

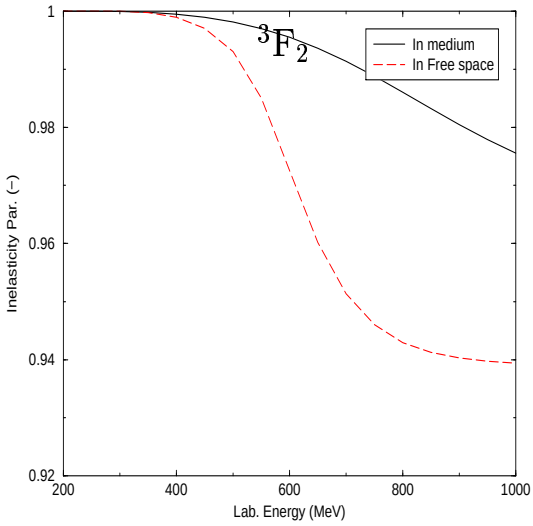
$^3F_2$
In medium
In Free space
Inelasticity Par. (–)
Lab. Energy (MeV)

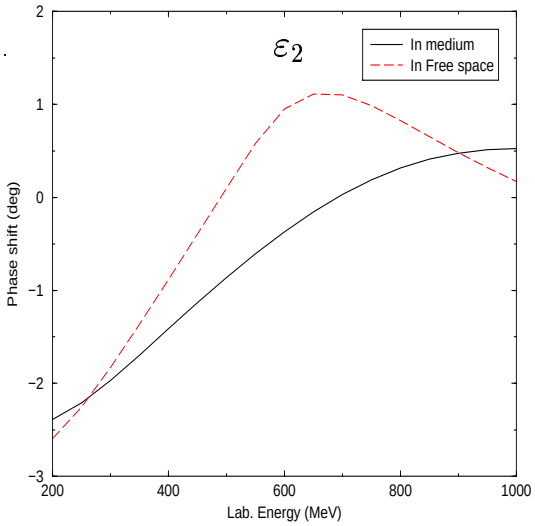
ε_2
In medium
In Free space
Phase shift (deg)
Lab. Energy (MeV)

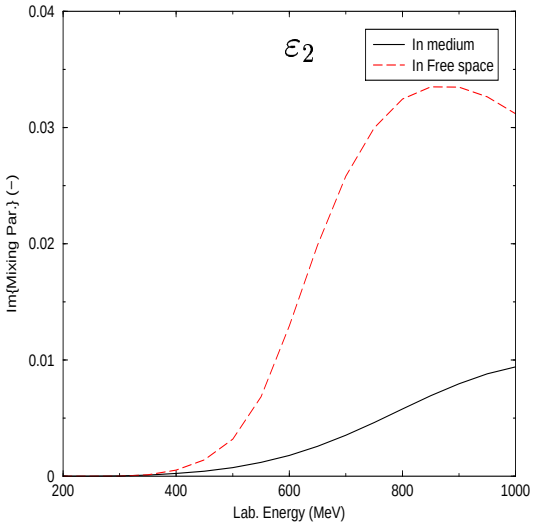
ε_2
In medium
In Free space
Im(Mixing Par.) (–)
Lab. Energy (MeV)

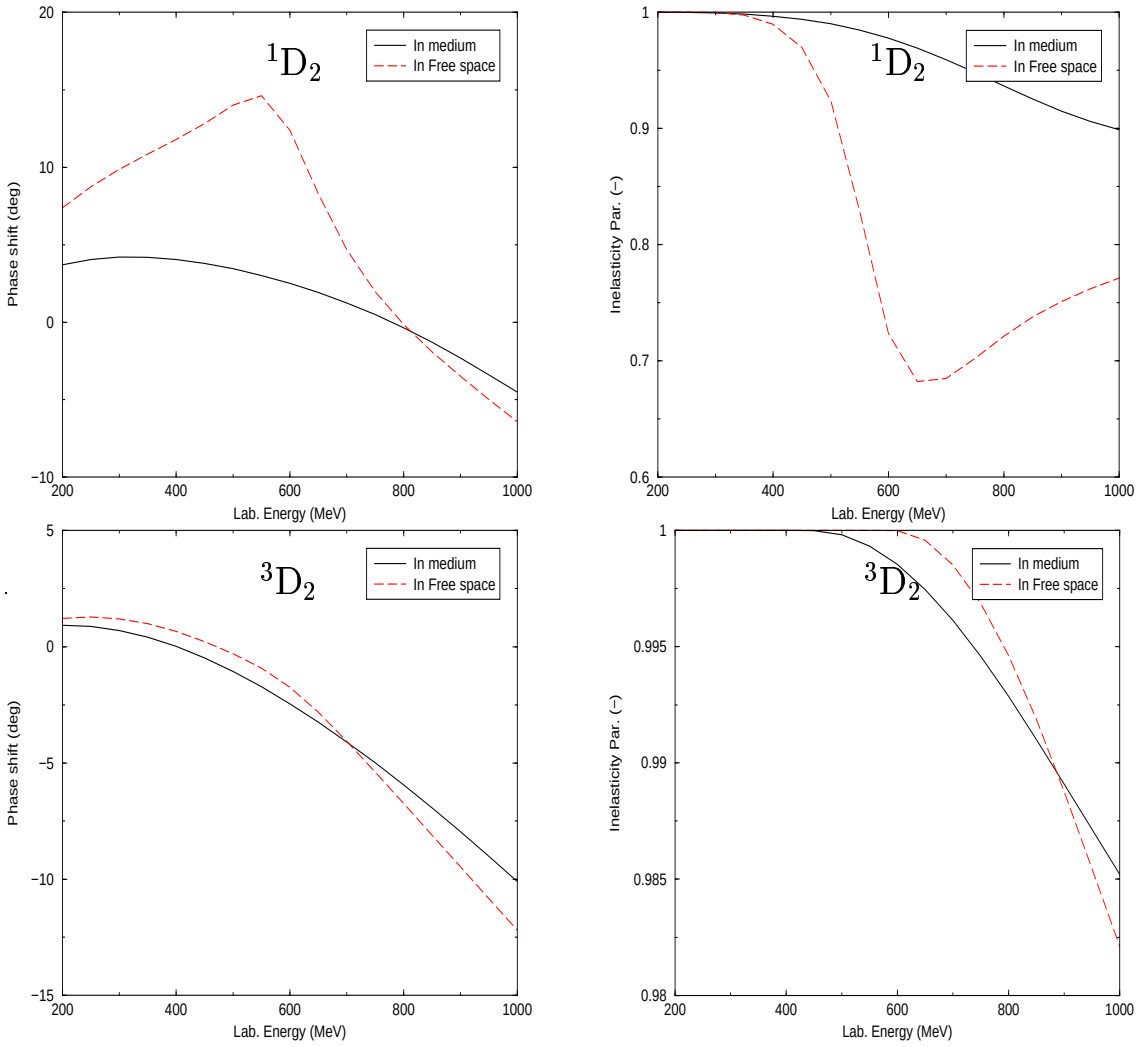

Figure 6.10: Free space and in nuclear matter phase shifts, inelasticities and mixing parameters, obtained for isoscalar np scattering, as a function of kinetic energy in the laboratory system. The nuclear matter is immobile in center of mass system.

Bibliography

[1] R. Machleidt, Adv. Nucl. Phys. **19**, 189, (1989)

[2] K. L. Kowalski, Phys. Rev. Lett. **15** 798 (1965)

[3] G. E. Brown and A. D. Jackson (1976)

[4] R. Machleidt, K. Holinde and C. Elster, Phys. Repts 149 (1987) 1.

[5] V. G. J. Stoks, R.A. M. Klomp, M. C. M. Rentmeester, and J. J. de Swart, Phys. Rev. C **48**, 2, (1993)

[6] R. A. Arndt, I. I. Strakovsky, and R. L. Workman, Phys. Rev. **C62**, 034005, (2000)

[7] K. S. Krane, Introductory Nuclear Physics, (1988)

[8] J. Blatt and L. Biedenharn, Phys. Rev. **C86** 399 (1952)

[9] H. P. Stapp, T. J. Ypsilantis and N. Metropolis, Phys. Rev. **C105** 302 (1957)

[10] G. Q. Li and R. Machleidt, Phys. Rev. **C48** 4 (1993)

[11] E. E. Salpeter and H. A. Bethe, Phys. Rev. **C84** 1232 (1951)

[12] R. Blankenbecler and R. Sugar, Phys. Rev. **C142** 1051 (1966)

[13] R. H. Thompson, Phys. Rev. **D1** 110 (1970)

[14] E. K. U. Gross, E. Runge and O. Heinonen, Many-Particle Theory, (1991)

[15] R. Machleidt, Phys. Rev. **C63**, 024001 (2001)

[16] K. Langanke, J. A. Maruhn and S. E. Koonin (R. Machleidt), Computational Nuclear physics 2 (1990)

[17] P. C. Hemmer, Kvante Mekanikk (2000)

[18] R. G. Newton, Scattering Theory of waves and Particles (1982)

[19] L. E. Engvik, Doctor Thesis (1999)

[20] F. Ravndal, Relativistic Quantum Mechanics (2001)

[21] J. J. Sakurai, Modern Quantum Mechanics (1994)

[22] Ch. Elster, J. H. Thomas and W. Glöckle, Phys. Rev. **C24** 5579 (1998)

[23] C. van der Leun and C. Alderlisten, Nucl. Phys. A380, 261 (1982)

[24] K. Holinde and R. Machleidt, Nucl. Phys. **A280** 429 (1977)

[25] K. Holinde, R. Machleidt, M. R. Anastasio,A. Faessler, and H. Müter, Phys. Rev. **C18**, 870 (1978)

[26] W. Rarita and J. Schwinger, Phys. Rev. **C60**, 61 (1941)

[27] Atomic Data and Nuclear Data Tables 17 (1976)

[28] B. H. Brandow, Ph. D thesis, Cornell University, (1964)

[29] Particle Data Group, Rev. Mod. Phys. **56**, 1 (1984)

[30] J. Fleischer and J. A. Tjon, Nucl. Phys. **A84**, 375 (1975)

[31] F. Gross, Phys. Rev. **C26** 2203 (1982)

[32] J. Fleischer and J. A. Tjon, Phys. Rev **D21**, 87 (1980)

[33] C. Itzykson and J.B. Zuber, Quatum field theory (McGraw-Hill, New York, 1980)

[34] S. Weinberg, Phys. Rev. Lett. **B18** 188 (1967)

[35] K. Holinde and R. Machleidt, Nucl. Phys. **A359** 495 (1975)

[36] G.E. Brown and W. Weise, Phys. Reports **22** 279 (1975)

[37] W. H. Dickhoff, A. Faessler, J. Meyer-Ter-Vehn and H. Müter, Phys. Rev. **C23**, 1154 (1981)

[38] M. Hjorth-Jensen, H. Müter and A. Polls, Phys. Rev. **C50**, 501 (1994)

[39] M.I. Haftel and F. Tabakin Nucl. Phys. **A158** 158 (1970).

[40] H.-J. Schulze, A. Schnell, G. Röpke, Phys. Rev. **C55**, 3006 (1997)

[41] W. H. Dickhoff, C.C. Gearhart, E. P. Roth, Phys. Rev. **C60**, 064319 (1999)

[42] B. H. Brandow, Rev. Mod. Phys. **39**, 771 (1967)

[43] A. D. Jackson, Ann, Rev. Nuc. Part. Sci. **33**, 105 (1983)

[44] H. A. Bethe, B. H. Brandow, and A. G. Petschek, Phys. Rev. **C129**, 225 (1963)

[45] J. P. Jeukenne, A. Lejeune, C. Mahaux, Nucl. Phys. **A245**, 411 (1975)

[46] T.-S. H. Lee, Phys. Rev. Lett **B50**, 1571 (1983)

[47] J. D. Jackson, J. M. Blatt. Rev. Mod. Phys. **22**, 77 (1950)